5-24-2010

# Microanalytical Investigations of Presolar SiC Grains as Probes of Condensation Conditions in Astrophysical Environments

Kathryn Hynes
*Washington University in St. Louis*

WASHINGTON UNIVERSITY IN ST. LOUIS

Department of Physics

Dissertation Examination Committee:
Thomas J. Bernatowicz, Chair
Charles M. Hohenberg
Martin H. Israel
William B. McKinnon
Frédéric Moynier
Ernst K. Zinner

# MICROANALYTICAL INVESTIGATIONS OF PRESOLAR SIC GRAINS AS PROBES OF CONDENSATION CONDITIONS IN ASTROPHYSICAL ENVIRONMENTS

By

Kathryn Mairin Hynes

A dissertation presented to the
Graduate School of Arts and Sciences
of Washington University in
partial fulfillment of the
requirements for the degree
of Doctor of Philosophy

December 2010

St. Louis, Missouri

# ABSTRACT OF THE DISSERTATION

Microanalytical Investigations of Presolar SiC Grains as Probes of Condensation Conditions in Astrophysical Environments

by

Kathryn Mairin Hynes

Candidate for Doctor of Philosophy in Physics

Washington University in St. Louis, 2010

Professor Thomas J. Bernatowicz, Chairperson

This thesis reports the microanalysis of sixteen presolar SiC grains that are thought to have condensed in several different types of astrophysical environments, including asymptotic giant branch (AGB) stars, J stars, born-again AGB stars, and Type II supernovae (SNe). The isotopic compositions and microstructural properties of a large number of presolar grains have previously been measured, but the two techniques have been combined in the analysis of only a handful of presolar grains. Detailed structural and chemical microanalytical studies, when combined with isotopic measurements, provide the most complete constraints on presolar grain formation and growth.

With the transmission electron microscope (TEM), I analyzed presolar SiC grains to determine the crystal size and structure of isotopically characterized SiC grains, as well as the elemental composition of the grains. I also obtained this information for internal subgrains found within the SiC grains. My combined analysis of these grains helped to place constraints on the growth conditions during grain condensation, revealed

differences between the physical conditions in different types of stellar sources, suggested the likely origin of these grains, and identified new types of presolar grains.

The types of internal subgrains I observed in the presolar SiC grains in this study varied according to the stellar source of the grains. During TEM analysis, I discovered two new types of presolar grains that are present as subgrains within the SiC grains. One of these types was determined to be iron-nickel silicide [$(Fe,Ni)_mSi_n$], which is found in SiC grains that originated in SNe. Although silicides are predicted stable SN condensates, they have not been previously observed in presolar grains. The other new type of presolar grain is oldhamite (CaS), found in a SiC grain that most likely condensed in the envelope of a J star. Oldhamite is one of the lowest temperature minerals that are predicted to condense with SiC and its presence, along with the observation of other low temperature condensates in the same SiC grain, indicates that thermochemical equilibrium must have been maintained over a wide range of temperatures during SiC grain condensation. I observed that SiC crystal domain size varies with stellar source, presumably as a result of the very different growth conditions that exist in the diverse circumstellar environments in which each type of SiC is thought to have condensed. However, I did not observe the crystal structure of the SiC grains to vary with stellar origin.

In addition to the TEM analysis of presolar SiC grains, I also compiled a database of all of the existing isotopic data on presolar grains, which is accessible via a website. This is both the first time that data on the more than twelve thousand presolar grains reported in the literature have been organized in a single place, and that a significant compilation of presolar grain data has been made available to the entire astrophysical

community. I designed the database as a tool to be utilized by both experimentalists and theorists, allowing them to readily compare their data or models to previous measurements and to serve as a simple, quick reference library of all the available presolar grain papers from which I obtained the original data.

# Acknowledgements

I owe a great debt to everyone on the 4th floor for all their help throughout my time here. This is truly an extraordinary place to work, and the 4th floor fosters an amazingly open, collaborative scientific environment that is rarely seen outside of its confines. First and foremost, I am forever beholden to my advisor, Tom Bernatowicz, for all of his help, guidance, and motivation, both scientific and personal. He has taught me not only how to be a good scientist, but also how to be a good teacher, which is a rare combination. I would also particularly like to thank the following people for their help: Ernst Zinner for imparting a vast amount of his scientific knowledge to me, for teaching me that there is always something new to learn, and for conveying an endless enthusiasm to learn it; Kevin Croat for teaching me all the ins and outs of the TEM and for walking all the way down to the first floor whenever a problem arose; Sachiko Amari for help with isotopic measurements and for her perpetual sunny disposition; Tim Smolar for teaching me almost everything I know about how to take things apart and put them back together again, and for always being entertaining in the process; Jan Foster for being a perpetual source of encouragement; and Eric Inazaki for his frequent effort to maintain a functioning internet connection.

I thank the Physics Department, the McDonnell Center for the Space Sciences, and NASA for monetarily supporting me throughout my time here. I am grateful to Pat Gibbons for keeping an old instrument in excellent working order. I thank Julia Hamilton, Sarah Hedley, and Linda Coffin for administrative assistance. I would also like to thank a number of my colleagues and collaborators: Ann Nguyen, Christian

Vollmer, Kuljeet Marhas, Phillip Heck, Larry Nittler, and Rhonda Stroud for many illuminating conversations; and especially Aaron Mertz and Emily Lebsack for their help with sample preparation. I am also indebted to several of my fellow students, both past and present: Scott Hughes for saving me in my first graduate school class and for more adventures than I can begin (or ever would want) to count; to Christine Geiger for many years of entertainment, from making Algebra bearable to more recent email distractions, among so many other things; and to Maitrayee Bose for excellent office company and her recent secretarial services.

Finally, I would be remiss if I did not thank the people who enabled me to get this far in the first place. In equal parts, my undying gratitude and love goes to my mother, Kathy Hynes, for always wanting to hear about what I was doing, read my academic papers, and see my conference talks - I would not be here without her boundless support and encouragement, which she has done far and above anyone else; my father, Robin Hynes, for always secretly being proud of me, despite insisting that if you cannot see a black hole, it cannot be there; my uncle, Pete Postol, for instilling a passion for science from the early days of air-layering and crack-the-whip torque demonstrations. I am forever beholden to my best friend, Frank Gyngard, for being my constant companion, sparring partner, and foil for eleven years, both scientifically and personally. And finally, I cannot thank my fiancé, Dan Wind, enough for all the love and support he has given me during the complete and utter bedlam that has been my life over the last few months. He has done more than I could have ever expected or hoped, and, amazingly, still wants to marry me in four weeks.

# Table of Contents

# List of Tables

# List of Figures

# Chapter 1

## Introduction

"We had the sky, up there, all speckled with stars, and we used to lay on our backs and look up at them, and discuss about whether they was made, or only just happened—Jim he allowed they was made, but I allowed they happened; I judged it would have took too long to *make* so many."

~from *The Adventures of Huckleberry Finn* by Mark Twain

One hundred and twenty-five years after its publication, people are still doing exactly the same thing that Huck and Jim did in *The Adventures of Huckleberry Finn*: marveling at the stars and attempting to fathom just how they came to be. It is the task of astronomers and astrophysicists to attempt to answer that question, or to at least contribute a proverbial drop in the ocean towards it. While the observation of stars, their physical properties, and their compositions were traditionally the realm of astronomers and telescopes, the discovery of stardust grains revolutionized these observations. These grains are, quite literally, microscopic pieces of preserved ancient stars that are available for analysis in the laboratory. It is now possible to actually analyze, in extremely precise detail, individual pieces of stardust with microscopes and mass spectrometers.

The process by which these grains of stardust, also known as presolar grains, reached the laboratory is illustrated in Figure 1.1. Through various mechanisms, many

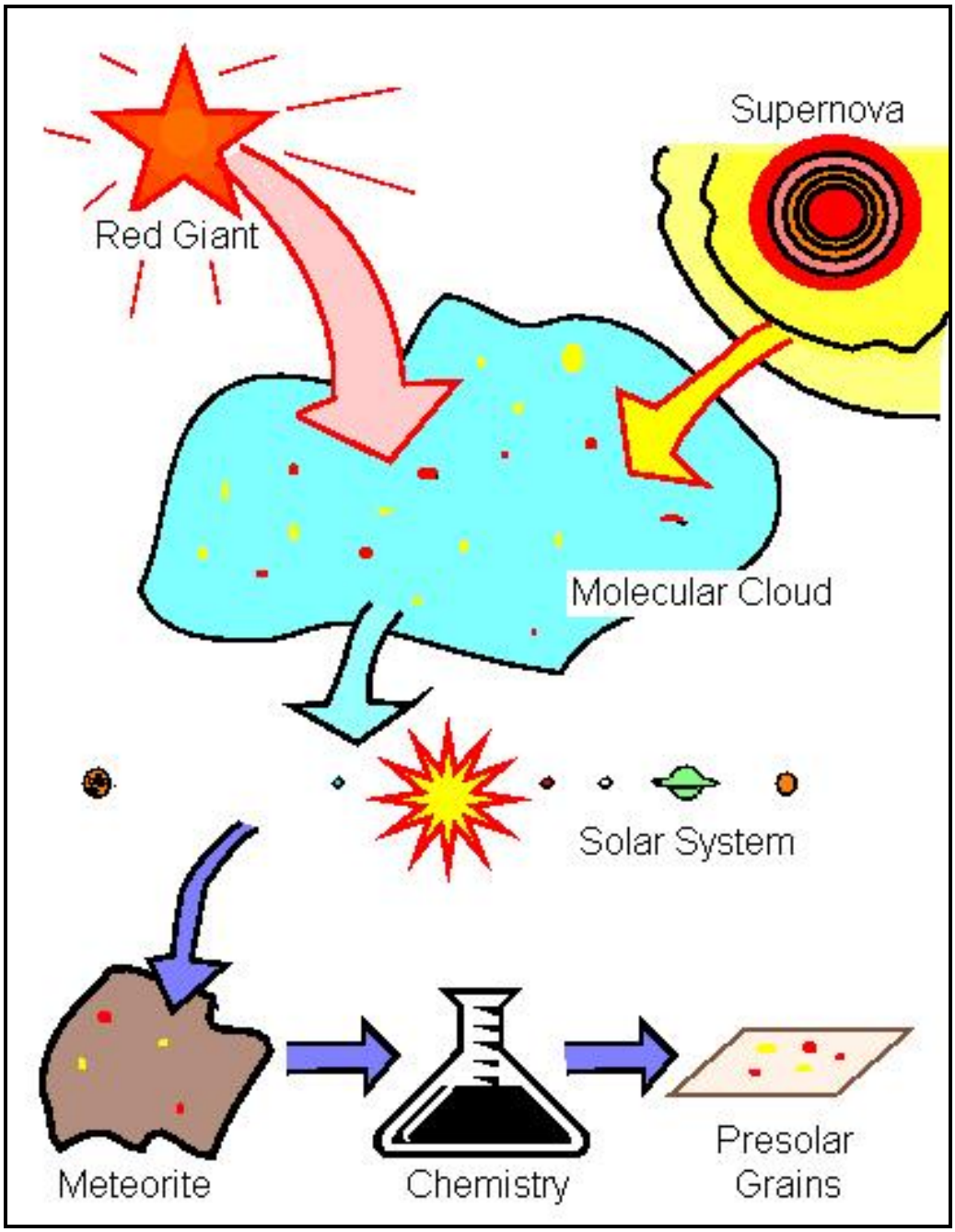


Figure 1.1: Cartoon illustrating the history of presolar grains: the initial formation in stars, subsequent ejection into the ISM, incorporation into the SS and eventually meteorites, and finally isolation in the laboratory for analysis. The cartoon represents ~4.6 x $10^9$ yrs from the beginning of the collapse of the SS to present day, with up to ~$10^9$ yrs of residence time in the ISM. The parent stars formed many millions to a few billion years before dust production, depending on the type of star. (Figure from Nittler 1996)

types of stars produced dust, which they subsequently ejected into the interstellar medium (ISM). These dust grains remained in the ISM for up to ~$10^9$ yrs (Gyngard et al. 2009; Heck et al. 2009), eventually becoming part of a molecular cloud, which then collapsed to form our Solar System (SS). In the early SS, most of these stardust grains were vaporized, then mixing and condensation homogenized their compositions, thereby erasing the individual isotopic signatures of their original stellar origins. However, some infalling grains survived entry into the nascent solar nebula and were incorporated into the matrices of primitive meteorites (i.e., meteorites that have not undergone extensive physical or chemical alteration since their formation ~4.6 x $10^9$ years ago). Eventually, these meteorites fell to Earth where they were collected, sent to museums and scholarly institutions, and eventually to laboratories. The most chemically resistant presolar grains are separated from the meteorite matrix with harsh chemical treatments (Amari et al. 1994), thereby allowing analysis of their isotopic, chemical, morphological, and crystallographic properties.

The analysis of presolar grains with microscopes and ion microprobes provides a complimentary approach to traditional astronomical observations, which utilize telescopes. While astronomers can pinpoint a particular star to measure, they are primarily limited to bulk measurements of the star's major elements, which can easily be obscured by dust or overall distance, and in only a handful of cases can isotopic measurements be made. However, although it is impossible to know from which individual star any given presolar grain originated, the type of star (e.g., a supernova) can be determined for each grain, based on extremely precise isotopic compositions for most

elemental systems (with errors as small as one part in a thousand), detailed structural data (down to the Å-scale), and measurements of phases too rare to be observed astronomically (an example of which is shown in Figure 1.2). These data, when combined with astronomical observations and theoretical calculations, can provide detailed constraints not previously possible with astronomical results alone. New insights into nucleosynthesis, stellar mixing, stellar evolution, physical conditions like temperature and pressure, grain formation timescales and sequences, Galactic Chemical Evolution (GCE), and ISM residence times are all possible since the advent of presolar grain research.

Many of these advances have been made possible largely by two kinds of equipment: secondary ion mass spectrometers (SIMS) and transmission electron microscopes (TEM). The NanoSIMS is a type of SIMS instrument that is capable of obtaining isotopic data on individual grains as small as 50 nm. Because each presolar grain represents a sample of a star at a particular stage of stellar evolution and under particular conditions, each grain therefore has a unique isotopic composition, making it critical to measure presolar grains individually in order to get precise constraints on nucleosynthesis and stellar mixing. When isotopic measurements are combined with TEM analysis, even greater constraints can be placed on stellar processes. The crystal size and structure, elemental composition, and any internal inclusions in each presolar grain can be analyzed to a nano- or even Å-scale level of detail with a TEM. These analyses permit valuable inferences to be made about condensation temperatures and pressures, nucleation rates, and elemental abundances that existed in the circumstellar formation environment. The bulk of this thesis will be dedicated to presenting the results

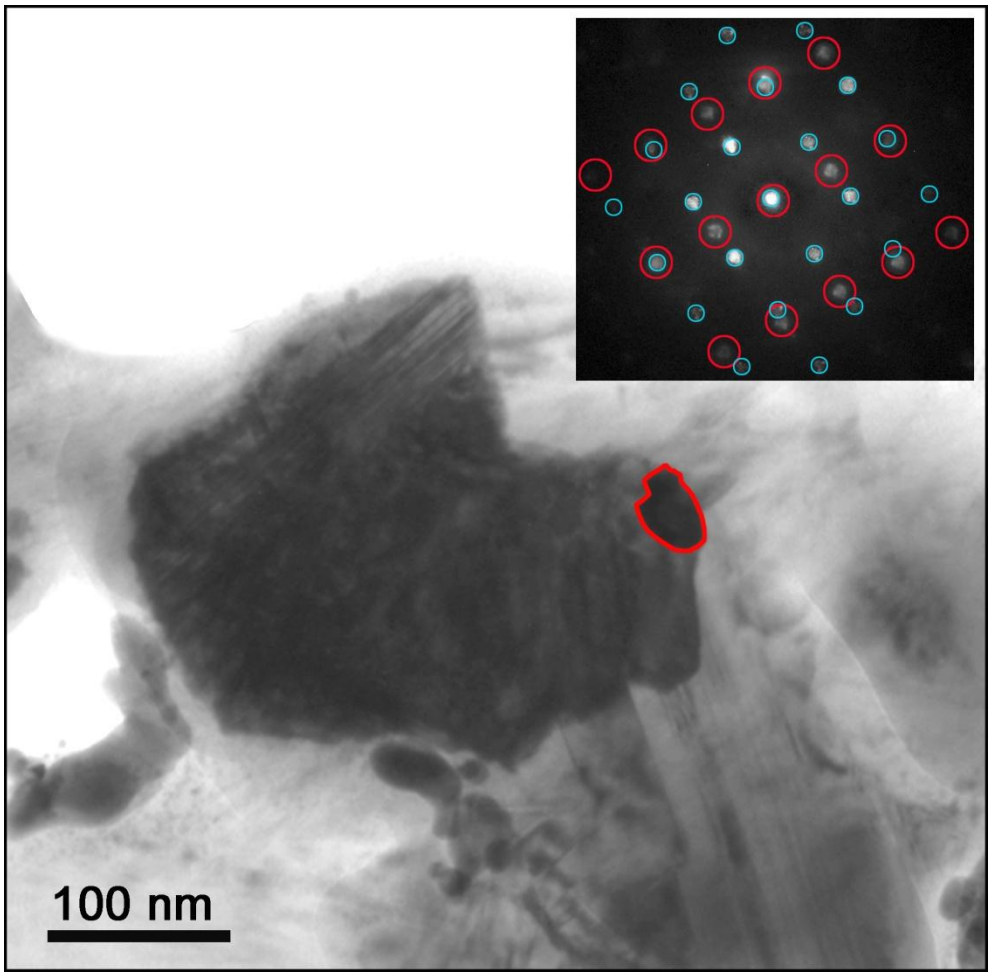


Figure 1.2: TEM bright-field (BF) image of a presolar SiC grain, which condensed in a supernova outlflow, with an Fe silicide inclusion (outlined in red). This is the first time presolar Fe silicide has been observed. The inset is an [011] electron diffraction pattern from the SiC crystal (diffraction spots circled in blue) superimposed on the diffraction pattern from the silicide subgrain (diffraction spots circled in red), which shows epitaxial alignment between the silicide subgrain and the SiC grain, with a slight mismatch of 1.5°. The silicide subgrain probably exsolved from the SiC. Additional details about these grains are discussed extensively in Chapter 2 of this work and in Hynes et al. (2010). (This image originally appeared on the cover of the April 2010 Meteoritics and Planetary Science)

of TEM analyses, combined with NanoSIMS measurements, of presolar grains, along with the inferences about grain formation and growth in several types of stellar sources, which can be drawn from these observations.

One of the fundamental goals of presolar grain research is to better understand the processes of nucleosynthesis and stellar evolution. As such, this chapter begins with an introduction to these topics, as well as a short history of the development of the theory of stellar nucleosynthesis. This history is adapted from the work of John Bahcall, who has a number of excellent articles describing the development of the theory of nucleosynthesis and experimental work from the nineteenth century to present day (Bahcall 2000). The chapter also contains a brief introduction to presolar grains, with a far more thorough treatment given in Chapter 4. Finally, the motivation behind the work in this thesis is described. Unfortunately, this thesis can only discuss in depth a small portion of the information that has been gleaned by the analysis of presolar grains. As such, the reader is referred to the reviews by Zinner (2007) and Nittler (2008), and the references therein, for additional information. Furthermore, although older, the book edited by Bernatowicz and Zinner (1997) does an excellent job in giving an overview of nearly every major topic associated with the analysis of presolar grains, the theoretical and experimental framework of this analysis, and the resulting astrophysical implications, and is therefore highly recommended.

## 1.1 Stellar Evolution and Nucleosynthesis

### 1.1.1 A Brief History of the Theory of Stellar Nucleosynthesis

The mystery of how the sun shines plagued astronomers and physicists for centuries. Leading physicists of the 19$^{th}$ century, such as Hermann von Helmholtz and Lord Kelvin, were convinced that stars produced energy from converting their gravitational mass into heat, a process that would allow the sun to shine for only ~30 million years (Helmholtz 1856; Kelvin 1862). This timescale was in direct opposition to the 300 million year age of the earth calculated by Charles Darwin, which he based on the erosion of the Weald Valley in England (1859). Scientists continued to struggle for the rest of the century to identify by what mechanism the sun could produce enough energy to sustain itself for hundreds of millions of years or more, but it was not until the formulation of the world's most famous physics equation, $E = mc^2$, by Albert Einstein in 1905, that the basis for how stars truly shine was supplied, although no one realized it at the time. The next major piece of the puzzle was provided by a series of mass spectrometry experiments by Francis Aston in 1920. While measuring the isotopes of Ne, he discovered that four H nuclei were heavier than a He nucleus. Later that year, Sir Arthur Eddington realized what Aston's experiments implied: according to Einstein's relation between mass and energy, the mass difference from converting H into He would theoretically provide enough energy for the sun to shine for about 100 billion years (1920). Although we now know that this is far too long by about an order of magnitude, the basic theoretical principle was correct. Finally, in 1939, the two fundamental

reactions by which H is fused into He (the PP chain and the CNO cycle – see section 1.1.1 for further description) were laid out by Hans Bethe. With these processes, he was able to develop a relation between stellar mass and luminosity that agreed with astronomical observations and to calculate the central temperature of the sun, which was within 20% of the current accepted value of ~16 x $10^6$ K.

Although the fusion of H into He in stars was now well understood, the creation of all the elements heavier than Li was still a mystery. Some physicists, such as George Gamow, believed that the heavy elements were primeval; after their creation in the post-Big Bang rapidly expanding universe, the amounts of all the elements other than H and He did not change (Gamow 1946). Competing theories, such as those advanced by Fred Hoyle, suggested that the heavy elements were made in stars, although all the relevant reactions were still unclear (Hoyle 1946). Eventually, spectral observations of red giant stars revealed the presence of Tc, which has no stable isotopes (the longest-lived isotope of Tc is $^{98}$Tc, which has a half-life of 4.2 x $10^6$ years) and is therefore no longer found in any terrestrial or meteoritic material, and confirmed that heavy elements are, indeed, synthesized in stars (Merrill 1952). Finally, the seminal paper by Margaret Burbidge, Geoffrey Burbidge, William Fowler, and Fred Hoyle (1957), and, independently, the work of Al Cameron (1957) set out, in detail, eight nuclear processes that could produce the heavy elements. Their theory, which included the s-process, the r-process, and the p-process, essentially laid out the modern theory of nucleosynthesis.

With a theory of nucleosynthesis in place, a description of stellar evolution was now possible. The Hertzsprung-Russell (HR) diagram traces out the life cycle of a star by plotting its luminosity and effective temperature relationship, an example of which is

shown in Figure 1.3 for a low-mass star. Although major differences arise in low- and high-mass stars at the Asymptotic Giant Branch (AGB) stage, most stars follow a similar path up to this point. A good discussion of stellar nucleosynthesis and evolution is presented by Meyer and Zinner (2006) and by Carroll and Ostlie (2007). The following summary is adapted from them.

### 1.1.2 Hydrogen and Helium Burning

Stars spend most of their lives on the main sequence, where their principal energy source for maintaining hydrostatic equilibrium is H burning. Low-mass stars (< 1.2 $M_{\odot}$) do this via the PP chain, in which (in the principal chain), two $^{1}H$ produce a deuteron, which in turn captures a proton to make $^{3}He$. Then $^{3}He$ captures another $^{3}He$, which produces $^{4}He$ and two protons to feed the cycle. In stars of higher mass and consequently higher temperatures, the CNO cycle dominates. Protons are captured by isotopes of C, N, and O, which produces $^{4}He$, as well as increases the $^{17}O/^{16}O$ and $^{14}N/^{15}N$ ratios while decreasing the $^{12}C/^{13}C$ ratio. These ratios are important for the study of presolar grains and will be discussed later in greater depth.

Once the H core is consumed and turned into $^{4}He$, all but the least massive stars leave the main sequence for the Red Giant Branch (RGB). With the depletion of the H core, the radiative pressure generated from fusion can no longer keep the star from gravitational contraction. The remaining H continues to burn around the He core, causing the star's luminosity to increase (Busso et al. 1999). The core also begins to expand, pushing out and cooling the H burning shell until it shuts off, once again triggering gravitational contraction. This time, however, the core temperature of the star

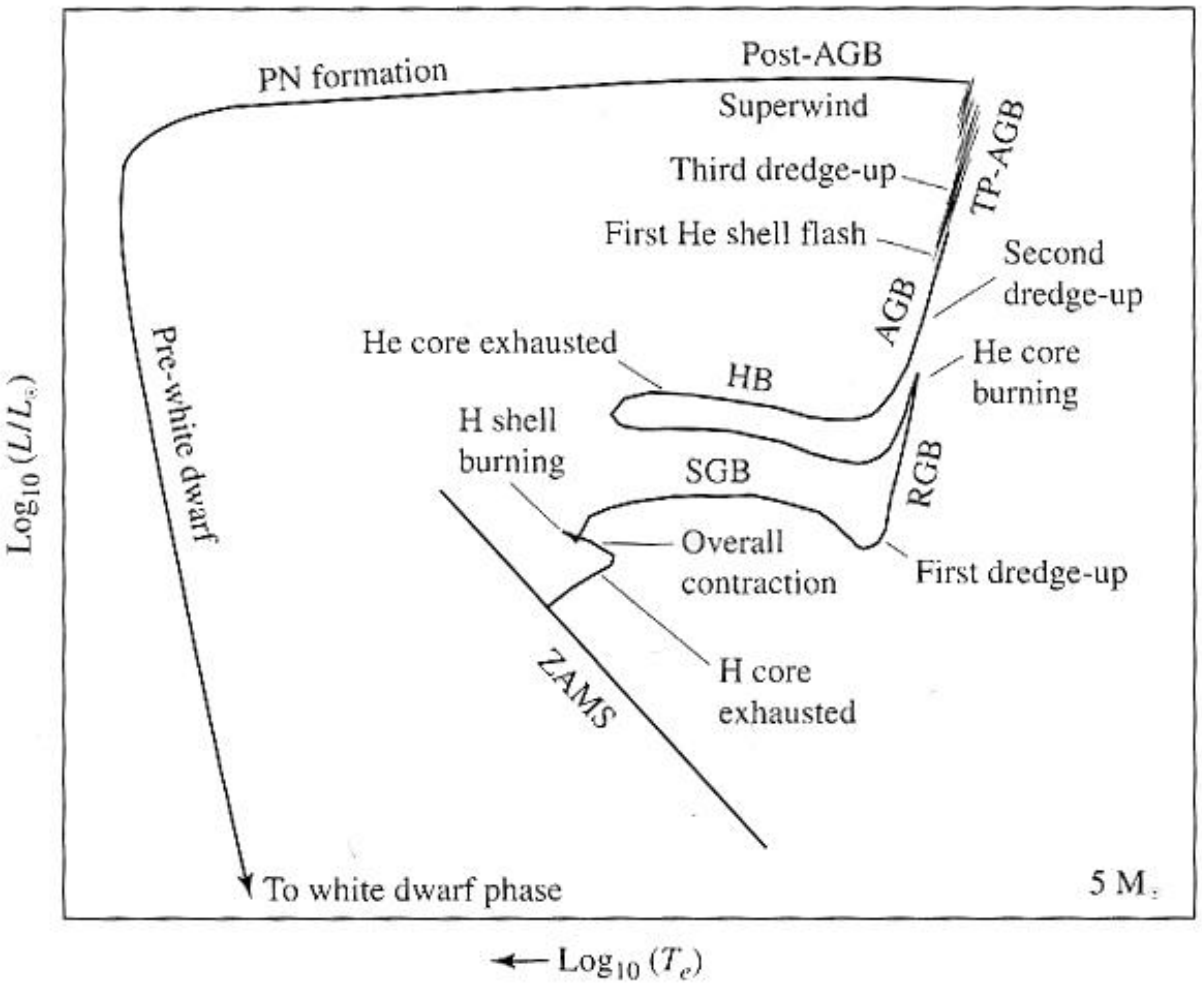


Figure 1.3: The HR diagram for a 5 $M_{\odot}$ star. HR diagrams plot the luminosity (L) of a star normalized to the sun's luminosity ($L_{\odot}$) versus the effective temperature of the star ($T_e$). The relationship between these two quantities shows the evolutionary stages of a star's life, from the main sequence (indicated as ZAMS on the figure for Zero-Age-Main Sequence), where stars spend most of their lives burning H, through He burning, and eventually to a white dwarf, the final stage of a low-mass star's life. (Figure from Carroll and Ostlie 2007)

becomes high enough for the He core to ignite and He burning to begin as the star moves to the Horizontal Branch (HB). During He burning, the triple-α-process fuses three $^{4}$He into $^{12}$C. Oxygen-16 is also produced via the addition of an α-particle to $^{12}$C. This continues until the He core is exhausted, leaving the star composed of a C and O core, surrounded by a He burning shell, a He intershell, a H burning shell, and finally a H-rich envelope (for a schematic, see Figure 1.4).

### 1.1.3 The Asymptotic Giant Branch

The AGB is one of the most important stages in a star's lifetime from the perspective of presolar grain research. Once He is exhausted in the core, the star begins burning He in a shell surrounding the core. In stars of > 8 $M_{\odot}$, this process is a relatively quiet continuation of He burning. However, for stars below this mass, the He shell flashes periodically, creating a thermally-pulsing (TP) AGB star. The previously dormant H burning shell reignites and dumps He ash onto the He intershell. As the mass of the He shell increases, the density rises and creates electron degeneracy at the shell's base. When the temperature is high enough, the base of the He shell ignites in a He flash, which drives the H burning shell outward, causing it to cool and cease burning. The He shell then subsides, the H burning shell shrinks, and the process repeats. These pulses can last between a few decades and a few centuries and occur every $10^4 - 10^5$ years for anywhere from 10s to 100s of cycles, depending on the mass of the star (Busso et al. 1999).

During the AGB phase, a number of important things occur in the star. Third dredge-up (TDU) brings nucleosynthetic material from the star's interior to the surface.

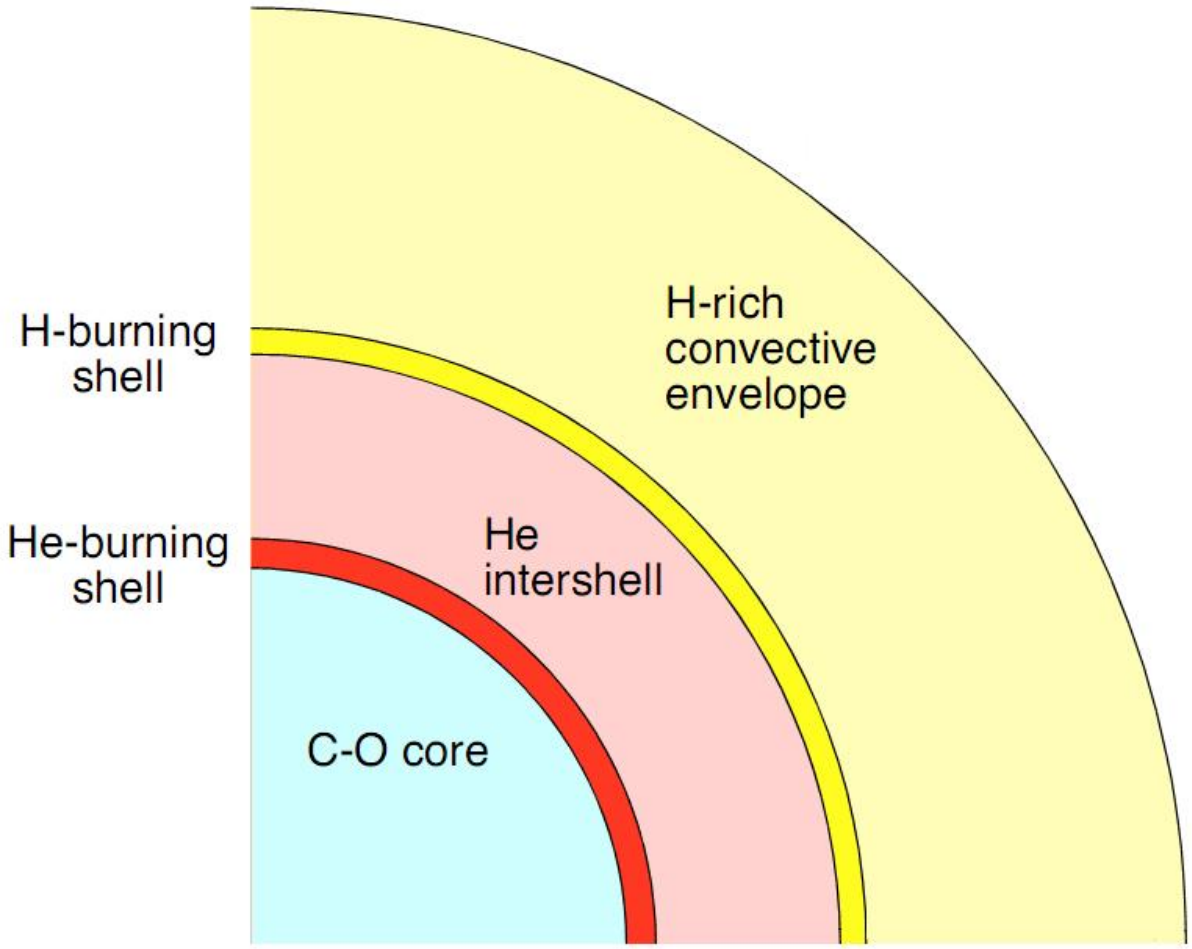


Figure 1.4: Cross-section of a low-mass AGB star (layers not to scale) showing the core, thin nuclear burning shells, intershells, and the large H envelope beyond which presolar grains condense during the TP-AGB phase. (Diagram courtesy of Andy Davis)

One of the most noteworthy results is that $^{12}C$ from the He intershell is brought to the surface, making the stellar envelope C-rich instead of O-rich and turning the star into a carbon star (Wallerstein et al. 1997). This is important for the formation of carbonaceous dust grains in AGB stars; in an O-rich environment, all of the C is tied up in particularly stable CO molecules, and therefore not available to form other molecules. In a C-rich environment, however, free C is available to form molecules other than CO, such as SiC and graphite. The temperature in the envelope also decreases during the He flashes, allowing dust grains to condense. Radiation pressure creates stellar winds that drive the grains out of the H envelope of the AGB star and into the ISM, resulting in rapid mass loss for the star, sometimes at rates as high as $10^{-4}$ $M_{\odot}$ $yr^{-1}$.

Another important process that occurs during the AGB phase is the main component of the s-process (Gallino et al. 1990). This process, so named because of the slow capture of neutrons due to low neutron densities, produces the elements heavier than Fe up to $^{208}Pb$ and $^{209}Bi$. Through a mechanism that is not well understood, protons from the H shell leak into the He intershell, where they react with the plentiful $^{12}C$, creating a "$^{13}C$ pocket". Through the reaction $^{13}C(\alpha,n)^{16}O$, abundant neutrons are released. During the TP, neutrons are also released via the high temperature $^{22}Ne(\alpha,n)^{25}Mg$ reaction. The newly released neutrons are added to existing nuclei; if unstable nuclei are created, they decay back down to the valley of stability via β-decay (Figure 1.5).

### 1.1.4 Beyond the Asymptotic Giant Branch

For stars < 8 $M_{\odot}$, He burning marks the end of their nucleosynthetic lives. The star continues to lose mass and expels its envelope, becoming a planetary nebula. With

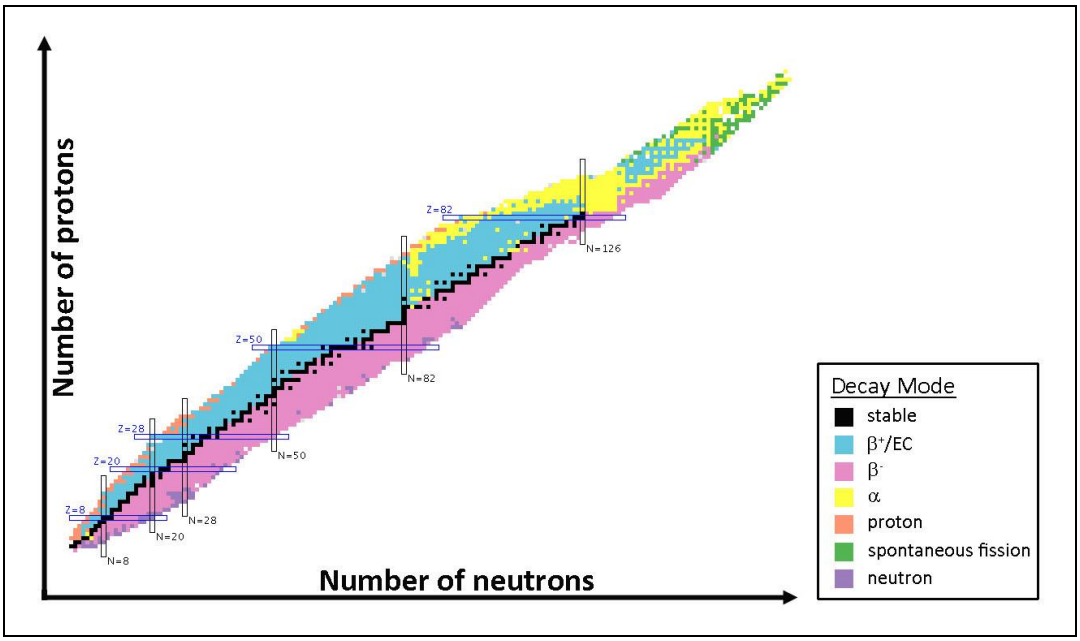


Figure 1.5: Schematic plot of the chart of the nuclides, showing the decay modes of the isotopes. The s-process, which occurs in both AGB stars and massive stars, and the r-process, which occurs only in SNe, produce isotopes along the valley of stability, indicated in black (Figure courtesy of Brookhaven National Laboratory)

only a thin amount of material in the H and He shells, the star is too cool to burn nuclear fuel and the degenerate C-O core remains as a white dwarf. However, for more massive stars, nucleosynthesis continues in the form of C burning. Once the C is exhausted, leaving a Ne core, stars 8 – 10 $M_{\odot}$ lose their envelopes and become O-Ne-Mg white dwarves.

Only in the most massive stars does nuclear burning continue in the core, first in the form of Ne burning, then as O burning, finally followed by Si burning. The final result of Si burning is an Fe-Ni core with the products of previous burnings stacked around it in an onion-like structure (Figure 1.6) (Meyer et al. 1995). Iron is the most tightly bound nucleus and therefore no energy can be released from the fusion of Fe. With no material left to burn, gravity causes the massive star to collapse in on itself and the star becomes a core-collapse supernova (SN). The inner core of the star collapses subsonically until it reaches nuclear matter density, which causes the collapse to cease and the core to "bounce". However, the outer core collapses supersonically and does not receive the signal from the inner core to halt its collapse, and it instead crashes into the inner core. This creates a shock wave that travels through the star and ejects the layers of material shown in Figure 1.6 into the ISM. During the explosion, heavy elements and neutron-rich isotopes are created by rapidly adding neutrons to Fe seed nuclei in the r-process (Woosley and Weaver 1995). Presolar grains also form during this period, and for additional details on presolar grains from SNe, the reader is referred to Chapter 2, which deals with presolar SiC grains produced in SNe (known as SiC X grains). After the SN explosion, either an extremely dense neutron star or a black hole is left behind.

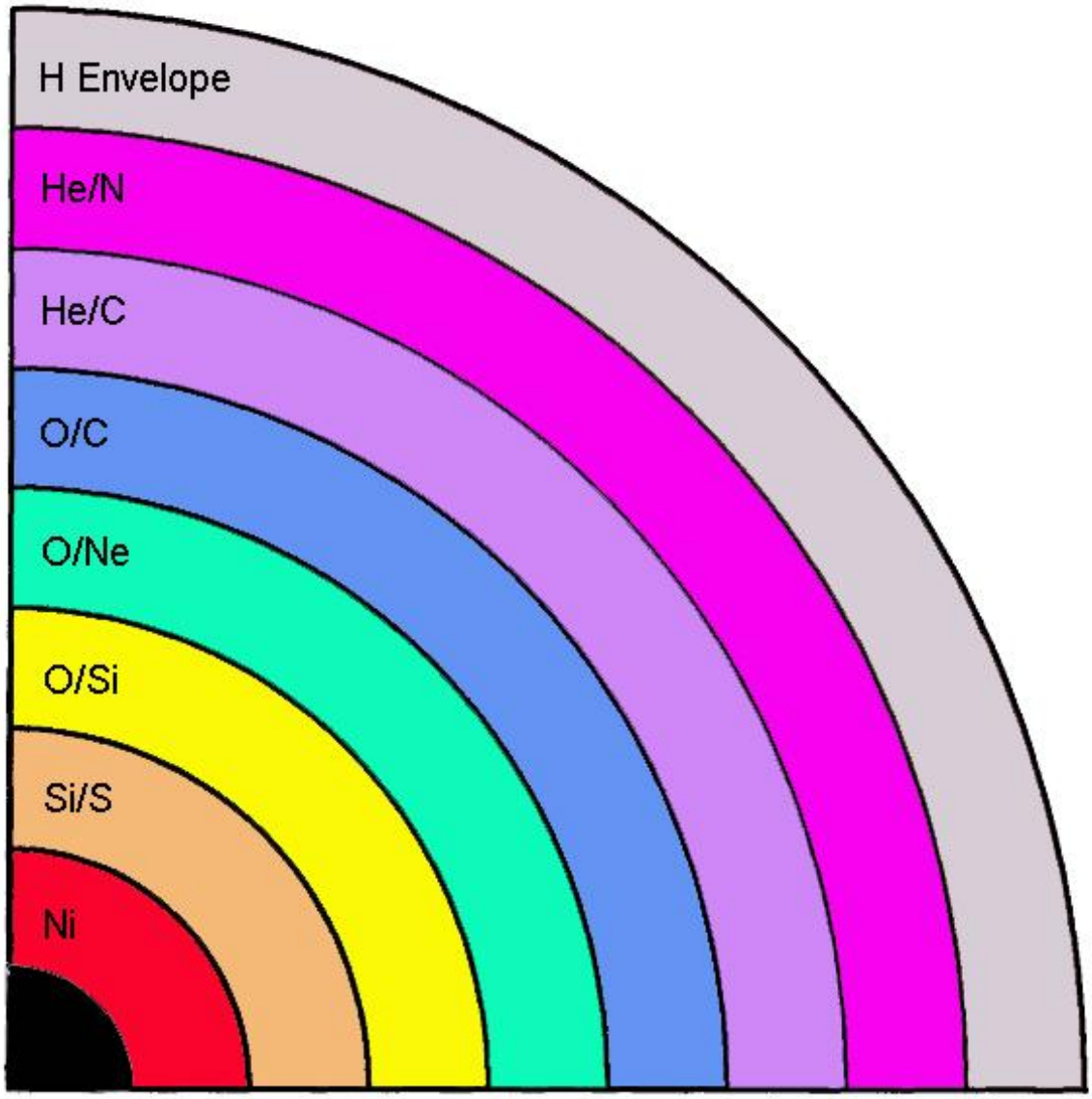


Figure 1.6: Cross-section of the pre-supernova structure of a 25 $M_{\odot}$ star (not to scale). Each zone of the onion-like structure is labeled by the major elements present in that zone. The zones have different isotopic compositions as a result of the nuclear burning the star underwent pre-explosion and from explosive nucleosynthesis during the SN explosion. The black area in the center of the diagram represents the neutron star or black hole remnant left behind after the explosion (Figure from Meyer et al. 1995)

## 1.2 An Introduction to Presolar Grains

The nucleosynthetic processes described above results in dust grains with a wide array of isotopic compositions that are highly dependent upon factors like the mass, metallicity, temperature, pressure, and C/O ratio of the parent star. This means that dust produced by different parent stars, or even by the same star at different times, can have distinctly different isotopic compositions. These dust grains are injected into the ISM, where they are incorporated into dark molecular clouds along with dust produced by other stars. Our SS eventually collapsed from a cloud like this and this material, which eventually formed the sun and planets, was vaporized and homogenously mixed. As a result, the material in the SS, whether the sun, primitive meteorites (the isotopic ratios of these two sources are collectively referred to as "solar" composition), differentiated bodies like the earth, or outer planets like Jupiter, all have nearly the same isotopic compositions, with only very small variations.

Until the 1970s, most people believed that processing in the early SS had homogenized all of the SS material and completely erased all traces of the original stellar isotopic signatures the material once carried. It was not until the discovery of O anomalies in Ca, Al-rich inclusions (CAIs) in 1973 (Clayton et al. 1973) that people believed material from the nascent SS did, in fact, survive. CAIs were the first solids to condense in the SS and they carry isotopic anomalies in many elements; however, it is important to note that they formed from reprocessed SS system material and are therefore not presolar. Additionally, the isotopic anomalies in CAIs are orders of magnitude smaller than those observed in presolar grains. For further information on CAIs, the reader is referred to a review by Becket et al. (2006) and references therein.

Ironically, the first clues that significant isotopic anomalies were preserved from the early SS were largely ignored, although they would eventually lead to the discovery of presolar grains. The discovery of Ne and Xe anomalies in primitive meteorites (Black and Pepin 1969; Reynolds and Turner 1964), as well as the suggestion that these anomalies were nucleosynthetic in origin (Black 1972), were, for the most part, disregarded at the time, largely because trapped noble gases are only a minor constituent of rocks and were not persuasive enough evidence to challenge the view of a homogeneous SS. However, after the discovery of isotopic anomalies in CAIs and the acceptance of a heterogeneous SS, attempts were undertaken to discover the carrier of the noble gas anomalies. A group at the University of Chicago, led by Edward Anders, pioneered a very extensive and systematic series of harsh chemical treatments, along with size and density separates, that were targeted at eliminating all meteoritic material except for the anomalous noble gas carrier(s). This process took more than a decade to develop (Amari et al. 1994), a method dubbed "burning down the haystack to find the needle". Eventually, this process led to the discovery of presolar diamond (Lewis et al. 1987), presolar SiC (Bernatowicz et al. 1987; Zinner et al. 1987), and presolar graphite (Amari et al. 1990).

Since their discovery, presolar grain research has progressed considerably. Additional types of presolar grains have been discovered, including oxides (Huss et al. 1993; Hutcheon et al. 1994; Nittler et al. 1994), $Si_3N_4$ (Nittler et al. 1995), silicates (Nguyen and Zinner 2004), and a host of inclusions within these grains (Bernatowicz et

al. 1991; Bernatowicz et al. 1996; Croat et al. 2003; Croat et al. 2005; e.g., Hynes et al. 2010) (a list of the major types of presolar grains, their abundances, and size ranges are listed in Table 1.1). The presolar origin of these grains is clearly indicated by the significant isotopic anomalies that have been measured in nearly every isotopic system. For example, the variations in the $^{16}O/^{17}O$ and $^{16}O/^{18}O$ ratios of all SS material, including the Sun, Earth, Jupiter, or meteorites, at their most extreme, are only ~5%. In contrast, the isotopic ratios measured in presolar grains are several orders of magnitude different than SS material. The only possible explanation for these large anomalies is that the grains retained the original nucleosynthetic signatures from circumstellar formation; no other known processes, such as radioactivity, fractionation, or cosmic ray exposure, can create anomalies as large as those observed in presolar grains. Furthermore, isotopic measurements on presolar grains of a variety of isotopic systems match theoretical nucleosynthesis predictions (e.g., Lattanzio and Boothroyd 1997; Rauscher et al. 2002), providing further evidence of their circumstellar origin.

Many of these measurements have only become possible with the high spatial resolution and high sensitivity of the NanoSIMS. These measurements, in turn, have provided better constraints on nucleosynthetic models, supplied insights into grain formation and growth conditions around the parent stars, and an enhanced understanding of the chemical evolution of the galaxy. An extensive discussion of several types of SiC grains constitutes the bulk of this thesis, but a more thorough description of the other types of presolar grains, their isotopic anomalies, the techniques employed to measure them, and the importance of these measurements is given in Chapter 4 of this work.

Table 1.1. Summary of abundances, sizes, and origin of various types of presolar phases[a]

| Phase | Abundance (ppm) | Size | Stellar Source(s) |
|---|---|---|---|
| Nanodiamonds | 1400 | 2 nm | SNe |
| Silicates in IDPs[b] | > 375 | 0.2 – 1 μm | RGB, AGB, SNe |
| Silicates in meteorites | > 180 | 0.2 – 0.9 μm | RGB, AGB, SNe |
| Oxides | > 100 | 0.15 – 3 μm | RGB, AGB, SNe |
| SiC mainstream grains | 15 | 0.1 – 40 μm | AGB |
| Graphite | 1 – 2 | 1 – 20 μm | AGB, SNe, born-again AGB? |
| SiC AB grains | 0.2 | 0.1 – 11 μm | J stars, born-again AGB |
| SiC X grains | 0.06 | 0.1 – 30 μm | SNe |
| $Si_3N_4$ | 0.002 | ~1 μm | SNe |
| Carbides (e.g., TiC)[c] | ~0.0003 | ~10 – 200 nm | AGB, SNe |

Notes: [a] Abundances adapted from Zinner (2007).

[b] Interplanetary dust particles (IDPs) are some of the most primitive objects in the SS and can contain presolar grains. For additional information on IDPs, the reader is referred to Bradley (2007).

[c] Found as subgrains within graphite and SiC.

## 1.3 The Work of This Thesis

Over the last two decades, the field of presolar grain research has amassed isotopic data on over twelve-thousand grains, with more data added every year. When used collectively, these data constrain models, suggest trends, or provide a comparison to new data. These data, however, were dispersed in hundreds of papers and abstracts, making such applications difficult, at best. In addition to describing presolar grains in greater detail, Chapter 4 deals with an undertaking to provide presolar grain researchers, and the astrophysical community as a whole, with a comprehensive collection of all the available isotopic data via a Washington University supported website.

However, a far more pressing need in the presolar grain community is for the microstructural analysis of presolar grains with the TEM. Coordinated isotopic and TEM

studies can provide the most complete insights into presolar grains. Isotopic analysis provides valuable information on nucleosynthetic processes and stellar sources. This is complemented by TEM data: crystallographic size and structure give insight into grain formation conditions; chemical composition indicates important trace elements that have been incorporated into the grains and for which NanoSIMS isotopic measurements can later be done; and internal subgrains and their relationship to the surrounding grain provide information on growth conditions, condensation sequences, and temperature and pressure constraints.

While there are almost nine thousand grains with isotopic measurements for SiC alone, there is a severe dearth of TEM analyses of these grains. Prior to the work of this thesis, only one refereed paper on TEM analyses of presolar SiC existed (Daulton et al. 2003). While the work of Daulton et al. provides an excellent characterization of the crystal structure (or polytype) of SiC and particularly on the most abundant type of SiC (known as mainstream grains, which account for > 90% of the total presolar SiC population, by number), the study does not, for the most part, have coordinating isotopic data, nor does it deal at all with the chemical composition or internal subgrains of SiC.

In an attempt to expand the number of SiC grains analyzed in the TEM, the main work of this thesis is the microanalysis, including the determination of the polytype, crystal size, chemical composition, and internal subgrains, of two of the minor types of presolar SiC, both of which have unusual origins. Chapter 2 deals with X grains (~1% of the total presolar SiC population), which originate in SN outflows and Chapter 3 deals with AB grains (~5% of the population), which have a somewhat uncertain origin, but are believed to originate from both J-type stars and from born-again AGB stars (see pages 74

– 77 of this work for an introduction to these types of stars). Seven X grains and, coincidentally, seven AB grains were analyzed in the TEM and the details about the properties of X and AB grains, their stellar sources, the specific methods used to analyze the grains, the results of TEM analyses, and the implications of these findings are described in detail in their respective chapters.

In addition to the work presented in Chapter 2, 3, and 4, I have been involved in several minor projects and collaborations on various aspects of presolar grain research not directly related to the work presented in the main body of this thesis. A brief description of some of these projects is presented in the Appendix.

# Chapter 2

# A Microanalytical Study of SiC X Grains

"When, according to my habit, I was contemplating the stars in a clear sky, I noticed that a new and unusual star, surpassing all others in brilliancy, was shining almost directly over my head…I was so astonished at this sight that I was not ashamed to doubt the trustworthiness of my own eyes."

~Tycho Brahe, on his discovery of SN 1572, from *De Nova Stella*

## 2.1 Introduction

Isotopic studies of presolar grains provide important information about stellar nucleosynthesis at an unprecedented level of detail (see Meyer and Zinner 2006). In addition, chemical, structural, and mineralogical microanalysis can offer valuable insights into grain formation in circumstellar outflows and SNe ejecta (see Bernatowicz et al. 2006). Laboratory studies indicate that the microstructural characteristics of presolar SiC grains are dependent upon the physical conditions, such as temperature and pressure, in which they condense. Detailed morphological studies on presolar SiC therefore provide important information for understanding the conditions in which these grains form at a level of detail that cannot be obtained through astronomical observation alone (Croat et al. 2005; Daulton et al. 2003).

For the most complete constraints on presolar grain formation, detailed structural and chemical microanalytical studies can be combined with isotopic measurements. An example of this analytical approach is the study by Croat et al. (2003) of ultramicrotomed sections of SN graphite grains from the Murchison meteorite. Isotopic characterization with the NanoSIMS revealed large excesses in $^{18}O$ and $^{28}Si$, indicating a SN origin. Microanalysis of the same presolar graphite sections with a TEM revealed the presence of internal TiC subgrains, which NanoSIMS analysis subsequently confirmed to be of presolar origin based on large Ti isotopic anomalies. These internal subgrains were found in all of the SN graphite grains studied, with a single graphite grain containing up to several hundred TiC subgrains. Some of these internal TiC subgrains have attached iron-nickel grains epitaxially grown onto one or more of the TiC faces. Further analysis of the chemistry, morphology, and crystallography of the SN graphite grains and their internal subgrains allowed inferences to be drawn concerning the physical conditions of the gas from which these graphite grains condensed. For example, grain morphology indicates the condensation sequence, with TiC condensing first, followed by the iron-nickel phases, and finally graphite. This sequence places bounds on the temperature and pressure of the gas in which these grains condensed. Additionally, the properties of the TiC subgrains were used to determine the minimum Ti number densities in the gas before condensation and suggest that turbulent mixing must have occurred in the SN outflows prior to TiC incorporation in the graphite.

In addition to the information learned from studying SN graphite grains, further understanding of SN outflows can be gained by studying another type of presolar grain with a SN origin, SiC X grains (Amari et al. 1992). While ≳95% of presolar SiC grains

originate in the outflows of AGB stars, X grains comprise only ~1% of all presolar SiC grains. The primary indicator of a SN origin for SiC X grains is large excesses of $^{28}$Si, which can only be produced deep within the interiors of massive stars (see Meyer and Zinner 2006). Most X grains are also characterized by isotopically light C ($^{12}$C/$^{13}$C > Solar = 89) and isotopically heavy N ($^{14}$N/$^{15}$N < Solar = 272), both of which are the result of nucleosynthesis in massive stars. These isotopic compositions are distinct from those of grains originating around AGB stars, so-called mainstream grains, which constitute most of the presolar SiC population ($^{29}$Si/$^{28}$Si, $^{30}$Si/$^{28}$Si, $^{14}$N/$^{15}$N > Solar; 10 < $^{12}$C/$^{13}$C < 100) (see Meyer and Zinner 2006). Some X grains also contain radiogenic isotopes from nuclides that are only produced in SNe, such as $^{44}$Ca from the decay of $^{44}$Ti (Nittler et al. 1996) and $^{49}$Ti from the decay of $^{49}$V (Hoppe and Besmehn 2002).

Unlike presolar graphite, which has only one basic crystal structure that occurs in varying degrees of structural perfection, SiC has ~250 crystal structures, or polytypes, which depend on the particular repetitive stacking sequence of Si-C bilayers (Kern et al. 1998). Most of these polytypes have only been produced in laboratories and only a few have ever been observed in nature. SiC polytypes are sometimes grouped into two categories: the unique cubic 3C polytype (also called β-SiC) and the hexagonal and rhombohedral polytypes (all the others collectively called α-SiC). For a thorough discussion of SiC polytypes, see Daulton et al. (2003).

Because the formation of particular presolar SiC polytypes is determined by the physical conditions of the stellar outflows in which the grains condense, knowledge of the microstructure of presolar SiC can provide valuable insight into formation conditions. Astronomical data are of limited use in this regard, however. Infrared spectra can, at

most, distinguish between the α-SiC and β-SiC polytypes and even the ability to make this distinction is subject to controversy (Speck et al. 1999). However, SiC polytypes can be distinguished from one another in the TEM. Utilizing analytical and high-resolution TEM to determine the polytypes of 508 randomly selected Murchison presolar SiC grains (500 nm average size), Daulton et al. (2003) observed only two polytypes: the cubic 3C (fcc; a = 4.36 Å) polytype (~79% by number) and the hexagonal 2H (a = 3.08 Å, c = 5.03 Å) polytype (~3%), as well as intergrowths of these two polytypes (~17%). Most of these SiC grains are single crystals, while the rest are twinned. A small number (~1%) of one-dimensionally disordered SiC grains could not be classified as any polytype. Because >90% of Murchison SiC grains are mainstream grains and because coordinated isotopic data have been obtained for only a small number of these SiC grains (Daulton et al. 2006), to first order, this polytype distribution largely represents mainstream SiC grains, which formed around AGB stars.

Laboratory studies of SiC growth show that the 2H polytype has the smallest unit cell and generally the lowest formation temperature, followed by 3C, and then by the higher-order rhombohedral and hexagonal polytypes. The temperatures at which the 2H and 3C polytypes form and remain stable in laboratory experiments are roughly consistent with theoretical equilibrium thermodynamics predictions for the circumstellar outflows of AGB stars (Lodders and Fegley 1995; Sharp and Wasserburg 1995). However, the higher number densities in SN outflows could conceivably result in the formation of higher-order polytypes in some SiC X grains, which may not have been observed by Daulton et al. due to the small number of X grains encountered in their study (presumably ~1% of the total).

While the polytype distribution of mainstream grains is well understood, very little is known about the microstructure of the minor types of presolar SiC, including X grains. Only one morphological study has previously been done on SiC X grains. Utilizing a focused ion beam (FIB) lift-out, Stroud et al. (2004) analyzed two X grains with the TEM. One grain is the 3C polytype, while the other is the 2H polytype. No higher-order polytypes were observed. Although several previous presolar SiC microanalytical studies (Bernatowicz et al. 1992; Stroud et al. 2002; Stroud and Bernatowicz 2005; R. Stroud, pers. comm.) have observed internal (Ti,V)C, AlN, Fe, Fe-Ni, and graphite subgrains in presolar SiC, all of these grains (three mainstream grains and one Z grain) originated in the outflows of AGB stars. In the Stroud et al. (2004) X grain study, no subgrains were found.

In this study, we present a coordinated TEM and NanoSIMS study of seven SiC X grains from the Murchison CM2 meteorite. These grains were selected on the basis of their isotopic compositions, namely large $^{28}$Si excesses, which were determined by NanoSIMS analysis. The seven X grains were then analyzed in the TEM for their chemical composition and structural characteristics, including polytype, crystal domain size, and subgrains. Two mainstream grains from the same size fraction as the X grains were also selected for TEM analysis to provide a basis for comparison with the X grains. The combined microstructural, isotopic, mineralogical, and chemical data on these X grains yield insights into the formation of SiC grains in SN outflows.

## 2.2 Experimental Methods

### 2.2.1 Isotopic Characterization

Silicon carbide grains were obtained from the KJG size separate (2.1 – 4.5 μm observed size) of the Murchison meteorite (Amari et al. 1994). An aggregate of grains was dropped onto a Au foil and subsequently analyzed for Si isotopes in a Cameca IMS 3f ion microprobe utilizing ion imaging to locate potential X grains (Amari et al. 2000). Because the IMS 3f has relatively low sensitivity, grains that had $^{28}Si/^{30}Si$ ratios greater than the solar value (29.75) were subsequently analyzed in a Cameca NanoSIMS with high mass resolution and high sensitivity to verify their grain type. Negative secondary ions of C, Si, and in some cases CN (for the N isotopes) were measured with a $Cs^+$ beam. No additional isotopes were measured with the NanoSIMS in order to minimize grain sputtering and to preserve as much of the grain as possible for subsequent analysis in the TEM. Mainstream SiC grains, also from the KJG size fraction of the Murchison meteorite, were similarly analyzed in the NanoSIMS for their C, Si, and N isotopic compositions.

### 2.2.2 TEM Sample Preparation and Characterization

After isotopic characterization, the grains were imaged in a JEOL 840A SEM to locate their positions on the grain mount. Seven SiC X grains and two mainstream grains were subsequently selected for study in the TEM. Each of the selected grains was picked from the ion probe mount with a sharpened tungsten needle held in a micromanipulator. The tip of the needle was kept clean and at a diameter of ~1 μm by electrochemically

sharpening the needle with a solution of sodium hydroxide. Utilizing an optical microscope to view the process, each SiC grain was placed at the bottom of a gelatin capsule, along with three carbon fibers to later aid in locating the grain. The capsule was slowly filled with LR White Hard resin and cured at 60º C for 24 hours. The gelatin capsule was then removed, leaving the SiC grain and the carbon markers embedded in the resin block. The top of the resin block was trimmed into a multi-step pyramid with a Reichert-Jung Ultracut E microtome equipped with a glass knife, with the top step having a side-length of ~0.5 mm and containing the SiC grain and the carbon markers. The top step was then sliced with the ultramicrotome fitted with a diamond knife attached to a water reservoir. The 70-nm-thick slices of SiC and the surrounding resin were removed from the water's surface with Pella 3 mm, 75 mesh Cu TEM grids covered with Formvar stabilized with carbon.

The microstructure and chemical composition of the SiC and their internal grains were determined with a JEOL 2000FX TEM equipped with a NORAN Vantage energy-dispersive X-ray spectrometer (EDXS). The Novar window of the EDXS allows identification of all elements with $Z \geq 5$. Background and peak fitting were performed on these spectra with Origin-based in-house software, described by Croat et al. (2003). In cases where elemental peaks (such as Al or Mg) were not detected, an upper limit of $2\sigma$ of the background counts in the energy region of interest was placed on their concentrations. Quantitative analyses were performed with k-factors for Al, Si, and Mg determined from a geologic standard (basaltic glass USNM 113498).

The polytype was determined for each SiC grain utilizing both selected-area diffraction (SAD) and convergent-beam electron-diffraction (CBED) patterns. Low-

index zones were located by tilting the crystals along both orthogonal axes of the sample stage goniometer. The diffraction patterns were subsequently analyzed to determine the polytype of each crystal.

Since inclusions of other phases contained within the SiC X grains were of interest, each slice was observed at high magnification (~$10^5$x) while the crystal was systematically rotated through ±30º about one axis of the sample stage goniometer. Diffraction contrast was used to identify candidate internal grains and their compositions were subsequently determined with EDXS. Once located, the grains were rotated to low index crystallographic zones from which CBED patterns were obtained. The known d-spacings of the surrounding SiC were used as a calibration standard for the d-spacings of internal grains. Utilizing this as the primary method of detection, internal grains as small as ~15 nm could be identified.

## 2.3 Results

### 2.3.1 Isotopic Composition

Isotopic measurements on all X grains and mainstream grains, made prior to TEM analysis, are reported in Table 2.1. The large excesses in $^{28}$Si relative to normal SS ratios clearly identify seven of the grains as X grains. In addition, they are all more depleted in $^{30}$Si than in $^{29}$Si and lie near the line of slope 0.6 defined by most X grains on a $\delta^{29}$Si/$^{28}$Si versus $\delta^{30}$Si/$^{28}$Si three isotope plot (Figure 2.1). These are the type X1 grains defined by Lin et al. (2002), as opposed to X2 grains which have relatively larger $^{29}$Si depletions. Most X grains plot well above the mixing line of slope 1 between solar system Si

Table 2.1. Isotopic compositions of SiC mainstream and X grains in this study (±1 σ errors).

| Grain label | Type | $^{12}C/^{13}C$ | $^{14}N/^{15}N$ | $\delta^{29}Si/^{28}Si^a$ (‰) | $\delta^{30}Si/^{28}Si^a$ (‰) |
|---|---|---|---|---|---|
| KJG-N2-31-1 | X | 250 ± 4 | | -309 ± 4 | -436 ± 5 |
| KJG-N2-129-1 | X | 111 ± 1 | | -187 ± 5 | -329 ± 6 |
| KJG-N2-253-2 | X | 162 ± 2 | | -231 ± 5 | -396± 6 |
| KJG-N2-411-2 | X | 216 ± 3 | | -298 ± 5 | -422 ± 6 |
| KJG-N4-185-1 | X | 127 ± 0.5 | 144 ± 1 | -296 ± 3 | -384 ± 4 |
| KJG-N4-263-1 | X | 156 ± 0.6 | 91 ± 1 | -249 ± 2 | -384 ± 3 |
| KJG-N4-585-2 | X | 409 ± 2 | 49 ± 0.5 | -310 ± 3 | -495 ± 4 |
| KJG-N4-439-2 | Mainstream | 47 ± 0.2 | 1818 ± 72 | 79 ± 3 | 70 ± 4 |
| KJG-N4-595-1 | Mainstream | 66 ± 0.2 | 2535 ± 80 | 12 ± 3 | 22 ± 4 |

Notes: [a] Values given in "delta" notation, defined as: $\delta^iX/^jX \equiv [(^iX/^jX)_{measured}/(^iX/^jX)_\odot - 1] \times 1000$.

($\delta^iSi/^{28}Si \equiv 0$) and pure $^{28}Si$ ($\delta^iSi/^{28}Si \equiv -1000$) (Nittler et al. 1995). The seven X grains from this study are enriched in $^{12}C$ and the three that were measured for their N isotopic compositions also have $^{15}N$ enrichments (Figure 2.2), which is typical of SiC X grains (Amari et al. 1992).

The two mainstream grains show enrichments in $^{13}C$, $^{14}N$, and $^{29,30}Si$ relative to the solar values, which are all indications of an AGB origin (Hoppe et al. 1994). Both the X grains and the mainstream grains in this study were selected as typical isotopic representatives of their respective grain types in order to make inferences about these grain populations, albeit from a limited sample size.

### 2.3.2 Chemical Composition

After isotopic analysis in the NanoSIMS and ultramicrotomy, sections of each grain were analyzed in the TEM. An EDXS spectrum was acquired at several spots on

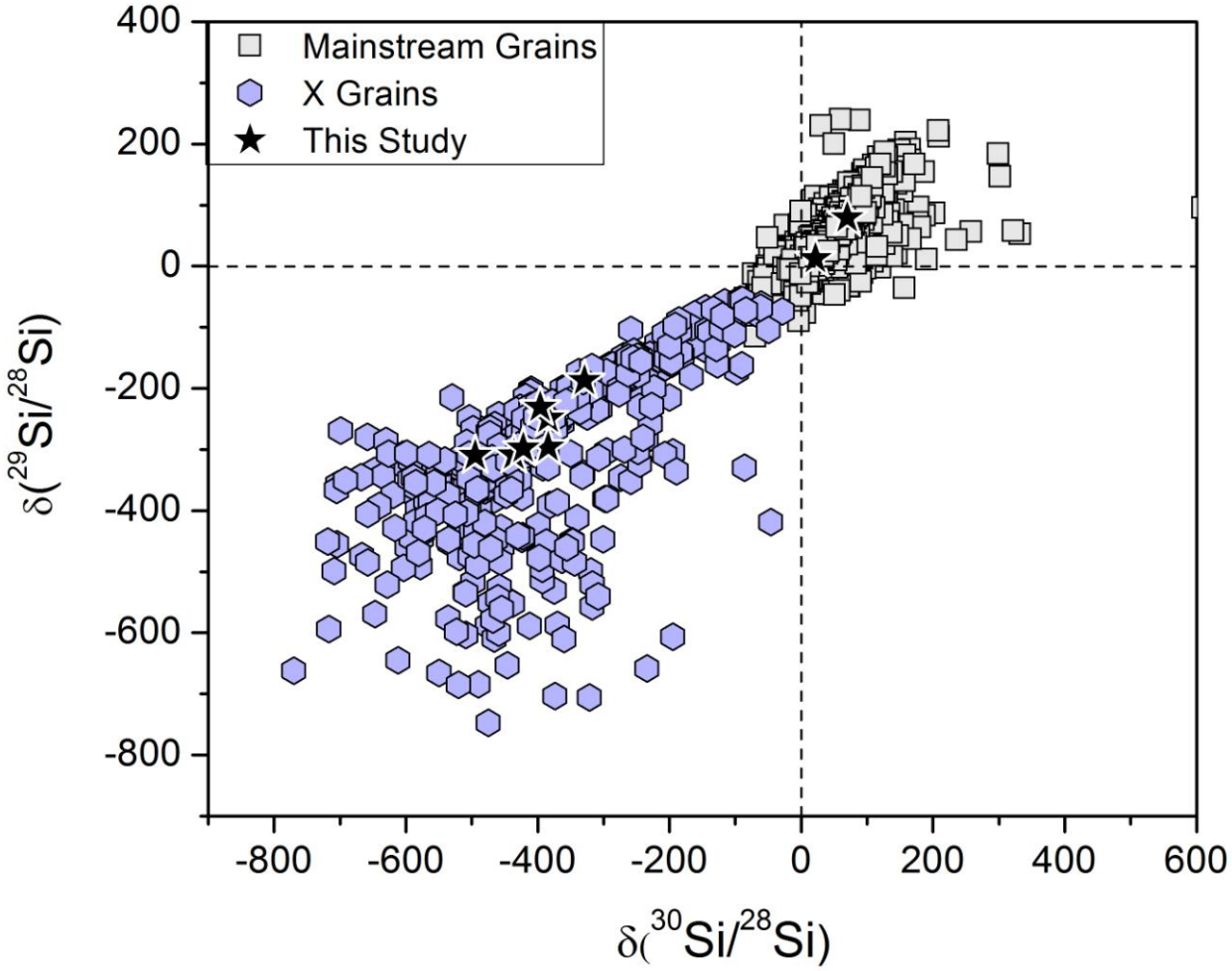


Figure 2.1: Plot of the Si isotopic ratios of the seven X grains and two mainstream grains in this study expressed as δ-values, or deviations from the solar isotopic ratio in parts per thousand (‰). The grains are plotted against isotopic data from other X grains and mainstream grains for comparison [grain data are from the Presolar Database (Hynes et al. 2009)].

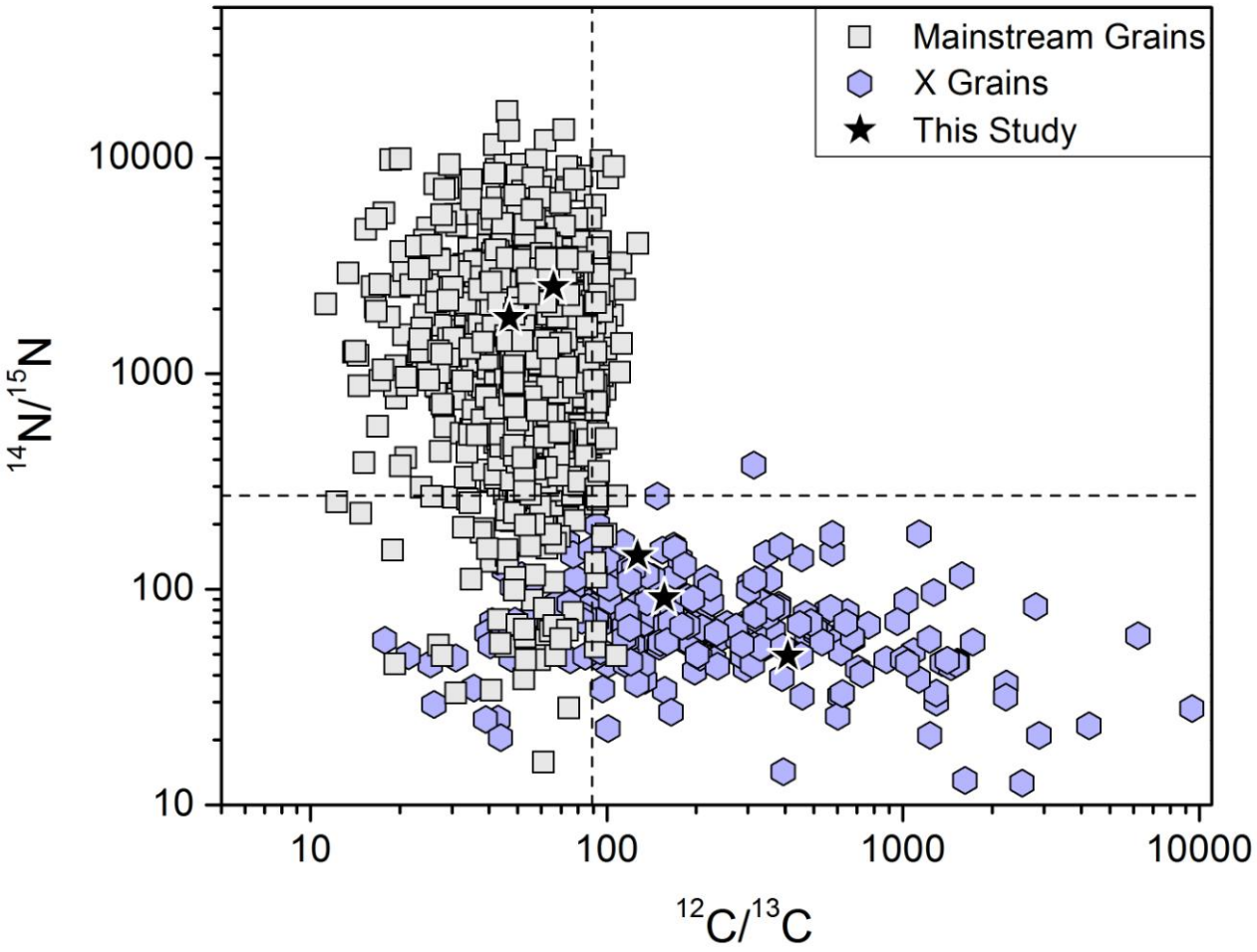


Figure 2.2: Plot of the C and N isotopic ratios of three X grains and both mainstream grains from this study; N isotopic data are not available for the other grains. As in Figure 1, the grains are plotted against isotopic data from other X grains and mainstream grains for comparison. Although there is growing evidence that the true $^{14}N/^{15}N$ ratio of the sun may be closer to that of Jupiter [$^{14}N/^{15}N$ = 448 (Abbas et al. 2004)] and the value of $^{14}N/^{15}N$ = 272 is more correctly the terrestrial value, in order to maintain continuity with earlier presolar grain research and models, the "solar" $^{14}N/^{15}N$ ratio will refer to the value of 272 throughout this thesis. For additional reading on the subject of $^{14}N/^{15}N$ ratios in the sun, the reader is referred to Marty et al. (2010).

each grain and for the grain as a whole. As expected, the spectra revealed mainly Si and C. Due to the large C background signal from the Formvar substrate and embedding resin, C is excluded from all elemental quantifications that follow.

Most of the SiC X grains (5 of 7) also contain minor amounts of both Al and Mg, ranging from 1.3 – 6.5 and 0.6 – 5.0 atomic % (at%), respectively (Table 2.2). In contrast, both mainstream grains show Al (1.7 and 1.5 average at%), but no detectable Mg, implying upper limits of 0.08 and 0.18 at%, respectively. Some variation in the Al signal occurs across the mainstream grains, ranging from undetectable to 2.0 at%. No separate crystals of Al-bearing phases were detected, suggesting that the Al is heterogeneously distributed in solid solution, possibly in the form of AlN, which is isostructural to SiC. The Mg/Al ratios for the X grains range from 0.43 – 0.74. Relatively high Mg/Al ratios are commonly observed in SiC X grains (Nittler et al. 1995), as discussed in detail later (see section 2.4.1). Of the two remaining X grains in this study, one contains no measurable Al or Mg, with upper limits of 0.7 and 0.2 at%, respectively, and the other grain contains measurable amounts of Al (1.3 at%), but no Mg. Both Al and Mg (when present) appear to be uniformly distributed within the X grains, although minor spot-to-spot variations of ~0.2% are observed. No other trace elements were observed in the grains.

### 2.3.3 Grain Morphology and Crystal Domain Size

SiC is one of the hardest naturally occurring materials, so it tends to shatter when ultramicrotomed with a diamond knife. The breakage can be seen by comparing SEM

Table 2.2. EDXS measurements of Al and Mg elemental content of presolar SiC grains.

| Grain label | Type | Atomic % Al | Atomic % Mg | Mg/Al |
|---|---|---|---|---|
| KJG-N2-31-1 | X | < 0.7 | < 0.2 | |
| KJG-N2-129-1 | X | 3.4 | 2.1 | 0.63 ± 0.05 |
| KJG-N2-253-2 | X | 1.4 | 0.6 | 0.43 ± 0.11 |
| KJG-N2-411-2 | X | 2.8 | 2.0 | 0.71 ± 0.08 |
| KJG-N4-185-1 | X | 6.5 | 5.0 | 0.74 ± 0.04 |
| KJG-N4-263-1 | X | 1.3 | < 0.15 | < 0.12 |
| KJG-N4-585-2 | X | 2.0 | 1.3 | 0.66 ± 0.05 |
| KJG-N4-439-2 | Mainstream | 1.7 | < 0.08 | < 0.05 |
| KJG-N4-595-1 | Mainstream | 1.5 | < 0.18 | < 0.12 |

Notes: Atomic % for Al and Mg are quantified for a grain assumed to be composed of only of Si, Al, and Mg. Carbon values are not quantified or included due to large background interferences from the grid substrate. Grain KJG-N2-31-1 is an intergrowth between the 3C-SiC and 2H-SiC polytypes; all other grains are the 3C-SiC polytype.

(Figure 2.3a) and TEM (Figure 2.3b) images of the same grain. Despite this, ultramicrotomy does have the advantage of producing multiple slices for study, which

sample the entire volume of the grain. In Figure 2.3, the smaller diameter of the TEM slice compared to the whole grain is mainly due to sampling the grain off-center, although some material is also lost during slicing.

Each SiC X grain is observed to be an aggregate of many smaller SiC crystals. Although ultramicrotomy causes the SiC to have a fragmented appearance, it does not affect our ability to determine the crystal domain size or structure. Multiple crystal domains are observed within each fragment of an X grain slice. Since the crystal domains are smaller than the fragments, the fracturing during ultramicrotomy does not result in an artificially small estimate of domain size. Six of the X grains are composed of crystals of similar size (Figure 2.4a, b). Most of the domains are in the size range of

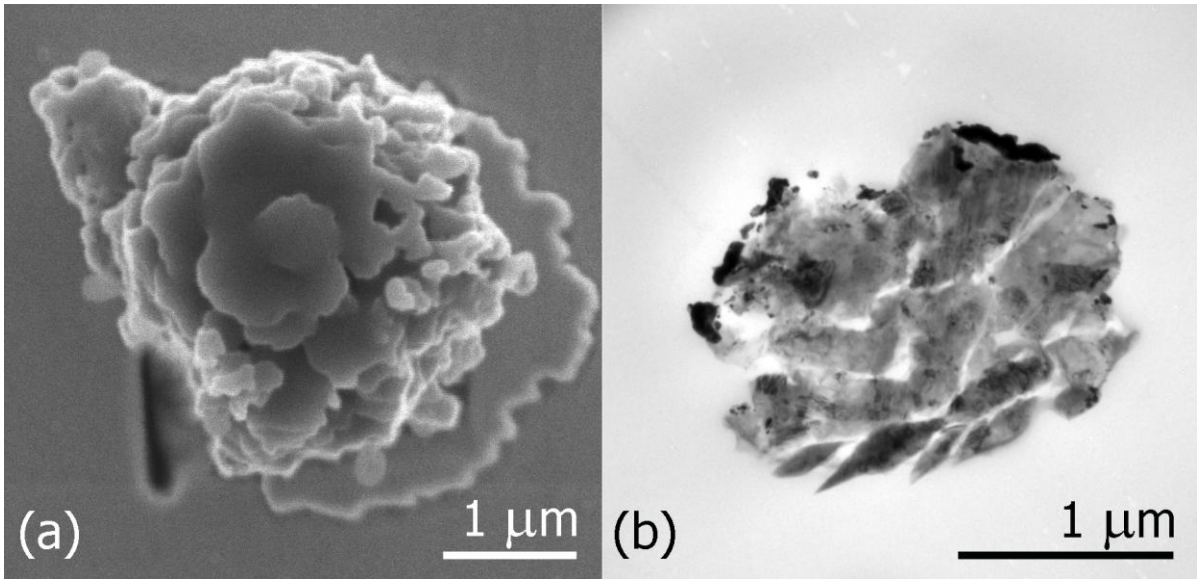


Figure 2.3: (a) SEM image of SiC X grain KJG-N4-585-2 after NanoSIMS analysis, but before slicing with the diamond ultramicrotome. (b) Typical example of a grain after slicing. This bright-field (BF) TEM image shows one 70-nm-thick slice of the same grain pictured in (a). Although it has a broken appearance due to the slicing process, crystallographic properties are unaffected. Individual crystals are visible within the grain due to diffraction contrast and the black areas at the top edge of the slice are Au deposited during NanoSIMS analysis.

~100 – 200 nm, although each grain contained a few crystals that were larger than this range, as well as some smaller crystals. The total range in crystal size for these six grains is 56 – 457 nm, with a median geometric crystal diameter of 140 nm. A similar crystal domain size was observed by Stroud et al. (2004) in one of the two X grains they analyzed. The other X grain in this study (KJG-N4-185-1) had a much finer-grained appearance (Figure 2.4c, d). This grain is composed of much smaller crystals than the other X grains, with crystal domains that range from 24 – 135 nm, and a median diameter of 51 nm. Despite its different crystal domain size, the isotopic and elemental compositions of this grain are typical for X grains and not significantly different from the other X grains in this study. The second grain in the Stroud et al. (2004) study has smaller crystal domain sizes (~10 nm crystals) than any of the X grains observed in this study.

Most previous TEM work on mainstream SiC has been done on relatively small grains (Daulton et al. 2003) that are 180 – 390 nm in diameter and are primarily composed of single crystals (66.4% of the population), although at least one grain larger than 1 μm has also been observed to be a single crystal (Stroud et al. 2005). Because the bulk of previously analyzed presolar SiC grains are much smaller than the ~3 μm SiC X grains analyzed in this study, interpretation of the differences in crystal domain sizes between studies is problematic. Moreover, both trace element abundances (Amari et al. 1995) and the abundance of SiC grains from different types of stellar sources (Hoppe et al. 1996; Zinner et al. 2007) have been observed to vary systematically with grain size. Therefore, the observed differences in crystal domain sizes between the X grains in this study and the mainstream grains in the Daulton et al. (2003) study could be the result of

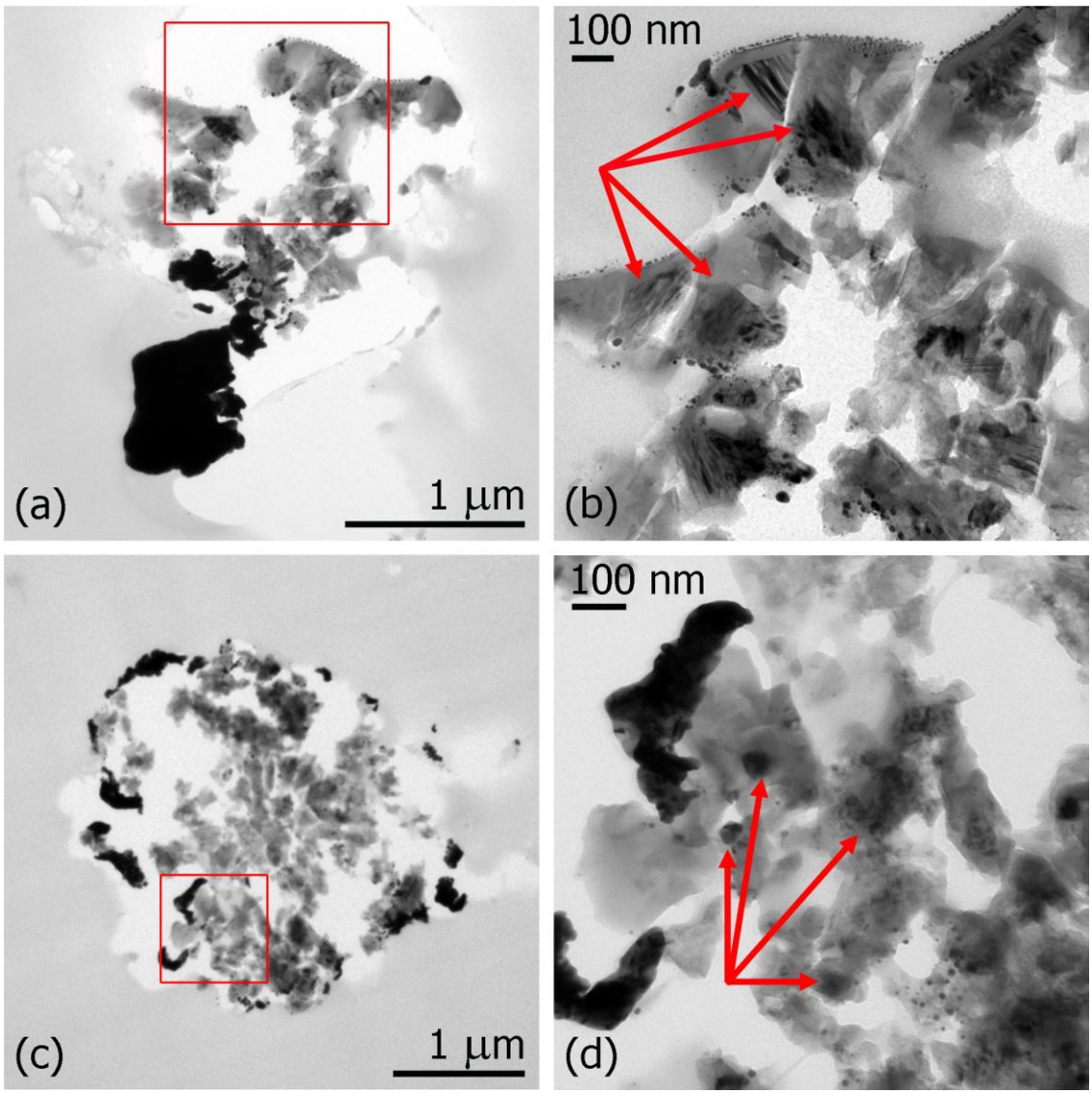


Figure 2.4: TEM BF images of SiC X grains and their crystal domain sizes. (a) The crystal domains (140 nm median diameter) observed in SiC X grain KJG-N2-411-2 are typical of six of the seven X grains. (b) Individual crystal domains (examples indicated by arrows) are visible within the broken fragments of the grain in this magnified view (shown at $10^5$ x magnification) of the area indicated by a box in (a). Intensity variations between domains are due to orientation-dependent diffraction contrast. (c) Grain KJG-N4-185-1 is composed of much smaller crystal domains (51 nm median diameter) than the other X grains. The smaller crystal domain size is visible in this image of the entire slice. (d) Magnified view (at $1.2 \times 10^5$ x magnification) of the area indicated by a box in (c) showing individual crystal domains (examples indicated by arrows).

analyzing two different SiC size fractions and not a result of the different stellar formation environments of mainstream SiC and X grains (AGB stars and SN outflows, respectively).

To facilitate a direct comparison with the X grains in this study, mainstream SiC grains from the same Murchison size fraction (KJG) as the X grains were analyzed for their crystal domain size and structure. The mainstream grains are also broken into several pieces as a result of ultramicrotomy, but unlike the X grains, no small crystals are visible within the fragments. To determine if each fragment is a separate crystal domain or if it is part of a larger crystal that had been shattered during slicing, a CBED pattern was obtained from a low index zone of one of the grain fragments. The grain was then tilted over an ~5º range around both axes of the sample stage goniometer to locate a nearby zone axis for each adjacent fragment. In this way, a CBED pattern was obtained for each fragment of the grain. The diffraction patterns were then analyzed to determine the polytype and crystal orientation of each fragment. Ideally, if the grain were a single crystal, at any given goniometer angle each fragment would be at the same crystallographic orientation. In reality, some minor displacement and rotation of the fragments occurs during ultramicrotomy, resulting in adjacent fragments having the same zone axis located at slightly different goniometer angles (a few degrees apart).

An example of this analysis is shown in Figure 2.5, in which all of the fragments in mainstream grain KJG-N4-595-1 were indexed to either the [-112], [011], or [013] zone axes (of the 3C-SiC polytype), all found within ~8º of one another. In a single crystal, the angles of separation between <112> and <011>, <112> and <013>, and <011> and <013> zones are never less than 30°, 25.4°, and 26.6°, respectively. Since the

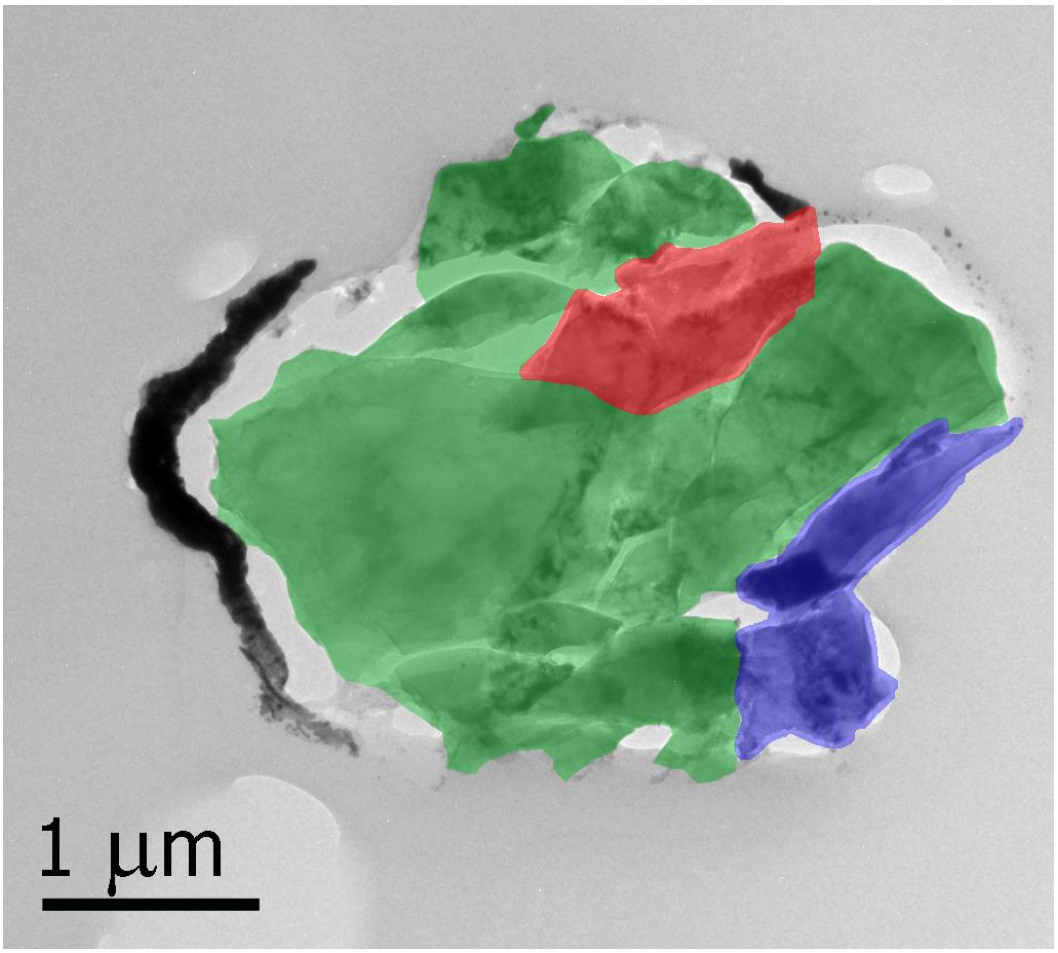


Figure 2.5: TEM BF image of mainstream grain KJG-N4-595-1. Although the grains were broken into several pieces, the mainstream grains were actually composed of only 2 – 3 crystals. The three crystal domains observed in the grain are indicated by the different colors; the blue and red colored areas show the two smaller crystal domains and the remaining green part of the grain is the larger third domain.

zones in this grain are observed with smaller relative rotations (≤ 8°), the SiC grain in Figure 2.5 must therefore be comprised of three separate crystal domains.

Utilizing this method, it was determined that both mainstream grains are composed of only a few large crystals. Grain KJG-N4-439-2 contains two crystal domains and the other, described above, contains three crystal domains. The crystal domains range in size from 0.5 – 1.7 μm. Because some material was probably lost during slicing, this is a lower limit on the domain size of these grains.

### 2.3.4 Polytype Identification of KJG SiC Grains

The crystal structure was determined for each SiC grain, mainly with CBED patterns. Kikuchi bands were observed while tilting around both axes of the sample stage goniometer and used as a guide to locate low-index zones. In this way, several zone axes were located for each of the crystal domains analyzed. The <011> zones were used primarily for 3C-SiC polytype identification since these zone diffraction patterns are distinct from any formed by hexagonal or rhombohedral polytypes.

Due to the small crystal size of each SiC X grain (140 nm median crystal domain size for six grains, 51 nm for one grain), it is extremely difficult to analyze every crystal domain within each SiC X grain. Therefore, between five and eleven crystal domains were randomly selected from each grain for analysis for most of the grains. Unfortunately, only three crystal domains were available to be analyzed for two of the grains: one of which had only a limited area available for analysis and one in which the grid support failed. All but one of the crystal domains analyzed are the 3C polytype (see below). This is the most commonly observed polytype in mainstream grains (79.4% by

number) (Daulton et al. 2003) and was also previously observed in one X grain (Stroud et al. 2004b).

Polytype identification of many of these crystals was complicated by the presence of additional diffraction spots in <011> zones, indicating twinning. In the Daulton et al. (2003) study, the one third of SiC grains that are not single crystals are twinned. Twinning is the most common type of grain boundary in many cubic materials (see Daulton et al. 2003). It occurs across close-packed tetrahedral planes when a stacking fault suddenly reverses the stacking sequence of the SiC crystal and creates a mirror image of itself. A first-order coherent twin boundary is formed for a <011> zone when a stacking fault creates a rotation of 70.53º (plus an additional 180º to align the C-Si bonds) around an axis perpendicular to a {111} plane. Because bond lengths and angles are not changed, a low-energy interface results (Miura et al. 1990). All twinned crystals in this study and more than 95% of the twinned grains in the Daulton et al. study were of this type (the remaining ~5% in the Daulton et al. (2003) study were higher-order twins, which can result from rotations around axes perpendicular to {011} planes). First-order twinning is observable in a <011> diffraction pattern as a dimmer extra spot located at an interval of ⅓ along the spots caused by one {111} plane (Figure 2.6b). This additional spot is caused by an extra reflection that arises from plural scattering from the twinned domain, which also normally contains less material than the matrix, and thus has a lesser intensity (Bender et al. 1986). Although the crystal has four unique {111} planes, twinning is only resolvable in <011> zones along the two planes with interfaces parallel to the electron beam (for a more extended discussion, see Bender et al. 1986).

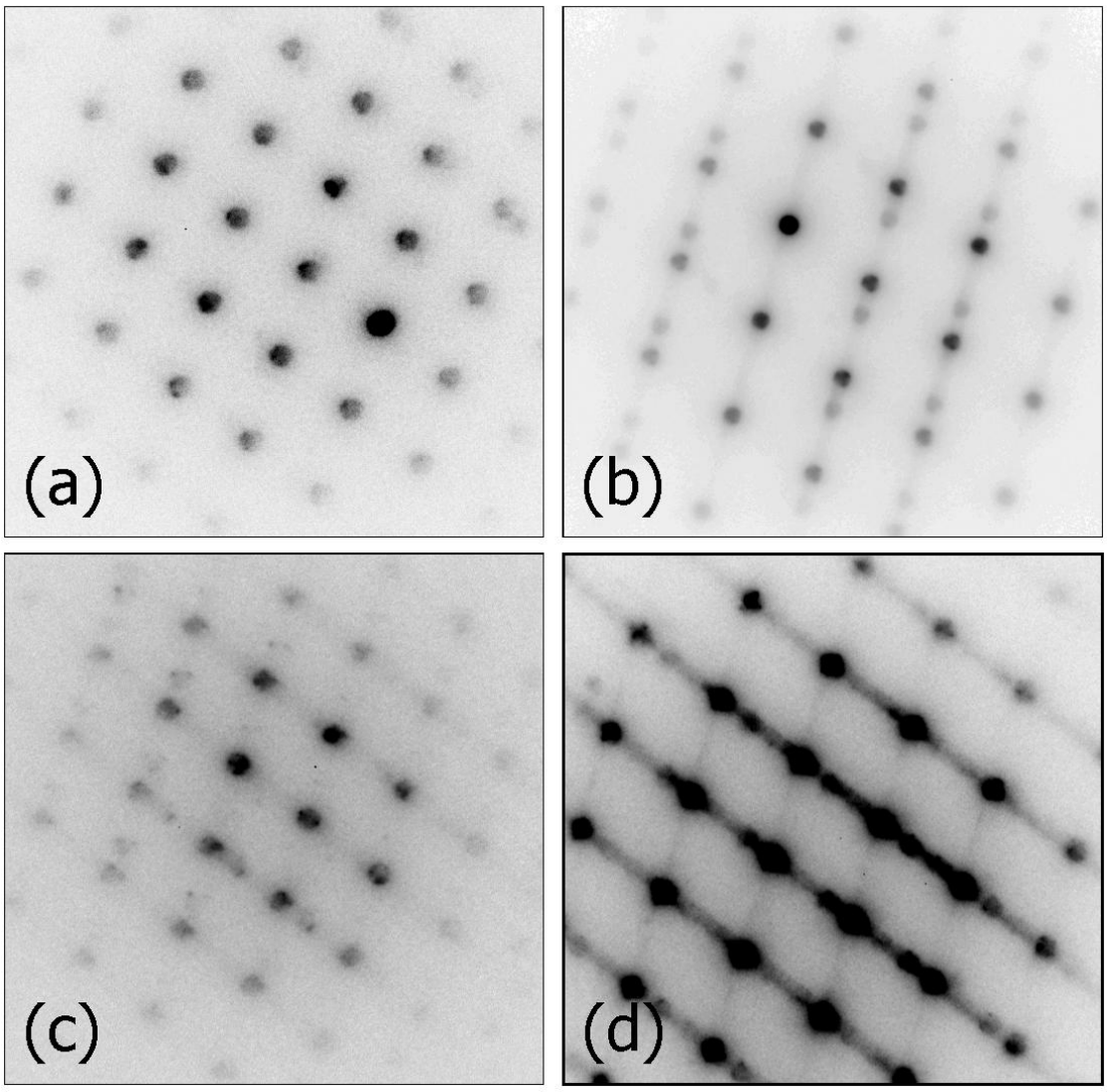


Figure 2.6: Diffraction patterns of [011] zones showing examples of twinning along the {111} plane in SiC X grains (b-d) and an untwinned [011] diffraction pattern from a crystal domain in KJG-N4-585-2 for comparison (a). (b) Extra spots are visible at intervals of ⅓ in this diffraction pattern from a crystal domain in KJG-N2-253-2, indicating a twin boundary. Twinning was observed in ~33% of SiC X grains. (c) Extra diffraction spots are visible at intervals of ⅓ in two directions when a crystal is twinned along both possible {111} planes, as is the case for this crystal domain in KJG-N4-585-2. (d) Streaking can also occur along twinned {111} planes, as seen in this pattern from KJG-N2-129-1.

In this study, six of seven X grains show first-order twinning along one of the sets of {111} planes. It is possible that the seventh X grain (KJG-N4-263-1) was also composed of twinned crystals, but none were observed, probably due to the small number of crystal domains available for study in this grain. Approximately one-third of the crystals analyzed are twinned, but this is clearly a lower limit since only two of four unique {111} planes that could potentially show twinning lie within the tilt limits of the TEM goniometer. To confirm the twin identification, diffraction patterns from another <011> zone (located 60º away in tilt from the original <011> twin boundary zone) were obtained from each side of the twin boundary. These patterns are rotated 70.5º from one another, providing conclusive evidence of a twinned 3C-SiC structure. Only one crystal showed twinning along both {111} planes (Figure 2.6c). Some crystals also show streaking along the {111} planes, indicating stacking faults in this direction (Figure 2.6d). The precise orientation relationship required for a twinned structured is further evidence that the observed small crystal domain sizes in X grains are not a result of ultramicrotome damage. If larger crystals were simply broken apart during slicing (as it appears for the mainstream grains), then it is highly improbable that the crystals would still display the same crystallographic twinning relationships that they do.

In order to further investigate the relationship between crystal domains in SiC X grains, CBED patterns were obtained at similar sample orientations for low index zones from neighboring crystal domains in an unbroken portion of an X grain. Analysis of these diffraction patterns indicated that neighboring crystal domains share a common growth plane. An example can be seen in Figure 2.7. For the crystal domains thus analyzed, a mismatch of 1.7º - 7°, with all but one crystal domain aligned within 4.4°,

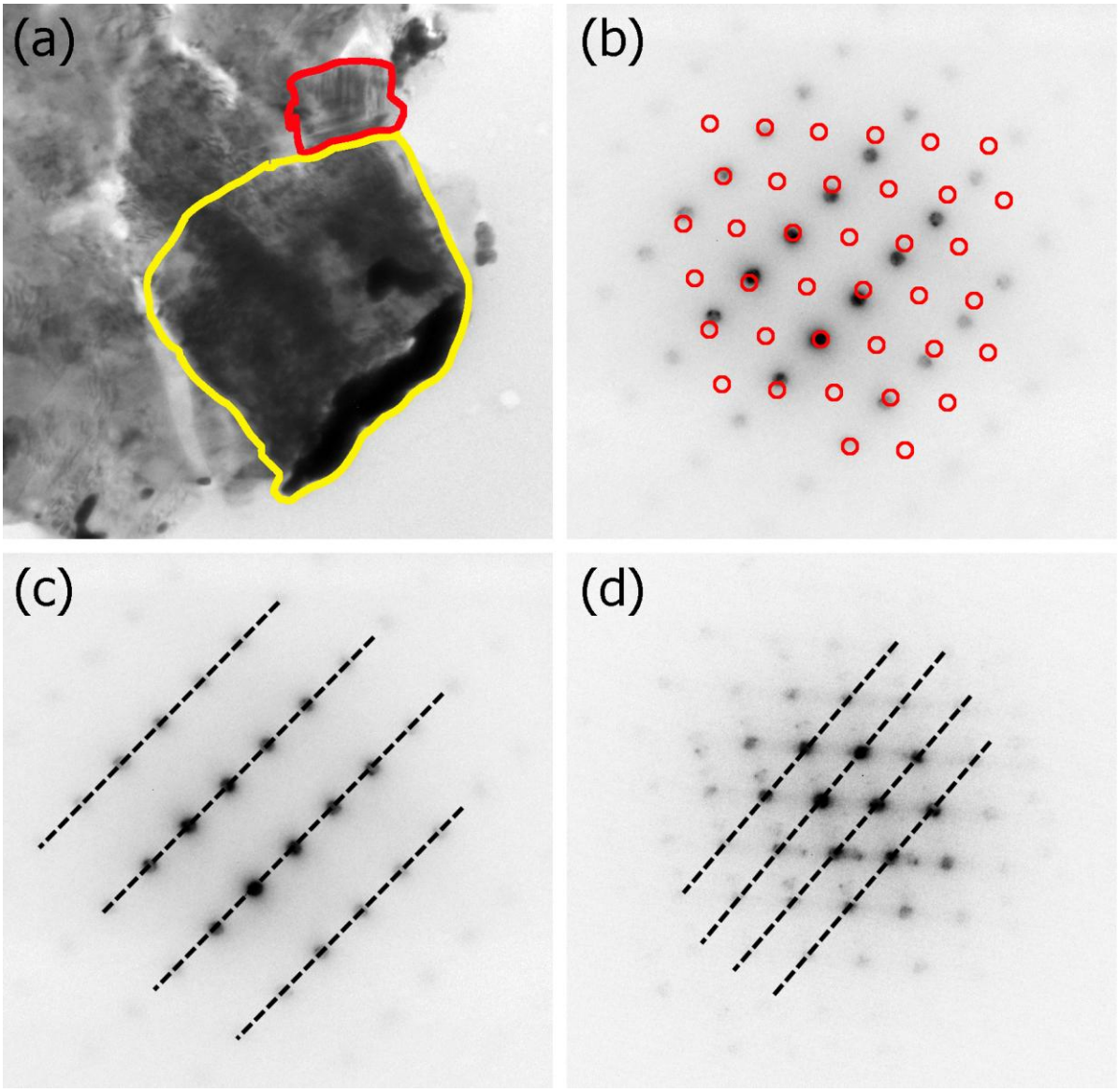


Figure 2.7: Diffraction patterns at similar goniometer angles from two neighboring crystals were obtained from X grain KJG-N4-585-2 (a). A [-112] diffraction pattern was obtained from the crystal outlined in yellow (c) and a [011] pattern from the crystal outlined in red (d). The epitaxial growth of these two crystals is evident in (b) when pattern (d) is overlaid onto pattern (c). For clarity, the spots in the [011] pattern are drawn as empty red circles. The (1-11) and (200) planes of the [-112] and [011] zones, respectively, are almost perfectly aligned (with a 4° mismatch), indicating epitaxial growth. These planes are indicated with dashed lines in figures (c) and (d). Other adjacent crystals have similarly closely aligned planes, with most mismatches varying from ~2° - 4.5º.

was observed, clearly indicating an epitaxial relationship between neighboring crystal domains. For groups of neighboring crystal domains in other grains, similarly well-aligned planes were observed. This close alignment would be extremely unlikely if the crystals grew independently and then randomly coalesced into a mechanical aggregate.

Only one grain contains a crystal domain that does not index to the 3C polytype; this was found in grain KJG-N2-31-1 and appears to be an intergrowth of the 3C and 2H polytypes (Figure 2.8). A [112] diffraction pattern from this crystal domain also contains extra, lighter rows of spots between the (11-1) planes of the [112] zone. The spacing of these extra spots is inconsistent with twinning or another 3C-SiC domain. Instead, the extra pattern indexes to the [0001] zone of the 2H-SiC polytype. The {11-1} spots of the [112] 3C-SiC pattern are aligned with the {10-10} spots of the [0001] 2H-SiC zone, indicating an intergrowth. Additional diffraction patterns from this crystal indicate that it is predominantly 3C-SiC, but dark field (DF) images obtained from diffraction spots unique to the 2H-SiC polytype show a signal emanating from the entire grain, indicating that the 2H-SiC intergrowth occurs throughout the grain as well. This suggests a close intergrowth between the two polytypes that switches back and forth between the two throughout the grain. No streaking or additional spots are evident in any of the other 3C-SiC patterns obtained from this crystal. Although intergrowths between the 3C and 2H polytypes have not been previously reported in X grains, they occurr in ~17% of the grains in the Daulton et al. (2003) study. However, unlike the X grain crystal domains in the present study, their grains were composed of a distinct crystal domain for each polytype, with the proportion of 2H-SiC to 3C-SiC varying greatly between grains, from primarily 3C-SiC to primarily 2H-SiC.

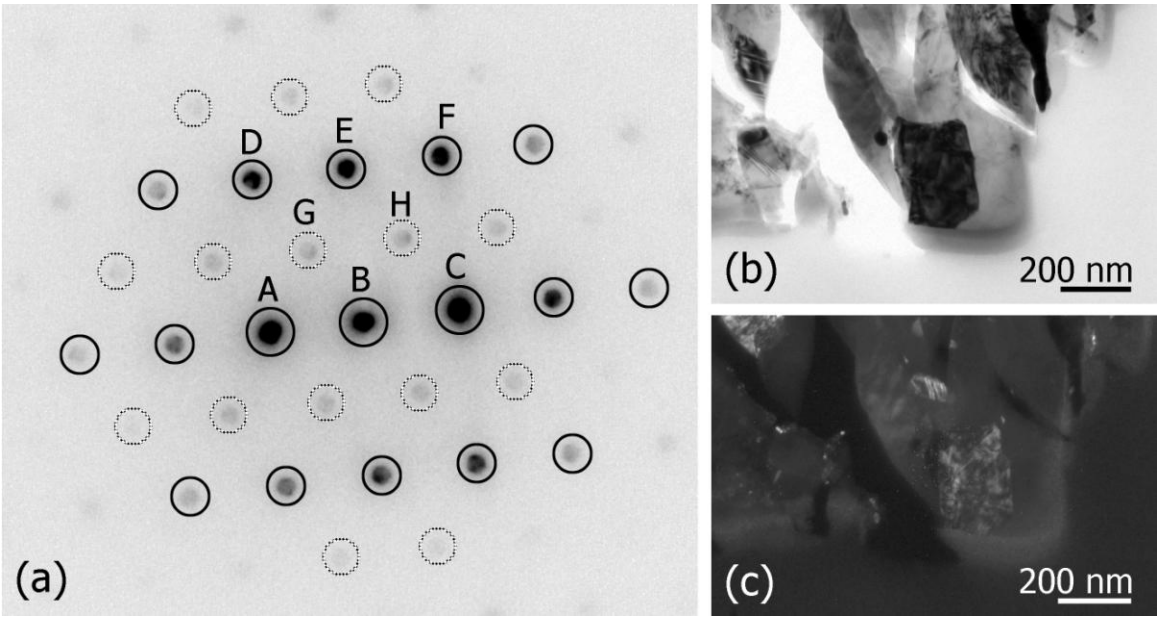


Figure 2.8: A diffraction pattern (a) from one crystal in SiC X grain KJG-N2-31-1 shows an intergrowth between the 3C-SiC and 2H-SiC polytypes. The dark spots (indicated by solid circles) index to both the [112] zone of 3C-SiC and the [0001] zone of 2H-SiC. These spots are shared by the {10-10} plane of 2H-SiC and the {11-1} plane of 3C-SiC. The minor difference in d-spacings between the 2H-SiC {10-10} and 3C-SiC {11-1} diffraction spots (nominally 6%) is not seen. The lighter spots (indicated by broken circles) index to only the [0001] zone of 2H-SiC. The letters above some of the spots represent indexing of the diffraction spots that correspond to: A = (-1-10)/(-1010) spots; B = (000)/(0000); C = (11-1)/(10-10); D = (-311)/(-2200); E = (-220)/(-12-10); F = (-13-1)/(02-20); G = (-1100); and H = (01-10). Comparison of a BF image (b) and a DF image (c) (taken with the diffraction spot indicated by "H") shows signal emanating from the entire crystal, while additional diffraction patterns indicate the entire crystal is 3C-SiC This suggests a close intergrowth of the two polytypes instead of distinct domains of the crystal for each polytype.

Unlike the small crystal domains in SiC X grains, each SiC mainstream grain section is only broken into ~10 – 15 fragments. Zone axes were located for each fragment in the two mainstream grains. All the fragments were conclusively indexed to the 3C polytype. Although each grain is composed of several crystal domains, the grain, as a whole, is a single polytype. In this study, limited crystallographic information was obtained for the mainstream grains, as they were analyzed primarily to provide a comparison to the crystal domain size of the X grains of comparable total grain size (~3 μm). The reader is referred to Daulton et al. (2003) for additional crystallographic information on SiC mainstream grains.

### 2.3.5 Internal Grains within SiC X Grains

Eight internal subgrains were identified in a total of two X grains, making them the first subgrains identified in SiC X grains (Hynes et al. 2006). Seven of the eight subgrains were identified in grain KJG-N2-129-1 (Figure 2.9a). The internal grains, as well as their relative positions within the SiC grain, are shown in Figure 2.9a-e, and their sizes and compositional information are listed in Table 2.3. All of the grains are located within a single slice of KJG-N2-129-1 and five of the grains are clustered in a small area ~200 nm in diameter; only sg3-a and sg3-b are located ~500 nm away from the others. The subgrains are all relatively small, ranging in size from 11 – 45 nm. They are, however, only slightly smaller than some of the SiC crystal domains. The morphology of the subgrains is euhedral to subhedral, with growth faces clearly visible. Only a single subgrain is located in KJG-N4-185-1 (Figure 2.9f), but the extremely small crystal domain size of this grain makes it difficult to locate subgrains in this SiC. Despite the smaller SiC domain size of grain KJG-N4-185-1 compared to the other SiC X grains, its

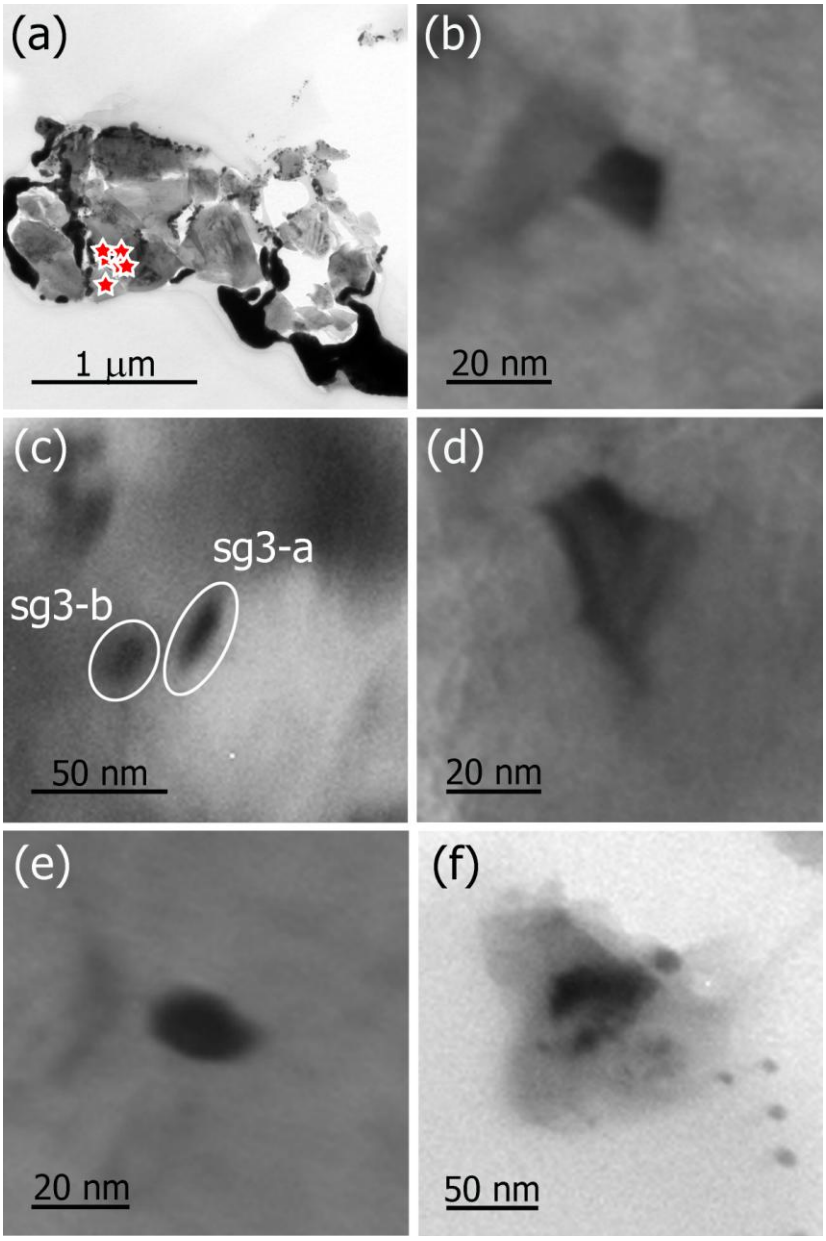


Figure 2.9: TEM BF images of four of the seven internal subgrains in KJG-N2-129-1 (b – e) and one subgrain in KJG-N4-185-1 (f). The internal subgrains in KJG-N2-129-1 are all localized in an area of a few hundred nanometers in the grain. The location of each of these subgrains is indicated by a star in (a). Subgrains 3-a and 3-b are only a few nm apart from one another and are therefore indicated with a single star. The subgrains pictured are: from KJG-N2-129-1, sg1 (b); sg3a and sg3b (c); sg4 (d); sg5 (e); and from KJG-N4-185-1 sg1 (f).

Table 2.3. Summary of internal subgrains within SiC X grains.

| Grain label | Subgrain label | Size (nm) | Ni/Fe[a] | Ti/Fe[a] |
|---|---|---|---|---|
| KJG-N2-129-1 | sg1 | 18 x 13 | 1.60 | |
| KJG-N2-129-1 | sg2 | 44 x 29 | 0.18 | |
| KJG-N2-129-1 | sg3-a[b] | 45 x 22 | 0.34 | 3.15 |
| KJG-N2-129-1 | sg3-b[b] | 26 x 15 | 0.12 | <0.1 |
| KJG-N2-129-1 | sg4 | 33 x 21 | 0.40 | |
| KJG-N2-129-1 | sg5 | 23 x 11 | 0.41 | |
| KJG-N2-129-1 | sg6 | 40 x 37 | 0.18 | |
| KJG-N4-185-1 | sg1 | 28 x 50 | 1.61 | |

Notes: [a] Due to the small size of the grains, all Ni/Fe and Ti/Fe ratios have large errors of 5-10%. [b] Subgrain was originally labeled as sg3, but appears to be composed of two unique pieces: sg3-a and sg3-b. Due to their proximity, some signal overlap may occur.

internal grain is of a similar size to those found in KJG-N2-129-1. However, the subgrain appears to be subhedral compared to those in KJG-N2-129-1.

EDXS analysis indicates that all but one of the eight internal grains are composed of only Fe and Ni (in addition to the elements present in the surrounding SiC). The Ni/Fe ratios are highly variable, ranging over almost an order of magnitude from 0.18 – 1.61 (Table 2.3). Unfortunately, these subgrains are probably too small to be analyzed in the NanoSIMS to determine their isotopic composition. Only sg3 in KJG-N2-129-1 has detectable amounts of another element. This subgrain contains significant amounts of Ti. While the subgrain at first appeared to be a single crystal, a more detailed examination revealed the subgrain to actually be two subgrains. Although some of the EDXS signal likely overlapped between the two pieces of sg3 (sg3-a and sg3-b), they have detectably different compositions, with sg3-a containing nearly all of the Ti and sg3-b containing almost none, which is compositionally consistent with a TiC subgrain with an attached metal phase. Both portions of sg3 are Fe-rich, although sg3-b contains significantly more

total Fe than sg3-a. Unfortunately, due to failure of the support substrate, crystallographic information could not be obtained for these subgrains to further identify them and clarify their relationship.

Diffraction patterns were obtained from the rest of the subgrains in KJG-N2-129-1, as well as from the adjacent SiC crystals. Utilizing the known d-spacings from the SiC crystals as calibration, the d-spacings and interplanar angles from the subgrains' diffraction patterns were calculated. The d-spacings from at least one diffraction pattern for each of the subgrains are too large by 22 – 29% to be kamacite (bcc; a = 2.87 Å) and by 18 – 25% to be taenite (fcc; a = 3.60 Å), which are the only Fe-Ni metal phases previously observed in carbonaceous presolar grains (Croat et al. 2003). An accuracy of better than ~5% is expected with the internal calibrations, clearly indicating that the subgrains are a different phase than any previously observed. Further analysis showed that all the subgrains are inconsistent with any purely metallic Fe-Ni phase. Possible minerals are also limited by the EDXS composition. Given that the sizes of the subgrains are less than the thickness of an ultramicrotome slice, significant EDXS contributions from the SiC matrix are unavoidable. For this reason, the C and Si elemental content of the subgrains cannot be determined, since the strength of these elemental peaks depends on the relative contribution from the SiC background, which varies greatly depending on subgrain size, TEM beam orientation, and other factors. However, the relative strength of the O peak did not change when measuring the subgrain versus the bulk SiC, indicating that the O is just background signal, and eliminating oxides and silicates as possible candidates. Comparison of the d-spacings and the interplanar angles from the

subgrains' diffraction patterns were used to further rule out carbides, nitrides, and minerals containing Al and Mg.

Silicides [e.g., $(Fe, Ni)_3Si$, $(Fe,Ni)_2Si$ ], however, are good candidates that match the diffraction patterns and d-spacings of the subgrains. The diffraction data for all of the subgrains are consistent with a silicide identification. Silicides also have a broad range of compositions, widely varying in both Ni/Fe and metal to Si ratios. However, with a limited number of subgrain candidates, it is difficult to conclusively determine the stoichiometry and crystal structure of the silicides that are present in SiC X grains. Due to the large compositional range, large crystal lattices, and similar diffraction patterns produced by many silicides [e.g., $(Fe, Ni)_3Si$; monoclinic; a = 6.972 Å, b = 6.254 Å, c = 7.656 Å, β = 87.75° and $(Fe,Ni)_2Si$; orthorhombic; a = 3.73 Å, b = 5.00 Å, c = 7.04 Å], several silicide compositions can match the data from a single subgrain.

## 2.4 Discussion

### 2.4.1 Trace Elements in Presolar SiC Grains

One of the definitive characteristics of SiC X grains is their high level of radiogenic $^{26}Mg$ from the decay of $^{26}Al$ (half life = 7.4 x $10^5$ yrs), which is synthesized mainly in SNe, although smaller amounts can also be produced in AGB stars. The $^{26}Mg$ is assumed to be radiogenic for both chemical and isotopic reasons. First, Al preferentially condenses into SiC, giving Al/Si ratios of up to several weight percent in both SiC X grains and mainstream grains (Hoppe and Ott 1997). However, unlike Al, Mg does not readily condense into SiC, leading to typical concentrations in mainstream

SiC grains of only ~100 ppm (Amari et al. 1995). Presolar SiC grains have isotopically normal $^{25}Mg/^{24}Mg$ compositions, but show enrichments in $^{26}Mg$, further supporting the idea that the bulk of the $^{26}Mg$ measured in presolar SiC grains is due to the decay of $^{26}Al$. Based on this assumption, the inferred initial $^{26}Al/^{27}Al$ ratio can be calculated from Mg isotopic data. The inferred $^{26}Al/^{27}Al$ ratios for SiC mainstream grains are typically very low ($\sim 10^{-3} - 10^{-4}$) (Hynes and Gyngard 2009), with correspondingly low Mg/Al ratios (< 0.05) (Amari et al. 1995). SiC X grains, however, have much higher inferred $^{26}Al/^{27}Al$ ratios ($\sim 10^{-2} - 10^{-1}$) (Hynes and Gyngard 2009), ranging as high as 0.6 (Nittler et al. 1995).

Our EDXS data are consistent with previous isotopic findings. The mainstream grains do not show any measurable Mg, while most of the X grains have very high Mg/Al ratios (up to 0.74). With such low Mg concentrations in mainstream grains (in both TEM and isotopic measurements) and the $^{26}Mg$ excesses measured in presolar SiC grains generally being very high, with sometimes even monoisotopic $^{26}Mg$ (Hoppe and Ott 1997), it is possible to estimate the inferred $^{26}Al/^{27}Al$ isotopic ratios from elemental Mg/Al ratios. Within a $2\sigma$ error, the $^{26}Al/^{27}Al$ ratios inferred from our Mg/Al elemental ratios are consistent with the $^{26}Al/^{27}Al$ ratios inferred from isotopic data: $< 0.12$ to $0.74 \pm 0.04$ and $0.003 \pm 0.002$ to $0.61 \pm 0.04$, respectively (Hynes and Gyngard 2009).

The Al in SiC grains has been postulated to be in the form of AlN, an idea that has been supported by TEM observations of AlN subgrains in a SiC mainstream and Z grain (Stroud et al. 2005). Materials science research indicates that the solubility of AlN in solid solution varies with SiC polytype. Aluminum nitride was found to be most soluble in 2H-SiC and extremely insoluble in 3C-SiC (Zangvil and Ruh 1988). Contrary

to these findings, there is no obvious difference between Al-Mg content and polytype evident in this study; in fact, the only SiC grain indexed to 2H-SiC (grain KJG-N2-31-1, an intergrowth between the 3C and 2H polytypes) contains some of the lowest Al-Mg concentrations. Unfortunately, to the best of our knowledge, measurements of Al-Mg concentrations in presolar grains with coordinated crystallographic analyses are only available for the grains in this study. Additional Al-Mg measurements on grains with the 2H polytype are needed to determine if Al content in presolar SiC grains is correlated with polytype.

### 2.4.2 Effects of Stellar Environment on Grain Formation and Crystal Growth

The SiC X grains and mainstream grains were observed to have significantly different crystal domain sizes. SiC X grains, both from this study and from previous studies, are polycrystalline, even X grains that are submicron (Stroud et al. 2004b), whereas mainstream grains are either single crystals (Daulton et al. 2003; Stroud et al. 2005), or composed of only a few large crystals. In this study, the crystal domains in the mainstream grains range from several times to over 30 times larger than those in the X grains. The difference can be explained as resulting from the different environments in which these grains formed. The large number of crystals in each SiC X grain implies a large number of nucleation sites, which, in turn, suggests conditions of high supersaturation in the parent gas. If the gas is not supersaturated, small condensation nuclei that form will quickly redisperse due to free energy constraints because the free energy of a seed nucleus is higher than that of the bulk gas. However, crystallites will form and reach critical size under conditions of supersaturation. These conditions foster

both rapid nucleation and growth, with new crystallites nucleating at the expense of the growth of other crystals, resulting in many small crystals growing together into a single grain, as was observed in the X grains. Lower degrees of supersaturation would lead to lower nucleation rates and increased growth, producing fewer, but larger crystals within a single grain, as was observed with the mainstream grains.

It is useful to compare these growth scenarios to previous theoretical and experimental works on the growth conditions around AGB stars and SN outflows. An origin in the envelopes of low-mass carbon AGB stars has been well established for mainstream SiC, as well as for some graphite grains (Bernatowicz et al. 1996; Meyer and Zinner 2006). Bernatowicz et al. (2005) sought to determine the physical conditions, including stellar mass and timescale, required to form micron-size presolar graphite grains and their internal TiC subgrains in the outflows of AGB stars, beginning with the fundamental idea that in order for stars to contribute to the presolar grain population, they must have sufficient mass to reach the AGB phase soon enough to contribute dust to the solar nebula. The resulting mass limit excludes hot carbon stars, leaving carbon variable (CV) stars, which have radii, luminosities, and effective temperatures that vary periodically with time, as the likely source of presolar SiC and graphite with an AGB origin. Using equilibrium thermodynamics calculations and kinematics, as well as mass-loss rates and outflow velocities of CV stars from astronomical observations, they determined the radii at which the grains would form and the effective temperatures at which grain growth would begin and cease. With these parameters, they calculated a time interval (governed largely by the range of the luminosities of CV stars) of ~2 – 10 yrs during which graphite growth could occur. This timescale begins with nucleation and

ends when the number density in the gas drops so low that grain growth effectively ceases. These calculations were done for graphite and TiC, but they can be adapted for SiC. Grain growth largely depends on the number density of each species and is therefore limited by the less abundant species. The solar ratio of Si/C is 0.14, but when only free C is considered (C not tied up in CO molecules and thus free to form carbonaceous grains), for C/O ratios of 1.05 – 1.15, the ratio of Si/C ranges from 1.42 – 0.47 (Lodders 2003). At a C/O ratio of 1.05, the formation of graphite and SiC remove roughly the same amount of C from the total C (Lodders and Fegley 1995), suggesting that both SiC and graphite will continue to grow over similar timescales.

A timescale for the formation of SiC X grains in SN ejecta has also been estimated. Hoppe et al. (2002) measured the Ti and V isotopic compositions of SiC X grains. The radioactive isotope $^{49}$V (half-life = 338 days) is produced from the decay of $^{49}$Cr (half-life = 42 mins) by explosive Si, O, and He burning in the Si/S and Ni zones of a SN (Meyer et al. 1995). Vanadium-49 then decays into $^{49}$Ti, which allows a timescale for grain formation to be estimated. If the time of formation were much longer than the half-life of $^{49}$V, it would have decayed into $^{49}$Ti before its incorporation into the SiC grain and resulted in no correlation between Ti and V (measured as $^{49}$Ti/$^{48}$Ti and $^{51}$V/$^{48}$Ti). If, however, the formation timescale were shorter than the half-life of $^{49}$V, live $^{49}$V would be incorporated into the grains and subsequently decay into $^{49}$Ti, resulting in a correlation between Ti and V. Hoppe et al. (2002) found a positive correlation between $^{49}$Ti/$^{48}$Ti and $^{51}$V/$^{48}$Ti, suggesting that the $^{49}$Ti excesses are due to the incorporation of live $^{49}$V into the X grains. Additionally, $^{46,47,50}$Ti/$^{48}$Ti were close to solar values. The presence of live $^{49}$V during grain formation led them to calculate that the timescale for SiC X grain formation

was a period of months, and with uncertainties included, no more than 25 months. This timescale begins with the SN explosion (and the creation of $^{49}V$) and ends when grain growth effectively ceases. However, grain formation does not begin with the SN explosion, in which temperatures reach ~5 x $10^5$ K and all surrounding material is vaporized (Wooden 1997); this timescale estimate does not take into account the time necessary for the ejecta to cool enough for grains to condense. Although astronomical observations of dust around Type II SNe are limited, SN 1987A had strong infrared emissions, indicating the onset of dust condensation between ~350 – 500 days after the explosion (Wooden 1997). Although the dust emission was dominated by grains with featureless spectra, such as metallic C and Fe grains, the timescale for dust formation agrees with that predicted by Hoppe et al (2002). However, their estimated timescale is an upper limit on the time available for X grain formation, particularly if grain formation does not begin until ~500 days after the SN explosion, suggesting that the actual time for grains to form may be less than a year.

The total size to which a SiC grain can grow is directly proportional to both the growth timescale and the average total pressure, which affects the availability of condensable species. In SN ejecta, these conditions vary rapidly. The explosion itself is incredibly powerful, releasing ~$10^{46}$ J of energy. The gas then rapidly expands, with initial speeds of (4 – 30) x $10^3$ km $s^{-1}$, and quickly cools; observations of SN 1987A indicate that the temperature drops from ~500,000 K to ≤ 2000 K in only 350 days, with a corresponding decrease in pressure (Wooden 1997). The radioactive decay of isotopes like $^{56}Ni$ heats the ejecta, while instabilities, such as high temperature Rayleigh-Taylor fingers, create turbulent mixing throughout the SN ejecta. In this rapidly evolving

environment, SiC X grains are thought to condense. High initial pressure, which ultimately leads to the growth of large grains, coupled with sharp drops in pressure and rapid cooling would favor supersaturation with rapid and prolific nucleation and crystal growth, in agreement with the large number of crystal domains observed in X grains. This is also consistent with astronomical observations of SN 1987A, in which dust condensation occurred rapidly enough to fill 50% of the ejecta volume after just 500 days (Wooden 1997). With the short timescale available for X grain growth suggested by both astronomical observations (Wooden 1997) and isotopic measurements (Hoppe et al., 2002), each individual crystal domain does not have time to grow very large before being encroached upon by adjacent growing crystal domains, resulting in many small crystal domains in a single SiC X grain, consistent with the observations in this study. The conditions in the AGB outflows in which SiC mainstream grains condense, however, are quite different. Pressures and temperatures remain relatively constant. Although temperatures and pressures typically are ~2000 – 2500 K and ~100 N $m^{-2}$ in the photosphere of an AGB star, these temperatures are far too high for grain condensation to occur. At larger radii where SiC grains can condense, temperatures (~1400 – 1700 K) and pressures (roughly 0.01 – 10 N $m^{-2}$) are much lower (Lodders et al., 1995). Under these conditions, nucleation would occur at a slower rate than in SN ejecta and would result in fewer nucleation sites. However, some variation in condensation conditions in AGB stars likely occurs throughout the period of grain growth and between individual stars, resulting in some mainstream grains being composed of a single crystal domain, while others are polycrystalline. In addition to slower nucleation in AGB stars, given the growth period of years for mainstream grains to grow in AGB outflows calculated by

Bernatowicz et al. (2005), these crystals would have a significantly longer time to grow and to cool than their counterparts in SN outflows, resulting in relatively large, but few, crystal domains in each mainstream grain, also in agreement with the observations of this study. Therefore, both the timescale for grain formation and the nucleation rates lead to the growth of many small crystal domains in X grains, relative to mainstream grains with the same total grain size.

Based on the different grain formation conditions and environments in AGB stars and SNe, which are manifested in the different isotopic characteristics and different crystal domain sizes measured in mainstream SiC and X grains, it may seem plausible that these different environments would also be reflected in the presence of different polytypes in X grains and mainstream grains. However, the same polytypes have been observed to occur in both types of grains. Among the crystals in the X grains in this study and the two X grains analyzed by Stroud et al. (2004), examples of each polytype (3C and 2H) observed by the Daulton et al. (2003) survey are found, with the exception of 1-D disordered grains, which are less than 1% by number of presolar SiC grains and thus statistically unlikely to be observed in either our study or the Stroud et al. (2004) study, although Daulton et al. (2009) have recently identified a 1-D disordered X grain.

Some insights into why only the 2H and 3C polytypes are observed in presolar grains can be gained by looking at the experimental and theoretical work done on the conditions that affect SiC polytype growth in general. Due to the usefulness of SiC as a wide band gap semiconductor that can be used in hostile environments, it has found many uses in aerospace and defense applications, and even as coatings on very high temperature nuclear field reactors. Because some polytypes of SiC are better suited than

others for wide ranging applications, considerable research has been done by the materials science community over the last ~40 years to understand SiC formation and growth.

Despite much research on the subject, the theoretical details of the formation and growth of SiC polytypes are still not well understood and it is unclear what factors dominate formation in any individual case. Theories based on nucleation growth models and experimental results suggest a wide variety of factors may play an important role in determining which polytype forms. These include: the influence of physical conditions, such as temperature, pressure, and the C-flux; the effect of the Si/C ratio in the gas; the growth surface or nucleation seed and its polarity; the presence of impurities; the location and number of stacking faults present; the effects of non-equilibrium conditions; the presence of vacancies in the superlattice; and the differences between polytypes in formation energy and surface free energy (see Fissel 2000; Zhaoqing and Jun 2005, and references therein). Experimental results are also varied and are highly dependent on experimental conditions. Different growth methods can lead to the formation of the same polytypes at very different temperatures and can result in different transitions from one polytype to another, with possible intergrowths occurring at intermediary temperatures. For example, SiC vapor was observed to first crystallize as 3C-SiC and then begin to transition to the 6H polytype at temperatures of ~2100 – 2700 K (Anikin and Madar 1997; Yoo and Matsunami 1991). Above 2700 K, the SiC gas condensed directly to 6H-SiC. The same transition was observed to occur at ~1620 K for SiC grown with gas-source molecular-beam epitaxy (Kern et al. 1998). The 3C polytype can also form via transformation of the 2H polytype by annealing in an Ar atmosphere at temperatures

ranging from ~1673 – 1763 K (Krishna et al. 1971). In other experiments utilizing condensation of gaseous SiC onto graphite wafers, 2H-SiC was observed to start growing at temperatures ~1500 K and cease transitioning to 3C-SiC above ~1700 K (Patrick et al. 1966; Stan et al. 1994). In both vapor condensation and annealing experiments, the 2H to 3C to 6H-SiC transition has been frequently observed; however, 4H-SiC has also often been observed as an intermediary step after 3C-SiC. Both the 3C-SiC and 4H-SiC steps can also be omitted, resulting in a direct transition from 2H-SiC to 6H-SiC, even with techniques similar to those previously described. For example, 2H-SiC crystals, annealed in an Ar atmosphere, were observed to transition directly to 6H-SiC at 2673 K (Krishna and Marshall 1971).

Unfortunately, some difficulties arise in trying to apply the laboratory experimental conditions that result in a wide range of transitions and temperatures to the growth conditions in stars. No lab can accurately model the temperatures, pressures, gas-flux, growth surfaces, and possible non-equilibrium conditions present in SN outflows. Therefore, while laboratory experiments can provide a useful tool in understanding polytype formation, the exact temperatures of formation, conditions for possible intergrowth, and the transitions to higher-order polytypes are still uncertain.

However, despite large variations in temperatures, some general trends are clearly apparent. 2H-SiC is the lowest-order polytype that has been observed to form. Furthermore, only 2H-SiC has been observed at lower temperatures than 3C-SiC, marking 2H to 3C-SiC as the lowest temperature transition, with possible intergrowths between the two polytypes occurring at a range of intermediary temperatures. At even higher temperatures, both 2H-SiC and 3C-SiC become unstable and cease to form,

resulting in gaseous SiC crystallizing directly into higher-order polytypes like 6H-SiC. Transitions from higher-order polytypes to lower order ones, such as 6H-SiC to 3C-SiC, have not, however, been observed.

Equilibrium condensation calculations for the formation of SiC and graphite suggest that grain formation is limited to pressures of 0.01 – 10 N $m^{-2}$ and C/O ratios of 1.05 – 1.2 (Lodders and Fegley 1995; Sharp and Wasserburg 1995). Under these conditions, SiC is expected to condense at temperatures of 1390 – 1630 K. Some SN models predict SiC formation at a similar, although slightly higher, temperature of 1745 K (Lattimer et al. 1978). The temperatures predicted for SiC grain formation in stellar outflows are roughly in line with experimental evidence for the growth of the lower temperature polytypes, i.e., 2H-SiC and 3C-SiC. Although ~250 higher-order hexagonal and rhombohedral polytypes have been observed to form in laboratories, they require high temperatures above ~2800 K (Fisher and Barnes 1990), far too high for SiC to condense, given the low pressures in stellar outflows. However, these condensation models assume the grains form near thermochemical equilibrium, which is likely to be true in AGB stars, but may not be true in SNe (Ebel and Grossman 2000).

The presence of only the 2H and 3C polytypes, or intergrowths of the two, in presolar SiC suggests two possible explanations. The first is that the conditions under which SiC starts to form may not be that different in AGB stars and SNe, despite the fact that SN outflows may initially have significantly higher temperatures and pressures than do AGB outflows (Lattimer et al. 1978; Sharp and Wasserburg 1995). The other possibility is that polytype formation is not particularly sensitive to these conditions, at least at the ranges present in both kinds of stellar outflows. Other factors, such as the

Si/C ratio or the flux of C and Si onto growing particles, may play a more dominant role in polytype formation over the range of temperatures and pressures found in stellar ejecta and therefore contribute to the formation of the same polytypes in both mainstream and X grains. The resolution of this question requires a better theoretical understanding of the fundamental factors that dominate SiC polytype formation. As a final caveat, the number of X grains that have been analyzed in the TEM, though much improved, is still reasonably small, especially in comparison to the hundreds of mainstream grains analyzed, e.g., by Daulton et al (2003). In view of the somewhat limited sample size, it is still possible that higher-order polytypes may yet be discovered in SiC X grains.

While materials science experiments on polytype growth produce widely varying results, they agree with both this study and the Daulton et al. (2003) study that 3C-SiC is the preferred polytype at low temperatures. Daulton et al. (2003) suggested that the observed abundance of 3C-SiC over 2H-SiC can be explained for AGB stars by the formation of 2H-SiC at large circumstellar radii, where temperatures prevail that are low enough for only 2H-SiC to form. At smaller radii, the temperature would be high enough to allow for both the 2H and 3C polytypes to form, resulting in possible intergrowths between the two polytypes; at still smaller radii, even higher temperatures would cause 2H-SiC formation to cease, resulting in the formation of only 3C-SiC. The number densities are also higher at smaller radii, resulting in more 3C-SiC relative to 2H-SiC. In addition, more of the Si will have already condensed as 3C-SiC at smaller radii, resulting in fewer intergrowths and even less of the 2H-SiC polytype.

However, the observed preponderance of 3C-SiC is in stark contrast to nucleation theory, which predicts that 3C-SiC is never the stable polytype of SiC at any temperature.

3C-SiC has both a much higher total lattice energy (an important theoretical constraint on polytype formation) and a higher phonon energy (which is thought to stabilize polytypes by contributing to the free energy) than both 4H-SiC and 6H-SiC (Zhaoqing and Jun 2005). Of the most common polytypes, only 2H-SiC is less energetically favorable than 3C-SiC. However, the frequent experimental observations of 3C-SiC at low temperatures can be explained by its propensity to grow epitaxially (a phenomenon that was also observed in the formation of X grain aggregates in this study). SiC vapor growth can be viewed as a layer-by-layer process in which a single Si-C bilayer at a time is added to the crystal. At high temperatures, with each new bilayer, the crystal can rearrange itself to create the most energetically favorable stacking sequence, resulting in either 4H-SiC or 6H-SiC. However, at lower temperatures, the crystal is unable to reorient the already formed layers and must simply arrange the newest layer into a locally energetically favorable stacking, which results in the 3C polytype (Heine et al. 1991). This should also be the case far from equilibrium, where rearrangement of the Si-C bilayers is not possible (Fissel 2000). The composition of the gas from which the SiC grains condense has also been shown to affect polytype formation. 3C-SiC has been both theoretically predicted and experimentally observed to preferentially form over any other polytype at temperatures < 2000 K (at which 3C-SiC, 4H-SiC, and 6H-SiC have all been observed to form in a laboratory setting) under conditions of supersaturation of the C-flux and high Si/C ratios. However, at lower C-fluxes and Si/C ratios, 6H-SiC was observed to form and at still lower Si/C ratios, 4H-SiC formed (Fissel 2000). No clear theoretical reasons exist to explain the observed formation of 2H-SiC and the transition of 2H-SiC into 3C-SiC (Krishna et al. 1971) other than temperature constraints (Fissel 2000). Although the

applicability of laboratory experiments and nucleation theory has some limitations, until a more complete theory of polytype formation is developed, they provide possible scenarios for the observed polytype abundances in SiC X grains.

### 2.4.3 Subgrain Formation in Stellar Outflows

While not previously observed in SiC X grains, subgrains are quite common in carbonaceous presolar grains. Although a limited number of SiC grains have been sectioned for TEM analysis, subgrains have been found within four of eight presolar SiC grains studied (Bernatowicz et al. 1992; Stroud and Nittler 2004). Bernatowicz et al. (1992) observed TiC subgrains in a mainstream SiC grain. (Ti,V)C was also observed in two different pristine SiC grains, along with AlN subgrains, by Stroud et al. (2005). Finally, multiple graphite subgrains in SiC were observed by Stroud et al. (2002). All of these SiC grains originated in an AGB circumstellar environment.

Subgrains are also quite common in presolar graphite grains. Approximately 20% of the roughly 850 high-density graphite slices analyzed by Croat et al. (2005) contain subgrains. Most of these grains are (Ti, Zr, Mo, Ru)C with s-process enrichments of up to ~200 times the solar value, indicating an AGB origin for these graphite grains. SiC subgrains were found within six different high-density graphite sections (Croat et al. 2010b). Of those SiC-containing graphite grains measured for Si isotopes, two of three show extreme $^{29,30}$Si enrichments that could only originate in massive stars. In a few rare cases, kamacite, iron carbide, and metallic (Os)RuFe phases were also found (Croat et al. 2005). Additionally, subgrains have been found in SN graphite grains; all eleven low-density SN graphite grains studied by Croat et al. (2003) contain refractory carbides, with

a single graphite often containing hundreds of internal TiC subgrains. Many of these TiC subgrains (30 – 230 nm) have epitaxially grown kamacite and taenite grains (8 – 76 nm in diameter), providing clear evidence of Fe condensation in SN ejecta. Independent kamacite subgrains are also present, but are far less abundant.

Iron-nickel subgrains, which are detected as significant increases in the Fe signal in isotopic depth profiles, have been independently observed in isotopic measurements of SiC X and Z grains in the NanoSIMS (Hynes et al. 2009; Marhas et al. 2008). Most of the grains have highly anomalous Fe and Ni isotopic compositions and at least half of the X grains (and several of the Z grains) contain subgrains, which are the apparent carriers of the Fe anomalies. These subgrains show a wide range of Ni/Fe ratios, in agreement with the TEM observations in this study. However, the bulk Ni/Fe ratios of ~5.5 that were measured in the isotopic studies are not only much higher than the solar ratio of 0.059, but they are also much higher than those observed in this study.

While a wide array of subgrain types have been observed in presolar grains, to the best of our knowledge, this is the first reported observation of silicides. They are, however, not unexpected. Lodders (2006) predicted the formation of silicides in the He/C, Si/S, and Fe/Ni zones (named for their most abundant elements by mass) of Type II SNe as part of her calculations to explain the observations by Croat et al. (2003) of graphite containing internal TiC with attached Fe-Ni grains (suggesting a condensation sequence of TiC – metal – graphite). Several problems existed in explaining these observations. First, the calculated condensation sequence for mixtures of the He/C, O/C, and He/N zones is TiC – graphite – SiC – silicides. Also, except in the Fe/Ni zone, Si is as abundant as Fe, leading to the condensation of silicides (previously unobserved) over

the observed Fe-Ni metal. Deep in the outflowing Fe/Ni zone, however, the Si abundance is so low that titanides [i.e., $(Fe,Ni)_nTi_m$] could form in place of silicides and would then need to be transported to outer zones where a thermochemically favorable reaction would convert the titanides to TiC and Fe-Ni metal grains.

Although the existence of silicides is theoretically predicted and they are expected to readily form in SNe, the question of how they are incorporated into SiC remains. Three possible scenarios exist for the formation of subgrains in an astrophysical environment: independent formation of the subgrains prior to SiC and subsequent capture via collisions and sticking, similar to TiC subgrains observed in graphite (Croat et al. 2003); heterogeneous nucleation and growth of the subgrains onto the surface of SiC, similar to the growth of kamacite grains onto TiC (Croat et al. 2003); and the formation of subgrains after SiC formation via a solid-state reaction, such as the exsolution of the silicides from solid solution at the SiC grain boundaries, similar to the formation of TiC subgrains in SiC mainstream grains (Bernatowicz et al. 1992).

Crystallographic, morphological, and chemical properties of the subgrains can help limit the possible scenarios for silicide formation. Diffraction patterns from at least two subgrains in KJG-N2-129-1 indicate a likely epitaxial relationship with the surrounding SiC. These subgrains are aligned within ~1 – 5° of the SiC plane. Other diffraction patterns from the subgrains and the surrounding SiC are inconclusive. The likelihood of a subgrain forming independently, then sticking to a SiC crystal at a random orientation that happened to be crystallographically aligned with the SiC is unlikely, and it is even more improbable that this would occur twice in a single SiC grain, effectively

eliminating this scenario as a possibility for subgrain formation. Crystallographic alignment could, however, be expected for both heterogeneous nucleation and exsolution.

Examination of TEM BF images of the subgrains show that the subgrains are located at SiC crystal domain boundaries, rather than in the interior of a SiC crystal. Several of the subgrains (such as sg 4, see Figure 2.9d) even have concave boundaries with the surrounding SiC domains, a clear sign of secondary formation. This morphology is not consistent with subgrains that formed independently of the SiC and were later incorporated, nor does it resemble subgrains that nucleated onto the surface of another grain, such as the kamacite subgrains on TiC grains, which are found in SN graphite grains (Croat et al. 2003).

Both the crystallographic alignment and the morphology of the subgrains suggest an exsolution process, although the considerable compositional variation among the multiple subgrains in grain KJG-N2-129-1, which are only hundreds of nm apart, could be explained by the formation of silicides prior to SiC. However, the compositional variation can also be explained if the grains exsolved from solid solution. Crystallographic data indicates that there is not a single equilibrium silicide phase that can form over the observed compositional range. This suggests that at a SiC grain boundary, there may not be an equilibrium phase that exists for the Ni/Fe ratio present there. The subgrain would form, for example, as an Fe-rich silicide that contains as much Ni as the phase allows, while the excess Ni is pushed out of the grain, leading to the later formation of extremely Ni-rich silicides. The compositional data for the subgrains all fall into ranges of either high (Ni/Fe $\geq$ 1.6) or low (Ni/Fe $\leq$ 0.41) Ni/Fe ratios, but no subgrains have been observed with Ni/Fe ratios in between these values, supporting the

idea that the formation of equilibrium phases may only be possible at either high or low Ni/Fe ratios.

The morphological characteristics of the subgrains, their observed compositional range, and the epitaxial alignment of the subgrains with the surrounding SiC all point towards the silicides co-condensing in solid solution with SiC and then exsolving at lower temperatures as the most likely formation mechanism for the subgrains. This scenario also agrees with the predicted formation sequence in the He/C zone of a SN in which SiC condenses before silicides (Lodders 2006). However, additional theoretical calculations, such as those recently carried out by Fedkin et al. (2009), coupled with additional observations of subgrains in SiC X grains, particularly those X grains containing multiple subgrains, are still needed to gain a more complete understanding of grain formation in SN outflows.

## 2.5 Summary and Conclusions

Our TEM observations have revealed several unique characteristics of SiC X grains. The crystal domains in X grains are significantly smaller than those of SiC mainstream grains, indicating conditions of supersaturation and rapid formation in the SN environment, which is consistent with previous conclusions from both astronomical observations and isotopic measurements. Despite the fact that X grains form in the ejecta of Type II SNe, they exhibit the same polytypes as mainstream grains, which form around AGB stars. Although temperatures and pressures, which are thought to play a large role in polytype formation, are possibly quite different in AGB and SN outflows at

the time of grain formation, this difference appears to have little or no effect on polytype formation in presolar SiC. This suggests either that polytype is not particularly sensitive to the range of temperatures and pressures in which SiC can condense in astrophysical environments or that other factors, such as the Si/C ratio, which may not be that different in regions of SiC formation in AGB and SN outflows, may play a more dominant role in polytype formation. Additional experimental and theoretical work is needed to determine the reason that no differences in the polytypes present in mainstream and X grains have yet been observed.

We have also observed the first subgrains in SiC X grains. These subgrains have an epitaxial relationship with the surrounding SiC crystal domains, as well as a large range of Ni/Fe ratios, even between subgrains less than a hundred nanometers apart, suggesting that they were likely present in the SiC in solid solution and later exsolved at the SiC crystal domain boundaries as discrete phases dependent upon their Ni/Fe ratios. The crystallographic data from the subgrains are inconsistent with any previously observed presolar phase. Based on their crystallographic structure, we conclude that these subgrains are silicides. Silicides are, in fact, predicted stable SN condensates, although more work needs to be done to explain their formation and incorporation into SiC. Additional subgrains from a larger suite of SiC X grains would also help in identifying specific silicide phases and providing additional compositional and morphological information. Finally, although the number of SiC X grains that have been microanalyzed has been significantly increased, the study of many additional grains is needed to provide better statistics, possibly reveal rare SiC polytypes or subgrain types

that were not observed in the limited number of grains studied thus far, and generally provide a more comprehensive understanding of the formation of SiC X grains.

# Chapter 3

# A Microanalytical Study of SiC AB Grains

"On the subject of stars, all investigations which are not ultimately reducible to simple visual observations are ... necessarily denied to us…We shall never be able by any means to study their chemical composition or their mineralogical structure... I regard any notion concerning the true mean temperature of the various stars as forever denied to us."

~Auguste Comte, from *Cours de Philosophie Positive*, 1835, twenty-five years before Gustav Kirchhoff and Robert Bunsen published their three laws of spectroscopic analysis

## 3.1 Introduction

SiC is the best-studied type of presolar grain. Many thousands of so-called "mainstream" SiC grains, which represent over 90% of the total presolar SiC population by number, have been measured for their isotopic compositions (Hynes and Gyngard 2009). The $^{12}C/^{13}C$ ratios of mainstream grains ($10 < {}^{12}C/{}^{13}C < 100$; solar = 89) closely match both the theoretical predictions (Gallino et al. 1990; Lattanzio and Boothroyd 1997) and the astronomical observations (Lambert et al. 1986; Smith and Lambert 1990) of the range of $^{12}C/^{13}C$ ratios in low-mass ($1 – 3\ M_{\odot}$) N-type carbon stars, indicating that mainstream grains condensed around this type of AGB star. This inferred origin is further supported by measurements of $^{14}N$ and $^{29,30}Si$ excesses, relative to solar, as well as

the presence of s-process enrichments in the heavy elements (Gallino et al. 1990; Nicolussi et al. 1997), that have been measured in SiC mainstream grains.

The Si isotopic compositions of mainstream grains are indicative of an origin in AGB stars of close-to-solar metallicity. However, these $^{29}$Si and $^{30}$Si enrichments are not unique to mainstream grains; another sub-population of presolar SiC, known as SiC AB grains, has Si isotopic ratios that are indistinguishable from mainstream grains. SiC AB grains are quite distinct, however, from mainstream grains in their C and N isotopic compositions. AB grains, which make up just 4 – 5% of the total presolar SiC population, are defined as having $^{12}$C/$^{13}$C < 10, in addition to having a wide range of $^{14}$N/$^{15}$N ratios ($39 \leq {}^{14}\text{N}/{}^{15}\text{N} \leq 10{,}000$; solar = 272). Although mainstream grains also have a sizable range of $^{14}$N/$^{15}$N ratios ($179 \leq {}^{14}\text{N}/{}^{15}\text{N} \leq 9{,}800$), only ~3% of mainstream grains are enriched in $^{15}$N, compared to ~33% of AB grains (Hynes and Gyngard 2009). Roughly half of AB grains have enrichments in the s-process elements similar to those measured in mainstream grains; however, the other half have solar s-process abundances (Amari et al. 2001c; Pellin et al. 2000b)

The extremely low $^{12}$C/$^{13}$C ratios, coupled with the sub-solar $^{14}$N/$^{15}$N ratios and lack of s-process enrichments measured in some AB grains, pose significant problems for models of nucleosynthesis in AGB stars (Meyer and Zinner 2006). In these models, H burning in the CNO cycle creates large enrichments in $^{13}$C (the equilibrium value of the CNO cycle is $^{12}$C/$^{13}$C = 3.5). Nitrogen production is highly dependent on temperature, although, in general, material processed in the CNO cycle is typically greatly enriched in $^{14}$N, with $^{14}$N/$^{15}$N ratios up to ~30,000 (Amari et al. 2001c). The low $^{12}$C/$^{13}$C ratios produced by the CNO cycle closely match those measured in AB grains (or at least the

subset with high $^{14}N/^{15}N$ ratios), but the CNO cycle converts most of the C to N, and also produces large enrichments in $^{17}O$, leaving the star with C/O < 1. This is highly problematic, since in order for SiC to form in a stellar outflow, the C/O ratio there must be greater than unity; virtually all of the C and O atoms are tied up in stable CO molecules, which are the most tightly bound diatomic molecules (Sharp and Wasserburg 1995). Only if C/O > 1 will there be excess C available to form carbonaceous grains.

In order for the star to have C/O > 1 and form SiC, the products of He burning must be mixed with the convective envelope during repeated episodes of TDU. The main product of He burning is $^{12}C$, created via the triple-α-process (Meyer and Zinner 2006). A large abundance of neutrons are also released through the $^{13}C(\alpha,n)^{16}O$ and $^{22}Ne(\alpha,n)^{25}Mg$ reactions, fueling the strong s-process component, which is responsible for producing most of the elements from Fe up to $^{208}Pb$ and $^{209}Bi$ (Busso et al. 1999). Helium burning leaves the star rich in $^{14}N$ and the s-process elements, as well as C/O > 1, all of which are hallmarks of SiC mainstream grains. An extra-mixing process during third dredge-up (TDU), known as cool bottom processing (CBP), decreases the $^{12}C/^{13}C$ ratio in the star and can possibly match the $^{12}C/^{13}C$ ratios measured in AB grains (Amari et al. 2001b; Wasserburg et al. 1995); however, the low $^{14}N/^{15}N$ ratios and the lack of s-process enrichments are still problematic, at least for some AB grains. Hot bottom burning (HBB), a process that occurs in intermediate mass (4 – 7 $M_{\odot}$) stars, could also decrease the $^{12}C/^{13}C$ ratio to as low as ~3, but the $^{14}N/^{15}N$ ratios are expected to be as high as $3 \times 10^4$ and, more importantly, in stars of roughly solar metallicity (a condition that is indicated by the Si isotopic compositions measured in AB grains), HBB prevents the star from becoming C-rich, precluding the formation of SiC (Boothroyd et al. 1995).

AGB nucleosynthesis models have the greatest difficulty explaining the isotopic signatures of AB grains with solar s-process abundances and/or with $^{15}N$ enrichments. Also puzzling is that some AB grains have s-process enrichments, while others do not, and that AB grains display an enormous range of $^{14}N/^{15}N$ ratios. All of these considerations make pinpointing a stellar source for AB grains challenging. As discussed above, AGB stars, with the possible exception of those that undergo some CBP, are not able to reproduce the nucleosynthetic signatures of AB grains. The temperatures in the expanding envelope required for SiC condensation (1390 – 1630 K) (Lodders and Fegley 1995; Sharp and Wasserburg 1995) eliminate hot carbon stars, such as R-type stars (Dominy 1984), while the near-solar metallicity of AB grains eliminates low metallicity carbon stars, such as CH-type stars (Barbuy et al. 1997).

One possible source of AB grains with no s-process enrichments are the poorly understood J-type stars. These enigmatic stars are similar to N-type stars in many ways: both are cool, luminous stars located at the extreme red end of the HR diagram [although it is debated whether or not J stars are actually on the AGB (Abia and Isern 2000)] with similar effective temperatures (Amari et al. 2001c). Astronomical observations indicate that J stars have $^{12}C/^{13}C < 10$, are not enriched in the s-process elements over the other heavy elements, are of approximately solar metallicity, and likely represent 5 – 15% of the cool carbon star population (Abia and Isern 2000; Lambert et al. 1986). Also puzzling are the enhanced Li abundances in most J stars (Chen et al. 2007) and the silicate infrared emission features in their circumstellar disks, observed along with those emission lines characteristic of SiC, measured in ~20% of J stars (Little-Marenin 1986). Unfortunately, there are no reliable N isotopic measurements for J stars, except for a

study that places the very loose constraint that $^{14}N/^{15}N > 70$ in J stars (Wannier et al. 1991).

While over one hundred J stars have been discovered (Chen et al. 2007), their evolutionary history remains poorly understood. Observations of the low $^{12}C/^{13}C$ ratios and lack of s-process elements suggest that the CNO cycle is operating in J stars without the $^{13}C$ neutron source, but the reason for this is unclear. One of the leading hypotheses suggests that J stars are part of a binary system (Chen et al. 2007). Oxygen-rich material could be trapped in the disk of a companion star, which would explain the silicate emission features of J stars; however, a causal link between the binary system and the low $^{12}C/^{13}C$ ratios, Li abundances, and lack of s-process elements has yet to be explained, although some type of non-standard tidal-induced mixing has been proposed (Abia and Isern 2000; Chen et al. 2007). An alternate theory is that J stars are evolved R stars, and possibly even the evolutionary link between R stars and N stars (Abia and Isern 2000). In this scenario, CBP could account for the low $^{12}C/^{13}C$ ratios and the $^{18}O$ depletions measured in J stars and could also produce $^{7}Li$ via the Cameron-Fowler mechanism (Boothroyd and Sackmann 1999; Cameron and Fowler 1971). If J stars represent the early AGB phase, only a few TDU episodes would have occurred, leaving the star with little or no s-process element enhancements (many TDU episodes are required for the s-process enrichments observed in both N stars and mainstream grains). However, quantitative analysis of the full implications of this scenario is still lacking, as are the expected ranges of $^{14}N/^{15}N$ ratios for all of these scenarios.

Although J stars are not well understood, it is clear from many observations that they have solar s-process abundances. It is therefore impossible for them to be the source

of SiC AB grains that have significant s-process enrichments. This discrepancy prompted Amari et al. (2001c) to look for a second source for AB grains. They suggested that the most likely sources of SiC AB grains with s-process enrichments are born-again AGB stars. These are low- to intermediate-mass evolved stars that undergo a very late thermal pulse (VLTP) as they pass through the planetary nebula phase and descend along the white-dwarf cooling path (Fujimoto 1977). A VLTP is predicted to occur in 10 – 25% of stars that pass through the planetary nebula phase. During the VLTP, the star experiences a final He-shell flash, which drives the convection zone into the H-rich envelope and sends the star back to the AGB phase, where the remaining H is burned in the CNO cycle. Freshly synthesized material, rich in $^{13}C$, is mixed to the surface, leaving the star H-deficient and with a low $^{12}C/^{13}C$ ratio (Herwig 2001; Herwig et al. 1999).

Although a significant minority of low- to intermediate-mass stars are expected to go through the born-again phase, they are predicted to spend only 100 – 1000 years there, with observations indicating that the He-flash lasts only a few years (Asplund et al. 1999; Herwig 2001; Lawlor and MacDonald 2003). The brevity of this phase is why only three examples of born-again stars have been observed (FG Sagittae, V605 Aquilae, and V4334 Sgr), but it is fortunate that many detailed observations exist, particularly in the case of V4334 Sgr. This object, better known as Sakurai's Object, was first observed in 1996 and has been carefully studied since (Asplund 1999; Asplund et al. 1997; Asplund et al. 1999). The chemical and isotopic composition, along with the temperature, of Sakurai's Object were observed to change dramatically within just a year (Asplund et al. 1997). Unfortunately (from an observational standpoint), Sakurai's Object rapidly developed a dense wind in which grains could condense, completely obscuring any

optical observations. However, radio observations were able to continue and may indicate that Sakurai's Object is already entering the planetary nebula phase for the second time, suggesting it is evolving even more rapidly than theoretical models predicted (Hajduk et al. 2005).

Initial observations of Sakurai's Object indicated it was rich in C, N, and O, but deficient in H, with C/O > 1 (Duerbeck and Benetti 1996). Later, high-resolution spectroscopic data compiled over the ~3 years during which Sakurai's Object was optically visible confirmed that it is C-rich and further constrained the $^{12}C/^{13}C$ ratio to $1.5 \leq {}^{12}C/{}^{13}C \leq 5$ (Asplund 1999). During this period, it was also observed that in Sakurai's Object: the abundance of the s-process elements increased by a factor of 4, resulting in the largest enrichments in the light s-process elements in any AGB or post-AGB star ; the H abundance dropped by a factor of 10; the Li abundance increased dramatically, making Sakurai's Object more Li-rich than any AGB star; the temperature dropped by 1500 – 2500 K; and the C, N, and O abundances remained relatively constant (Asplund 1999). While only elemental abundances have been measured for N, theoretical models predict large enrichments in $^{14}N$ (Herwig 2001), suggesting born-again AGB stars could be the source of SiC AB grains with s-process enrichments and $^{14}N/^{15}N$ > solar; however, as discussed above, CBP in AGB stars cannot be ruled out as a possible mechanism for producing this subset of AB grains (Amari et al. 2001c).

Although the origin of AB grains and the mechanisms that produce the nucleosynthetic signatures of these grains are not well constrained, the compositions of the AB grains themselves are. However, for the most complete constraints on the formation of AB grains, isotopic analysis must be combined with TEM microanalysis

(e.g., Croat et al. 2003; Croat et al. 2005; Hynes et al. 2010). Detailed structural and chemical analyses done with the TEM can provide important insights into the formation conditions in circumstellar environments. TEM analysis also provides insight into new or rare presolar phases that are too small or too rare to be observed astronomically and sometimes even during isotopic analysis (e.g., Croat et al. 2003; Croat et al. 2005; Hynes et al. 2010). These rare phases are present in SiC as internal subgrains.

Extensive work on the microstructure of SiC grains has been done by Daulton et al. (2003), but for most of these grains, no corresponding isotopic data exist. It is therefore impossible to know what type (e.g., AB, X, mainstream) of SiC each grain is, but statistically, >90% of the grains are mainstream grains. While isotopic measurements exist on over 550 AB grains, only a handful have been studied in the TEM, and these have only been analyzed for their microstructure (Daulton et al. 2006; Daulton et al. 2009); no AB grains have previously been analyzed for their chemical composition, mineralogy, or internal subgrains. Because the origin of AB grains remains enigmatic and little is known about the most likely stellar sources of these grains, particularly J stars, a microanalytical study of SiC AB grains could yield important insights into some of the conditions present in the envelopes of the parent stars of AB grains during the time of grain growth and condensation, as well as place additional constraints on the type of stars that could produce these grains. Furthermore, since AB grains are the only type of SiC grains thought to originate from two different types of sources (Amari et al. 2001c), TEM analysis might reveal microstructural differences between AB grains from these sources.

In this study, we present a coordinated TEM and NanoSIMS study of seven SiC AB grains from the Murchison meteorite, selected on the basis of their low $^{12}C/^{13}C$ ratios. These seven grains were analyzed for the: isotopic and chemical composition; crystal structure, commonly referred to as the polytype; crystal domain size; and chemical and microstructural properties of any subgrains found within these SiC AB grains.

## 3.2 Experimental Methods

### 3.2.1 Isotopic Characterization

An aggregate of SiC grains from the KJG size separate (2.1 – 4.5 μm observed size) of the Murchison CM chondrite (Amari et al. 1994) was pipetted onto a gold foil for subsequent analysis. The $^{12}C/^{13}C$ and $^{28}Si/^{30}Si$ ratios were then measured by ion imaging with the Washington University IMS 3f ion probe. The grains with the lowest $^{12}C/^{13}C$ ratios were selected as the most likely AB candidates and their positions were located with a JEOL 840A SEM before further analysis in the Washington University Cameca NanoSIMS. The high sensitivity and high mass resolution of the NanoSIMS was necessary to obtain precise isotopic measurements on the grains, as well as to confirm the SiC grain type. Negative secondary ions of $^{12}C$, $^{13}C$, $^{12}C^{14}N$, $^{12}C^{15}N$, $^{28}Si$, $^{29}Si$, and $^{30}Si$ were measured with a $Cs^+$ ion beam in the NanoSIMS; no additional isotopes were measured in order to minimize grain sputtering and to preserve as much material as possible for later TEM analysis.

### 3.2.2 TEM Sample Preparation and Characterization

After conclusive isotopic identification as AB grains, seven of these grains were selected for additional study in the TEM. The grains were removed from the Au foil mount with a well-sharpened, clean tungsten needle with an ~1 μm diameter tip and were placed in a gelatin capsule, along with three carbon fibers to later aid in locating the grain, while the entire process was monitored with an optical microscope. The grain was then covered with ~20 μL of LR White Hard resin and cured in a vacuum oven for approximately 48 hours at 60 – 70˚ C to allow the resin to harden. Once the resin was sufficiently cured, the capsule was placed inside a second capsule, which was subsequently filled with resin and cured for 48 hours at 70˚ C in a regular oven to be certain that the resin was sufficiently hard for slicing. The gelatin capsule was then removed, leaving the SiC grain and the carbon fibers embedded in hard resin. The top of the resin block was trimmed with a Reichert-Jung Ultracut E microtome equipped with a glass knife into a multi-step pyramid structure, with the top step ~250 x 250 μm in size and containing the SiC grain and carbon fibers. The top step was then sliced with the ultramicrotome, now fitted with a diamond knife, into 70 nm-thick sections. The slices floated into an attached water reservoir, where they were picked up with a 3 mm wire loop and deposited onto holey carbon-covered 75 mesh Cu TEM grids.

Microanalysis of the SiC AB grains was performed with a JEOL 2000FX TEM. The polytype of each crystal domain in the SiC grains was determined primarily from CBED patterns. These were obtained by tilting the crystals along both orthogonal axes of the sample stage goniometer, employing Kikuchi bands as a guide to locate low-index zones for each crystal domain. Due to the hardness of SiC, significant fracturing of the

grains occurred during the ultramicrotomy process (Figure 3.1), although this did not affect our ability to determine the crystal size, structure, or epitaxial relationship of the grains, utilizing the procedure described in detail in Section 2.3. Briefly, the sample was tilted over an ~5˚ range around both axes of the sample stage goniometer to locate a zone axis for each piece of the SiC grain. A CBED diffraction pattern was acquired from each of these pieces and subsequently analyzed. If the individual pieces of SiC were part of a larger crystal domain that was broken apart during ultramicrotomy, these pieces would have the same crystallographic orientation, and therefore the same zone axis pattern, at roughly the same goniometer angle. However, if the pieces were orientated along different zone axes at roughly the same goniometer angle, then the pieces would be inferred to be separate crystal domains. If any ambiguity persisted, additional diffraction patterns were acquired at different crystallographic orientations to clarify the crystal domain size of the SiC pieces. Additional diffraction patterns were also obtained for low-index zones to confirm the polytype of each crystal domain. In this way, the polytype, crystal domain size, and epitaxial alignment among pieces of the SiC AB grains were ascertained.

The chemical composition of each grain was determined with a NORAN Vantage EDXS, which allowed the identification of all elements with $Z \geq 5$. Background subtraction and peak-fitting, with special attention paid to overlapping peaks, were done with a combination of in-house software, which is described in detail by Croat et al. (2003), and NORAN-based software. Qualitative analysis was performed with k-factors obtained from the basaltic glass USNM 113498 geologic standard. For cases in which

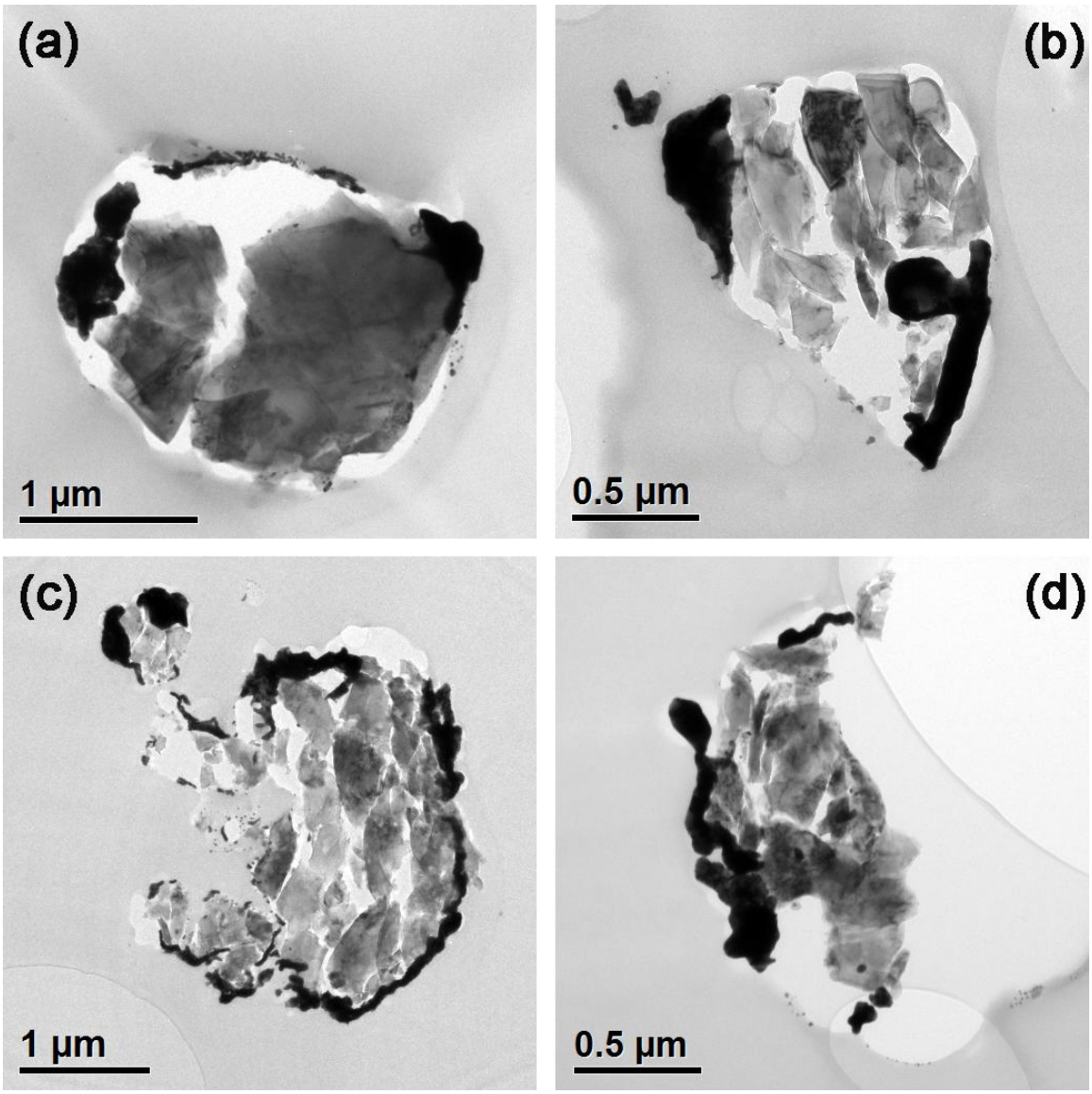


Figure 3.1: TEM BF images of 70-nm-thick slices of four SiC AB grains, showing typical examples of the general condition of the slices after ultramicrotomy. Although the slices have a somewhat broken appearance due to the slicing process, it does not affect the crystallographic properties of the grains. Individual crystal domains are visible in the slices due to orientation dependent diffraction contrast and the solid black areas around the perimeter of the slices are gold deposited on the slices during NanoSIMS analysis. (a) Grain KJG-N4-369-5. (b) Grain KJG-N4-259-1. (c) Grain KJG-N4-468-1. (d) Grain KJG-N4-354-5.

elemental peaks (such as Al) were not detected, an upper limit of 2σ of the background counts in the energy region of interest was placed on the concentration.

The AB grains were also analyzed for any internal subgrains present in the grain. Each slice was systematically rotated through ±30° about one axis of the sample stage goniometer while being observed at ~$10^5$x magnification for changes in the diffraction contrast. This method was used to identify potential subgrain candidates as small as ~15 nm and the composition of each subgrain candidate was then determined with EDXS. Once the composition of each subgrain was established, the crystal structure was determined by analyzing CBED patterns obtained after rotating the sample to low index crystallographic zones of the subgrains. The known d-spacings of the surrounding SiC were used as calibration.

## 3.3 Results

### 3.3.1 Isotopic Composition

The isotopic compositions of the seven AB grains in this study are reported in Table 3.1. All of the grains have $^{12}C/^{13}C < 10$, which clearly identifies them as AB grains. The $^{14}N/^{15}N$ ratios of the grains are also all anomalous, with the $^{14}N/^{15}N$ ratios of two grains appreciably higher than solar and the $^{14}N/^{15}N$ ratios of three grains significantly lower than solar; the $^{14}N/^{15}N$ ratios of the remaining two grains are only slightly less than the solar value. The small number of grains with $^{14}N/^{15}N >$ solar is not surprising, given the low $^{12}C/^{13}C$ ratios of all of the grains; low $^{12}C/^{13}C$ ratios tend to be

Table 3.1. Isotopic and elemental compositions of SiC AB grains (± 1 σ errors).

| Grain label | $^{12}C/^{13}C$ | $^{14}N/^{15}N$ | $\delta^{29}Si/^{28}Si$ [a] (‰) | $\delta^{30}Si/^{28}Si$ [a] (‰) | Atomic % Mg[b] | Atomic % Al[b] |
|---|---|---|---|---|---|---|
| KJG-N4-259-1 | 3.25 ± 0.01 | 71.5 ± 0.9 | -5.42 ± 2.44 | 12.75 ± 3.40 | < 0.2 | < 0.3 |
| KJG-N4-315-2 | 2.89 ± 0.01 | 94.0 ± 1.0 | -6.78 ± 2.42 | 10.08 ± 3.38 | < 0.2 | 1.6 ± 0.2 |
| KJG-N4-354-5 | 2.24 ± 0.01 | 121.4 ± 1.4 | 63.91 ± 2.48 | 49.85 ± 3.45 | 0.5 ± 0.2 | 6.3 ± 0.1 |
| KJG-N4-369-5 | 2.29 ± 0.01 | 246.9 ± 3.8 | -22.75 ± 2.45 | 17.79 ± 3.41 | < 0.3 | 1.0 ± 0.2 |
| KJG-N4-468-1 | 2.75 ± 0.01 | 351.6 ± 6.1 | -0.36 ± 2.40 | -4.47 ± 3.36 | 0.7 ± 0.2 | 17.3 ± 0.2 |
| KJG-N4-451-6 | 3.04 ± 0.01 | 882.0 ± 24.3 | -9.12 ± 2.50 | 7.11 ± 3.47 | < 0.2 | < 0.2 |
| KJG-N4-531-3 | 2.61 ± 0.01 | 246.2 ± 3.8 | 118.63 ± 2.45 | 89.33 ± 3.42 | 1.2 ± 0.3 | 7.1 ± 0.3 |

Notes: [a] Values given in "delta" notation, defined as: $\delta^{i}X/^{j}X \equiv [(^{i}X/^{j}X)_{measured}/(^{i}X/^{j}X)_{\odot}] - 1 \times 1000$.

[b] Maximum atomic percent of Al and Mg quantified in each grain, assuming a grain composed of only Al, Mg, and Si. Carbon is excluded from these quantifications due to large background interferences from the grid substrate.

accompanied by low $^{14}N/^{15}N$ ratios (Amari et al. 2001c). Due to the relatively low sensitivity during ion imaging of the IMS 3f, it can be difficult to distinguish some types of SiC from one another (e.g., an AB grain with $^{12}C/^{13}C = 8$ and a mainstream grain with $^{12}C/^{13}C = 12$). In order to ensure the best chance of selecting AB grains, SiC grains with the lowest $^{12}C/^{13}C$ ratios measured in the IMS 3f were selected as the most likely AB grain candidates and further analyzed in the NanoSIMS. As a result, this study contains predominantly grains with $^{14}N/^{15}N$ ratios less than the solar value as an unintentional consequence of grain selection. However, all of the grains still fall into the range that is typical of AB grains, which can be seen on the $^{14}N/^{15}N$ versus $^{12}C/^{13}C$ plot in Figure 3.2, comparing the grains in this study to other AB grains.

The Si isotopic ratios of all of the grains in this study are also typical of AB grains (Figure 3.3). They fall on or near the mainstream correlation line, which is the line of slope = 1.37 defined by most mainstream and AB grains on a $\delta^{29}Si/^{28}Si$ versus $\delta^{30}Si/^{28}Si$ three-isotope plot (Zinner et al. 2007). This indicates that the grains likely originated in stars of close-to-solar metallicity.

### 3.3.2 Crystal Domain Size and Structure in SiC AB Grains

After isotopic analysis, the grains were ultramicrotomed with a diamond knife in preparation for TEM analysis. During the ultramicrotomy process, the knife tends to shatter the SiC grains, giving each slice a somewhat fractured appearance (Figure 3.1). The degree of breakage varies significantly between grains. If the broken pieces are smaller than the crystal domains in the SiC grain, then the determination of crystal size would be lower limits, while the polytype determination remains unaffected. However,

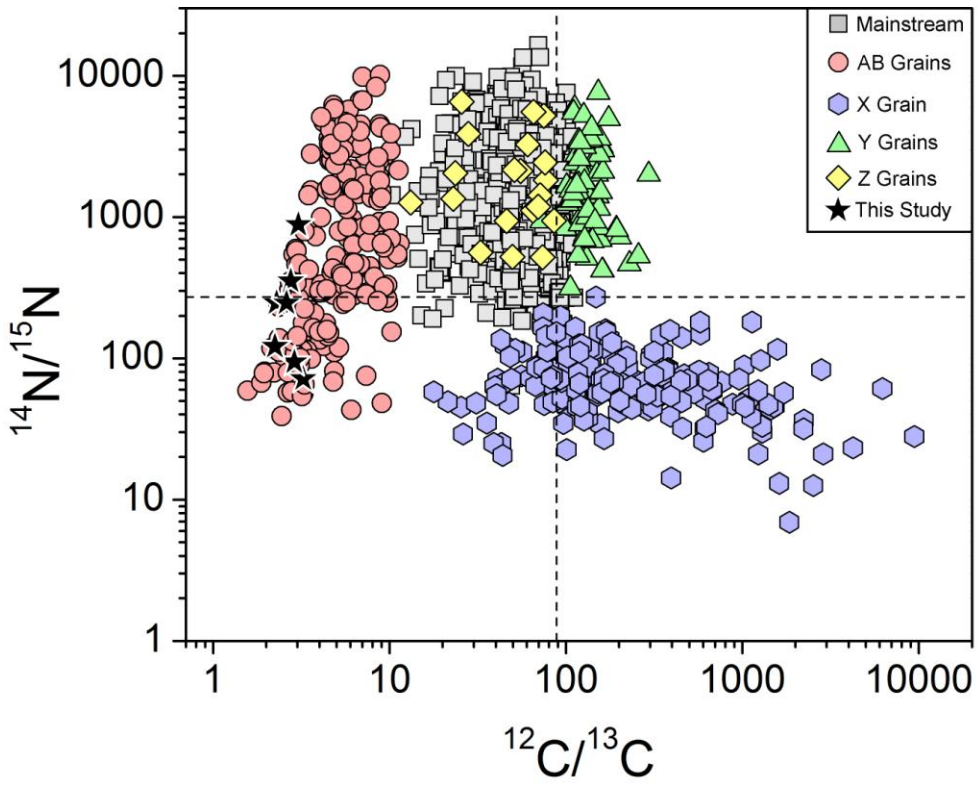


Figure 3.2: Plot of the C and N isotopic ratios of the seven AB grains in this study. For comparison, these data are plotted along with isotopic ratios of other presolar SiC grains (Hynes and Gyngard 2009). The plot clearly shows the characteristically low $^{12}C/^{13}C$ ratios and the significant range of the $^{14}N/^{15}N$ of the grains in this study and of AB grains in general. The dashed lines represent the solar $^{12}C/^{13}C$ and $^{14}N/^{15}N$ ratios.

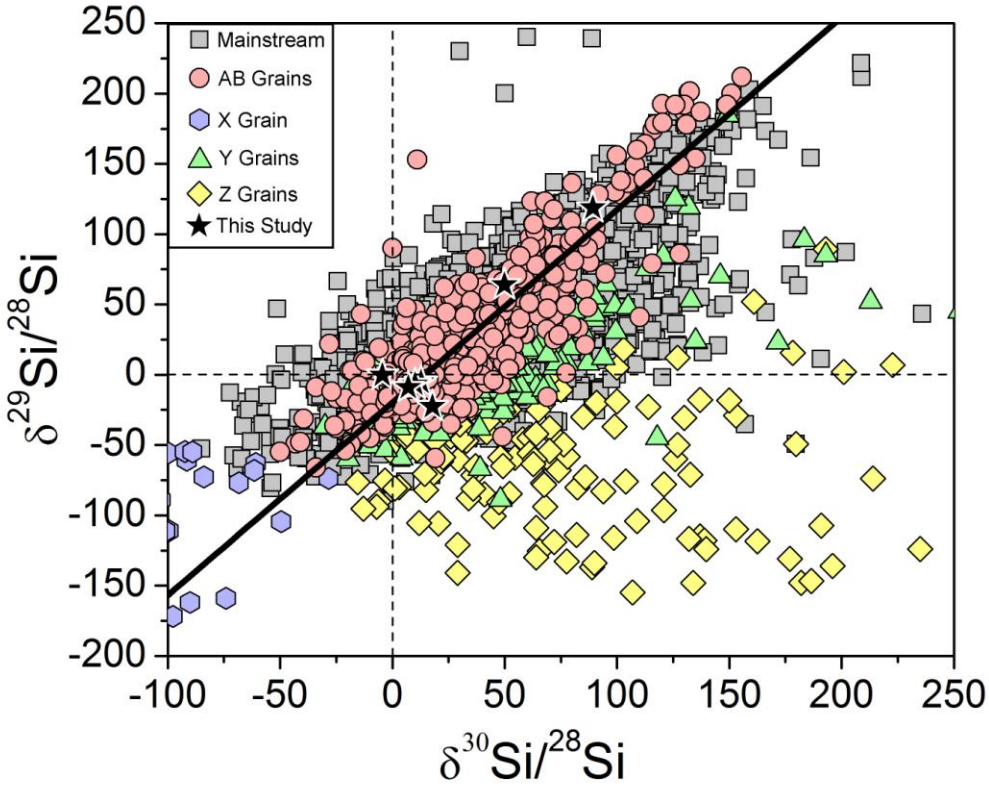


Figure 3.3: Plot of the Si isotopic ratios of the seven AB grains in this study expressed as δ-values, or deviations from the solar isotopic ratio (which is indicated by the dashed lines) in parts per thousand (‰). For comparison, these data are plotted along with delta values of other presolar SiC grains (Hynes and Gyngard 2009). The solid black line is the mainstream correlation line, along which most mainstream and AB grains fall (Zinner et al. 2007).

an advantage of ultramicrotomy is that it produces multiple slices of each grain from throughout the volume of the grain for analysis.

Each AB grain was observed to be an aggregate of several smaller SiC crystal domains; however, the number and size of the crystal domains varies significantly between grains and, to a lesser extent, between crystal domains in a single grain (Figure 3.4). The minimum number of crystal domains, the average size of the domains, and the polytypes observed in each SiC grain are listed in Table 3.2. Six of the SiC grains are composed of at least 3 – 6 crystal domains of roughly similar size, ranging from 130 – 720 nm in diameter, with a median diameter of 343 nm. Of these six grains, only two contain crystal domains as large as 700 nm, with one such domain in grain KJG-N4-451-6 and two in grain KJG-N4-468-1. Excluding these three larger domains, the rest of the crystal domains observed in these six AB grains have a much smaller range in size, from 130 – 470 nm. However, the exclusion of these three larger domains only changes the median diameter to 331 nm, indicating that the vast majority of the crystal domains are in the 200 – 400 nm range. It is important to note that these values represent lower limits to the size and number of crystal domains in AB grains. Some material can be lost during slicing and most of the slices sample the grain off-center. Only slices that are relatively intact are included in the crystal domain size estimates, so as to get the most accurate determination possible; slices that are very small or severely fractured are not included here, since the observed domain size in these slices is most likely not indicative of the true crystal domain size. The apparent crystal domain sizes of the most fractured slices of SiC are as small as 40 nm, which is probably artificially small.

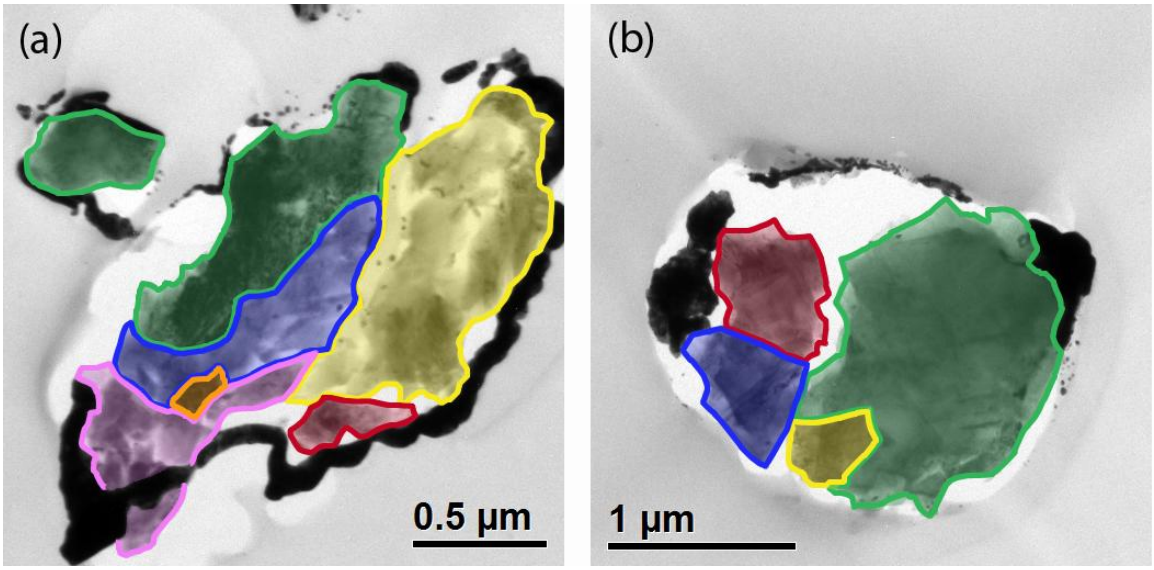


Figure 3.4: TEM BF images of two AB grains with false-color overlays indicating the crystal domains in each slice. (a) The crystal domains in grain KJG-N4-468-1 are typical of six of the seven AB grains in this study (343 nm average minimum domain size). This slice is composed of a minimum of six crystal domains, each indicated here by a different color. The yellow, orange, and blue domains index to the 3C polytype; the red and pink domains index to the 2H polytype; and the green domain indexes to an intergrowth of the 2H and 3C polytypes. (b) The average crystal domain size in KJG-N4-369-5 is significantly larger than any of the other AB grains. The large green domain (1.31 µm geometric mean diameter) is nearly twice the size of the largest domain observed in any of the other AB grains. This domain indexes to the 2H polytype. The red and blue domains (each ~500 nm mean diameter) are also larger than most of the crystal domains in the other six AG grains. The red domain and the small yellow domain both index to the 3C polytype, while the blue domain indexes to an intergrowth of the 3C and 2H polytypes.

Table 3.2. Grain morphology and crystal domain size in SiC AB grains.

| Grain label | Number of domains[a] | Median domain size (nm)[b] | Polytype |
|---|---|---|---|
| KJG-N4-259-1 | 3 | 33.4 | 3C |
| KJG-N4-315-2 | 5 | 33.0 | 3C, 2H |
| KJG-N4-354-5 | 4 | 42.3 | 3C |
| KJG-N4-369-5 | 4 | 53.6 | 3C, 2H, intergrowth |
| KJG-N4-468-1 | 6 | 34.3 | 3C, 2H, intergrowth |
| KJG-N4-451-6 | 5 | 32.8 | 3C, intergrowth |
| KJG-N4-531-3[c] | | | 3C |

Notes: [a] The minimum number of domains in each AB grain.
[b] The minimum geometric median diameter of the crystal domains in each AB grain. Due to the effects of ultramicrotomy, some material can be lost during slicing.
[c] Insufficient material was available for grain KJG-N4-531-3 to make an accurate estimate of the number of crystal domains or of their size.

Only one AB grain contains a crystal domain that is much larger than those observed in the other AB grains. Grain KJG-N4-369-5 is composed of four crystal domains (Figure 3.1a and Figure 3.4b). Two of the crystal domains are 516 – 555 nm in diameter, with a smaller 290 nm crystal between them. The largest domain comprises the bulk of the grain and is 1.31 μm, nearly twice the diameter of the next largest crystal domain observed in any of the AB grains in this study. Grain KJG-N4-369-5 is also the least fractured grain in this study; it has just a single fracture, with the two mid-sized domains cleaved from the other two domains. Since very little material was lost from this grain, the estimates of the crystal domain sizes in grain KJG-N4-369-5 are therefore probably very close to the true domain sizes in this grain.

To better understand how the AB grains formed, the relationship between adjacent crystal domains was also investigated. For each AB grain, diffraction patterns from low index zones were obtained from neighboring crystal domains at similar sample

orientations. Only contiguous crystal domains from an unbroken area of the AB grain were analyzed in this way. Analysis of these CBED patterns clearly indicates an epitaxial relationship between adjacent crystal domains, with planes of neighboring crystal domains aligned within 0.8° – 10°, and all but three of the domains aligned within 5°. This range was observed in all of the AB grains for which suitably intact slices were available. Close alignment between low index planes of neighboring crystal domains is expected if the domains grew epitaxially and implies that the individual crystal domains that compose the larger SiC grain share common growth planes; if the SiC grain were a mechanical aggregate of crystallites that formed independently and later coalesced, then well-aligned crystallographic planes between adjacent domains would be highly unlikely, particularly for multiple domains in a single grain. This type of epitaxial growth is consistent with what has been previously observed in SiC mainstream and X grains (Hynes et al. 2010).

The polytype of each crystal domain was determined along with its size. The majority (~78% by number) of the domains were conclusively indexed to the 3C polytype (fcc; a = 4.36 Å). This is consistent with previous observations of SiC grains, which indicate that 3C is the dominant polytype of presolar SiC (Daulton et al. 2003; Hynes et al. 2010). A common feature of cubic materials is the presence of twinning, in which a low-energy boundary is created when a stacking fault forms across close-packed tetrahedral planes. The abrupt reversal of the stacking sequence creates a mirror image of itself (for a more extensive discussion, see Chapter 2.3.4, as well as Daulton et al. 2003, and references therein). In presolar SiC, the most common type of twinning, occurring in ~95% of twinned SiC grains, is first-order coherent twin boundaries in <011> zones

created by a 70.5° rotation (plus an extra 180° to align the C-Si bonds) about an axis perpendicular to a {111} plane (Daulton et al. 2003). This can be observed as a slightly dimmer extra spot found at intervals of ⅓ the normal diffraction spot interval for one or both {111} planes in a <011> electron diffraction pattern. In this study, five of seven AB grains have first-order twinning along at least one {111} plane, equating to approximately ⅓ of the 3C-SiC crystal domains. This is similar to the percentage of twinned grains observed in other types of SiC, including mainstream grains and X grains (Daulton et al. 2003; Chapter 2 of this work). It is also likely that a higher percentage of 3C-SiC crystal domains in presolar SiC are actually twinned than the number measured. Only twinning that occurs along {111} planes that are parallel to the electron beam in the TEM can be resolved, resulting in twinning along two of the four possible {111} planes being unobservable (Bender et al. 1986).

All of the AB grains are primarily composed of crystal domains that index to the 3C polytype, but four of the AB grains also contained a second polytype of SiC: the 2H polytype (hexagonal; a = 3.08 Å, c = 5.03 Å). Three AB grains contained crystal domains that were indexed to only the 2H polytype, representing ~12.5% of the total number of crystal domains analyzed.

Intergrowths between the 3C and 2H polytypes were also observed in three AB grains, two of which also contained 2H-SiC crystal domains. This represents 9.5% of the total number of crystal domains analyzed in the SiC AB grains. Intergrowths are visible as a typical 3C-SiC diffraction pattern with extra spots that cannot be indexed to another 3C-SiC zone or be attributed to twinning. Instead, the extra set of spots indexes to a 2H-SiC zone. Additional diffraction patterns obtained from each intergrowth crystal domain

indicate that most of the crystals are predominantly 3C-SiC. However, DF images obtained from diffraction spots unique to the 2H-SiC zone in the intergrowth pattern indicate that the intergrowth occurs throughout the entire grain. In one grain this was reversed, with additional diffraction patterns indicating that most of the crystal is primarily 2H-SiC, but DF imaging suggesting that the 3C-SiC intergrowths occurs throughout the entire grain. All of the examples of intergrowth observed in the AB grains in this study suggest a fine-scale intergrowth between the two polytypes that occurs throughout the whole grain, not just at an interface of two distinct domains. The two polytypes likely switch back and forth throughout the entire SiC AB grain. No additional polytypes were observed.

The polytypes that were observed in the AB grains in this study, as well as the abundance of each type, are relatively consistent with previous analyses of polytypes in presolar SiC. In a study of 508 randomly selected SiC grains by Daulton et al. (2003), 3C-SiC was observed to be the most abundant polytype (79% by number), just as it was in this study. Daulton et al. also observed that 17% of the grains were 2H-3C intergrowths, while only 3% were 2H-SiC, in contrast to the results of this study, in which the 2H polytype was observed to be slightly more abundant than intergrowths. This discrepancy can likely be explained by the difficulty in observing intergrowths of the 2H and 3C polytypes. The SiC grains in the Daulton et al. study are primarily single crystals (not aggregates like the AB grains in this study) and in cases of an intergrowth between 3C and 2H, each polytype was observed as a distinct crystal domain. The proportion of each of these domains compared to the whole grain varies significantly, ranging from almost entirely 3C-SiC to almost entirely 2H-SiC. However, the

intergrowths observed in the AB grains in this study do not have distinct domains and instead appear to be a close intergrowth occurring throughout the crystal domain, similar to the type of close intergrowth that was previously observed in a SiC X grains (Figure 2.8). The variety of ways in which the 2H and 3C polytypes can create an intergrowth also makes them difficult to observe. If at most orientations, for example, the crystal domain indexes to only the 3C polytype, as was the case for most of the intergrowths observed in this study, it is possible to miss an orientation at which spots indexing to both the 2H and 3C polytypes are visible in the diffraction pattern. This would result in the crystal domain appearing to be only the 3C polytype, while, in reality, it is an intergrowth. The reverse could happen as well if the grain were primarily 2H-SiC. Additionally, the diffraction patterns produced by several major zone axes of 2H-SiC and 3C-SiC have similar d-spacings and interplanar angles, making these patterns inconclusive in determining the polytype of the crystal domain (e.g., the [-112] zone of 3C-SiC and the [01-10] zone of 2H-SiC). In an attempt to minimize these problems, multiple low-index crystallographic zones were located for each crystal domain. However, because significantly fewer crystal domains were analyzed in this study than in the Daulton et al. study (by more than an order of magnitude), a few crystal domains thought to be purely 2H-SiC or 3C-SiC that are actually intergrowths of the two polytypes would significantly change the percentage of each polytype that was observed, thus, at least qualitatively, putting the results of this study in more complete agreement with the Daulton et al. study.

Table 3.3. Internal subgrains within SiC AB grains.

| Grain label | Number of subgrains | Subgrain composition[a] | Abundance[b] (‰) |
|---|---|---|---|
| KJG-N4-259-1 | 2 | (Ti, Zr, Mo, V)C | 5 |
| KJG-N4-315-2 | 0 | | |
| KJG-N4-354-5 | 2 | (Ti,V)C | 3 |
| KJG-N4-369-5 | 5 | (Ti,V)C | 2 |
| KJG-N4-468-1 | 2 | (Ti,V)C | 1 |
| | 7 | CaS | 2 |
| | 6 | Fe carbide | 2 |
| KJG-N4-451-6 | 0 | | |
| KJG-N4-531-3 | 0 | | |

Notes: [a] Denotes the major compositional constituents of the subgrains in each AB grain. See the text for detailed compositional analysis.
[b] If subgrains were found in multiple slices of an AB grain, the abundance is averaged over the total area of the slices.

### 3.3.3 Internal Grains and Trace Elements within SiC AB Grains

Four of the seven SiC AB grains contain internal subgrains of various compositions, with a total of twenty-four subgrains observed in total. This represents the first direct observation of subgrains in SiC AB grains (Figure 3.5). Table 3.3 gives the number of subgrains found in each AB grain, as well as their general compositions and an estimate of their abundances.

EDXS analysis revealed the presence of Ti-rich subgrains in all four of the SiC AB grains in which subgrains were observed, with a total of eleven Ti-rich subgrains observed in total. Multiple Ti-rich subgrains were observed in each of the four AB grains, with as many as five subgrains observed in a single ultramicrotome slice. All of the Ti-rich subgrains are located at the SiC crystal domain boundaries and are euhedral, with well-defined crystal faces. The subgrains were identified as TiC (fcc; a = 4.39 Å),

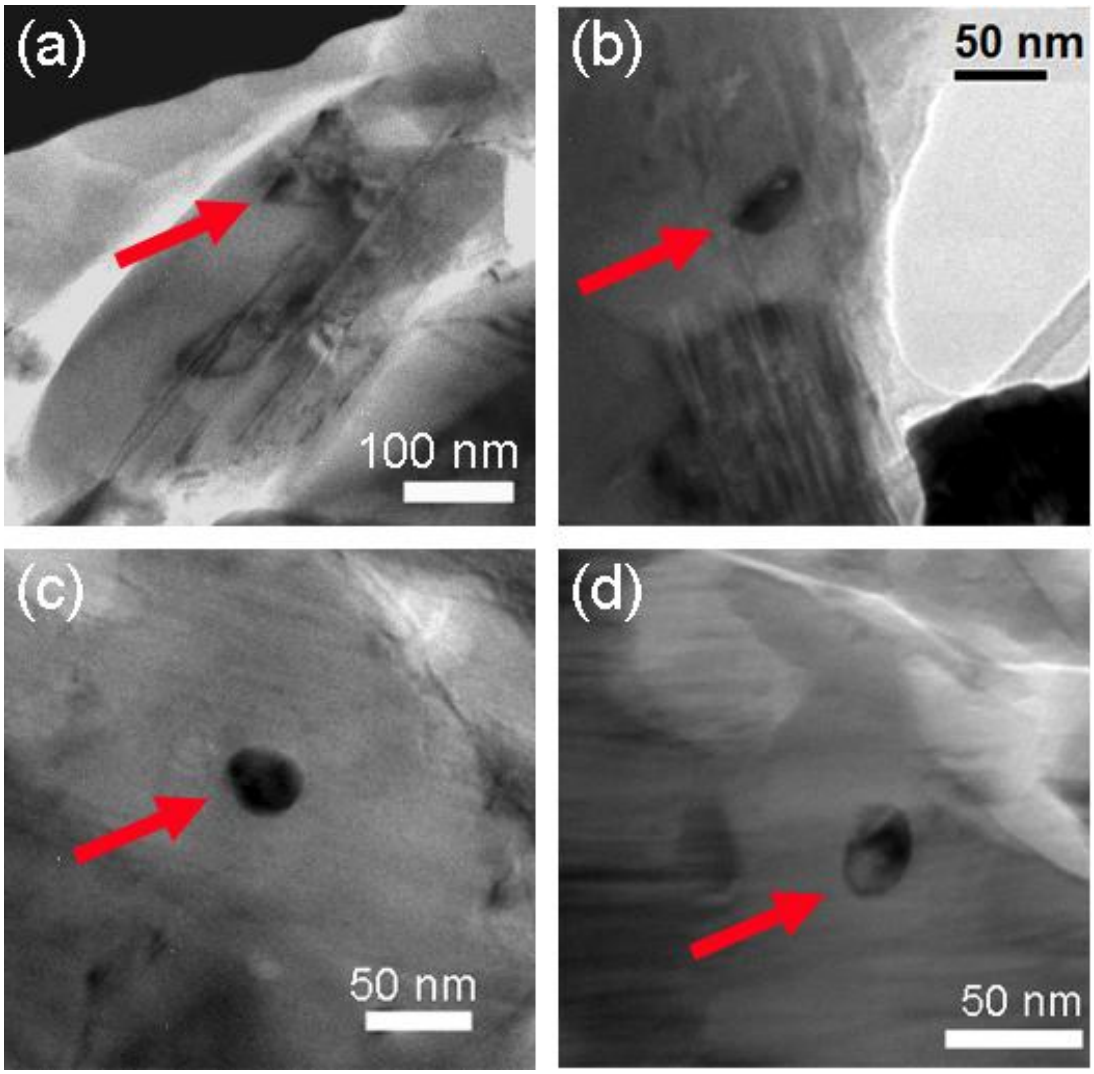


Figure 3.5: TEM BF images of an example of each of the major types of subgrains found in the AB grains in this study. (a) The well-defined crystal faces and the epitaxial alignment of this (Ti, V, Zr)C subgrain with the surrounding SiC domain from KJG-N4-259-1 are evident. Like this subgrain, all of the TiC subgrains were extremely euhedral in shape. (b) Typical example of an Fe carbide subgrain and (c, d) oldhamite subgrains from KJG-N4-468-1. While the Fe carbide subgrain is euhedral in morphology, both of the oldhamite grains are totally anhedral. Like the TiC subgrains, both the oldhamite and the Fe carbide subgrains are epitaxially aligned with the neighboring SiC crystal domains.

which is isostructural with SiC and has a unit cell that is 0.7% smaller than 3C-SiC. Diffraction patterns obtained from the subgrains and the surrounding SiC are consistent with TiC and display a clear epitaxial alignment between the SiC and the subgrains. The geometric mean diameter of the TiC subgrains ranges from 24 – 78 nm, with a median diameter of 38 nm. Utilizing the median diameter, this corresponds to an average abundance of 0.7‰ – 5‰ by volume for TiC subgrains in SiC AB grains. However, this is only a rough estimate of the total abundance, largely due to factors such as variations in the number of TiC subgrains in each slice of SiC, as well the size and the amount of material in the SiC slice.

EDXS analysis also revealed the presence of trace amounts of V in most (73%) of the TiC subgrains. The subgrains all have similar compositions, with approximate concentrations that range from $(Ti_{84}V_{16})C$ to $(Ti_{92}V_{8})C$ (this assumes a grain composed only of Ti and V; C is not quantified due to large interferences from the surrounding SiC and the C substrate). It is, however, not surprising to find small amounts of V present in the in the TiC subgrains, for two reasons. First, V is chemically very similar to Ti and both elements are highly refractory, with identical temperatures predicted for condensation in solid solution with SiC (Lodders and Fegley 1995). Furthermore, TiC and VC are isostructural, with C in the interstitial sites, which allows VC to be in solid solution with TiC, up to a solubility limit of 34 atomic percent (at%) at high temperatures (Upadhyaya 1996). The Ti/V ratios of the subgrains are well within this limit, with V present at ~10 – 20 at%. The V/Ti ratios measured in the subgrains are, however, close to the solar V/Ti abundance (12 at%) (Lodders 2003). An upper limit of

3.0 at% can be placed on the V content in the subgrains in which V was not detected, which corresponds to a V/Ti ratio that is only 25% of the solar abundance.

In studies for which the presence of internal subgrains was investigated, including the results of this study, TiC has been observed in seven of thirteen SiC grains that have an origin in low-mass carbon stars (Bernatowicz et al. 1992; Stroud and Bernatowicz 2005; Stroud et al. 2003; Stroud et al. 2002). However, this abundance is probably low, due to the FIB technique used to prepare several of these SiC grains for TEM analysis. While there are many advantages to FIB, one drawback of the technique is that it provides only one slice of the grain for analysis, which would limit the chances of finding a subgrain in the slice available for analysis. A similar situation exists for two of the SiC AB grains in this study for which no subgrains were observed; a limited number of slices of these AB grains were available for analysis. Therefore, it is likely that most SiC grains with an origin in low-mass carbon stars actually contain TiC subgrains.

This is further supported by indirect measurements in the NanoSIMS of TiC subgrains (Gyngard 2009). A large suite of 238 randomly selected presolar SiC grains were analyzed for their C, N, Si, Ti, and V isotopic compositions. The grains included all of the major types of SiC grains, with the exception of X grains, of which none were indentified amongst the 238 grains. In NanoSIMS analysis, Ti-rich subgrains can be identified in the depth profile of the grain as a significant increase and subsequent decrease in the Ti signal. Titanium-rich subgrains were observed in ~80% of the SiC grains in the study. Although NanoSIMS analysis cannot reveal the mineralogy of the subgrains or even definitively identify them as TiC, the detection of Ti-rich subgrains in the NanoSIMS, coupled with existing TEM evidence for the presence of TiC in presolar

SiC grains (e.g., Bernatowicz et al. 1992), strongly suggests that the Ti-rich subgrains are most likely TiC. NanoSIMS analysis also revealed that in most (97%) of the SiC grains in which both Ti and V were measured, the $^{51}V$ signal precisely matched the Ti signal, indicating that the subgrains are Ti-V-rich, or, most probably, (Ti, V)C. This is consistent with the observations of this study, which suggests that most of the TiC subgrains contain trace amounts of V, with V/Ti ratios close to the solar value.

S-process elements were only observed in the spectra of one AB grain in this study. Trace amounts of Zr and Mo, along with Ti and V, were measured in one subgrain in SiC grain KJG-N4-259-1, while only Zr, Ti, and V were measured in a second subgrain. The compositions of these two subgrains are $(Ti_{86.2}V_{8.7}Zr_{3.6}Mo_{1.5})C$ and $(Ti_{86.4}V_{8.1}Zr_{5.5})C$, which corresponds to an enrichment in the Zr/Ti and Mo/Ti ratios of 9 – 16 times the solar abundance of these elements (Lodders 2003). In the other SiC AB grains for which s-process elements were not detected, Zr and Mo could be present at concentrations up to 0.4 at% in the TiC subgrains, which corresponds to roughly solar abundance (Lodders 2003). Because the solar abundance of these s-process elements is very low, enrichments are required for detection above the EDXS background signal. Aside from their composition, the (Ti, V, Zr, Mo)C subgrains are indistinguishable from the other TiC subgrains, with similar size, shape, and structure. As with the (Ti, V)C subgrains, this is not surprising; Zr and Mo are both refractory elements, which are predicted to condense in solid solution with SiC at the same temperature as TiC (Lodders and Fegley 1995), and ZrC and MoC are isostructural with TiC, allowing them to be present in solid solution with TiC over a wide compositional range.

Only one of the seven SiC AB grains studied contains a type of subgrain other than TiC. Grain KJG-N4-468-1 contains seven Ca-S-rich subgrains and six Fe-rich subgrains, in addition to two (Ti, V)C subgrains. Each type of subgrain is present in multiple slices of the SiC grain, resulting in a total subgrain abundance of roughly 3 – 12‰ by volume. At the upper range, this is a higher abundance than was observed in any of the other AB grains, although as with the other SiC grains, abundances are difficult to precisely determine. The subgrains are all similar in size, ranging from 16 – 40 nm in diameter, with a median diameter of 27 nm.

Compositional and crystallographic analysis conclusively identified the seven Ca-S-rich subgrains as oldhamite (CaS; fcc; a = 5.696 Å), making it the first observation of oldhamite in presolar grains. Although oldhamite is commonly observed in enstatite and achondrite meteorites as the principal carrier of the Rare Earth Elements, it has not, to the best of our knowledge, been observed in any carbonaceous chondrites like the Murchison meteorite (e.g., Crozaz and Lundberg 1995; Floss and Crozaz 1993; Hsu 1998). This makes it unlikely that the oldhamite subgrains could be contamination from the meteorite matrix. Moreover, the oldhamite subgrains are distributed throughout the SiC AB grain, with no subgrains found at the edge of the SiC slice. When the sample is tilted over a large range of goniometer angles (±45°), the oldhamite subgrains are observed to clearly be internal to the SiC grain.

The oldhamite subgrains are all located along SiC crystal domain boundaries and are closely aligned with the SiC crystals. For example, for the subgrain shown in Figure 3.6, the (220) plane of the SiC is aligned within 1.8° of the (13-1) plane of the oldhamite subgrain, clearly indicating an epitaxial alignment between the two. Similarly close

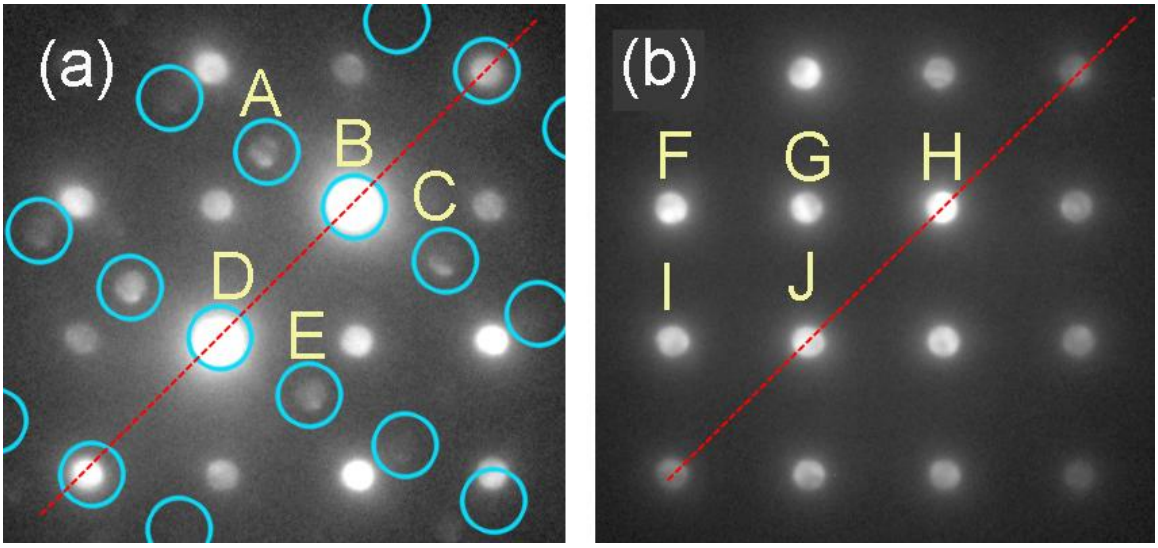


Figure 3.6: (a) Diffraction pattern of an oldhamite subgrain in KJG-N4-468-1 (subgrain pictured in Figure 3.5d at a different orientation). The [013] diffraction pattern (indicated by the blue circles) originates from the oldhamite subgrain, while the [001] diffraction pattern (uncircled spots) originates from the surrounding SiC crystal domain. Because the oldhamite subgrain is smaller than the thickness of the SiC slice, a contribution from the surrounding SiC crystal domain is unavoidable. (b) A [001] diffraction pattern from the SiC crystal domain that borders the oldhamite subgrain, taken at the same orientation as in (a), but away from the subgrain. The red dashed lines in (a) and (b) correspond to the (220) plane of the SiC and the (13-1) plane of the oldhamite, which are aligned within 1.8°, indicating an epitaxial alignment between the two. The yellow letters in (a) and (b) above some of the spots represent indexing of the diffraction spots from the oldhamite and SiC, respectively, that correspond to: A = (100); B = (000); C = (-100); D = (13-1); E = (-13-1); F = (100); G = (000); H = (-100); I = (110); and J = (010).

alignments were observed between the planes of the SiC crystals and the oldhamite subgrains for all seven cases. Although the oldhamite subgrains are located along the SiC crystal domain boundaries, there is no visible alignment between the SiC crystal domain faces and the oldhamite grains, such as was evident with the TiC subgrains, due to the anhedral morphology of the oldhamite subgrains (Figure 3.5c, d). They are all similarly rounded in shape, with no evidence of the crystal faces remaining. Although oldhamite is extremely soluble in water, recent exposure to water could not have caused the subgrains to become anhedral. Due to the nature of TEM analysis, a TEM is only able to provide imaging information on the morphology of the sample in the plane perpendicular to the electron beam; one is unable to obtain any information about the morphology of the third dimension of the sample, which is parallel to the beam. Therefore, although the subgrains were observed to be roughly round in shape and have an average diameter of 29 nm, with none of the subgrains exceeding 40 nm in diameter, it is only possible to estimate their total volume. However, given their roughly circular appearance in the TEM, it is reasonable to assume that the subgrains are approximately equant and have a maximum diameter of ~40 nm in all directions. This is considerably smaller than the 70-nm-thickness of the SiC slice, which suggests that most of the subgrains are surrounded by SiC material. This means the oldhamite is probably completely encased in SiC and effectively protected from any moisture. Evidence of this is found in the diffraction patterns obtained from the oldhamite subgrains, in which diffraction spots from the surrounding SiC are always present, along with those originating from the subgrain (e.g., Figure 3.6). It is also seen in the EDXS spectra of the subgrains, which always contain a strong Si peak. Furthermore, over the roughly seven

month period during which the oldhamite subgrains were intermittently analyzed, the morphology and size of the subgrains did not change. All seven of the oldhamite subgrains have nearly identical morphologies, and while it is possible that a single subgrain could be at the surface of the slice, it is extremely unlikely that all of the subgrains lie in a single plane that happened to be exactly the same plane through which a slice was made, and this scenario would have to occur for multiple slices of the SiC grain. This would result in the oldhamite subgrains being on the surface of the SiC slice, where they could be exposed to water.

Oldhamite is the most abundant subgrain type observed in AB grain KJG-N4-468-1, both by number and by volume, with a total estimated abundance ranging from 1 - 6‰ by volume. In general, the mineral oldhamite tends to be quite homogenous, but it can contain trace amounts of impurities, such as Mg, Na, and Fe (Hsu 1998). However, these are generally small and account for < 2 wt%. The compositions of most of the oldhamite subgrains in this study are close-to-stoichiometric CaS, with a maximum deviation of a few atomic percent. Only one oldhamite subgrain significantly differs from a composition of CaS, having a composition of $Ca_{47.0}Fe_{5.3}S_{47.7}$. Iron is commonly found in oldhamite, but the Fe content in this grain (7.9 wt%) is higher than the range usually measured in oldhamite (Hsu 1998). However, the relatively large Fe content of this grain could have an alternate explanation, as discussed below.

The final type of subgrain found in KJG-N4-468-1 is Fe-rich subgrains, of which six were observed, representing an abundance of 0.9 – 6.0‰ by volume. The Fe-rich subgrains are euhedral in shape and similar in size to the other types of subgrains, ranging in diameter from 22 – 36 nm, with a median diameter of 28 nm. Unfortunately, due to

the location of the grain on the sample mount, a conclusive determination of the mineralogy of the subgrains was not possible. However, diffraction patterns obtained from the subgrains, combined with EDXS analysis, were able to limit the likely mineralogy of the subgrains. Possible minerals were initially limited by the EDXS measurements, which revealed the subgrains were composed primarily of Fe, along with some Ni. Like the oldhamite subgrains, the Fe-rich subgrains are smaller than the thickness of the TEM slice and therefore contributions from the surrounding SiC grain are unavoidable. For this reason, the Si and C elemental content of the subgrains cannot be determined, since the strength of these elemental peaks depends strongly on the size of the subgrain (and the corresponding amount of SiC material), as well as on the beam orientation and other factors. However, the relative strength of the O peak, which is extremely low, was constant while measuring both the subgrain and the SiC grain away from the subgrain. This indicates that the O peak is due to the background signal and therefore oxides and silicates are ruled out. The only other trace elements observed in the subgrains' spectra were attributable to a slight overlap from nearby subgrains.

Diffraction patterns obtained from each of the Fe-rich subgrains further constrain the mineralogy of the subgrains. Kamacite and taenite are, by far, the most frequently observed types of Fe-Ni-rich subgrains in presolar grains (Croat et al. 2003; Croat et al. 2005). However, the d-spacings of at least one diffraction pattern from each of the Fe-rich subgrains in this study are too large by 30 – 35% to be either kamacite or taenite (both of which are Fe-Ni metals). An accuracy of better than 5% is expected with the internal calibrations based on the known d-spacings of the surrounding SiC crystal domain, which were used to determine the d-spacings of the subgrains. Additional

analysis showed that the Fe-rich subgrains in SiC AB grain KJG-N4-468-1 are inconsistent with any Fe-Ni metal phase, as well as with a number of other phases, such as troilite (FeS). The best fit to the diffraction and EDXS data are Fe carbides, like $(Fe,Ni)_3C$ (cohenite; orthorhombic; a = 4.518 Å, b = 5.069 Å, c = 6.736 Å) or $(Fe, Ni)_7C_3$ (hexagonal; a = 7.1 Å, c = 4.58 Å). Both of these phases have been observed in presolar graphite (Bernatowicz et al. 1999; Croat et al. 2005), but not to date in presolar SiC. Iron-nickel-rich subgrains were found in one SiC Z grain, but the phase was not conclusively identified (Stroud and Bernatowicz 2005; R. Stroud, pers. comm.). Iron-nickel silicides are the only Fe-rich subgrains that have been previously identified in presolar SiC, but these were found in SiC X grains, which originate in Type II SNe (Hynes et al. 2010). Diffraction patterns obtained from several of the Fe carbide subgrains indicate that they are epitaxially aligned with the SiC crystal domains within 6.2°.

The Fe carbide subgrains are well distributed throughout the SiC grain, both within a single slice of SiC and between slices, as are the oldhamite subgrains. Their distributions, however, are not independent of one another; for all six cases in which an Fe carbide subgrain was observed, an oldhamite subgrain was found 9 – 38 nm away from it (Figure 3.7). Conversely, only one oldhamite subgrain, described above as having an unusually high Fe content ($Ca_{47.0}Fe_{5.3}S_{47.7}$), was found without a companion Fe carbide subgrain.

One possible explanation for the relatively large amount of Fe present in the spectrum of this oldhamite subgrain (compared to the other oldhamite subgrains) is that there could be an unobserved Fe carbide subgrain nearby, resulting in a slight overlap

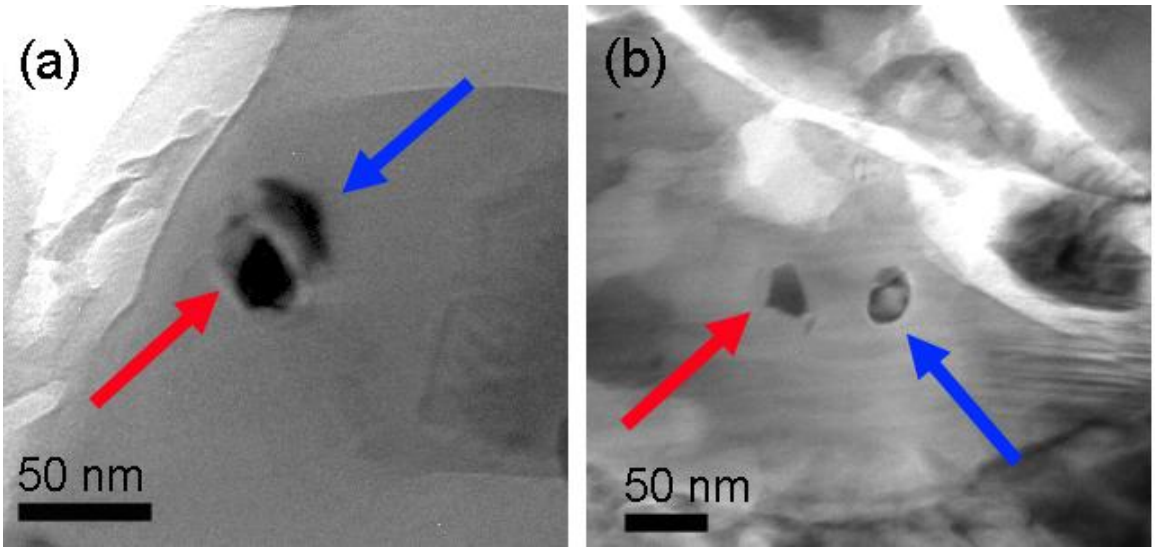


Figure 3.7: BF TEM images of subgrains in KJG-N4-468-1 showing the proximity of two examples of oldhamite and Fe carbide subgrains. The red arrows indicate the Fe carbide subgrains, while the blue arrows indicate the oldhamite subgrains. In all six cases in which an Fe carbide subgrain was observed, an oldhamite subgrain was located 9 – 38 nm away from the Fe carbide subgrain. The exact nature and cause of this relationship is, at present, unclear. Only one example of an oldhamite subgrain that did not have a companion Fe carbide subgrain was observed. However, a high Fe content in this oldhamite subgrain suggests that there could possibly be an undetected Fe carbide subgrain nearby.

between the signal from the oldhamite subgrains and the Fe carbide subgrain. All of the subgrains were initially detected by the observed change in diffraction contrast as the sample was tilted over a ±30° range of goniometer angles; however, due to the position on the sample mount of the slice of SiC in which this oldhamite subgrain is located, a more limited range is available over which the sample can be tilted. If an Fe carbide subgrain exists near the oldhamite subgrain, but does not have a low-index zone axis within the range of tilt that is available, it would be possible to not observe it.

Alternatively, there could have originally been an Fe carbide subgrain very close to the oldhamite subgrain, but the two subgrains were separated during ultramicrotomy. This would result in the two subgrains being located in different slices, with only a very small piece of the Fe carbide subgrain remaining in the same slice as the oldhamite subgrain, which might then contribute some signal to the EDXS spectrum. Although multiple slices of each SiC grain are available for study, they are not necessarily consecutive slices, due to a variety of factors, including the location of the slices relative to the Cu grid bars and the possible failure of the substrate under any given slice. If the two subgrains are in different slices of the SiC grain, it would be quite possible that one of the two slices is not able to be observed, which could explain why an Fe carbide subgrain was not observed without an oldhamite subgrain nearby.

A final possibility is that many or all of the oldhamite subgrains may have initially contained significant amounts of Fe in solid solution. The oldhamite subgrains could have subsequently begun to dissolve, allowing the formation of the euhedral Fe carbide subgrains and resulting in the observed anhedral morphology of the oldhamite subgrains. However, it is also possible that at least one oldhamite subgrain does not have

a nearby Fe carbide subgrain, suggesting that oldhamite subgrains can exist independently of Fe carbide, although the reverse has not been observed.

The only trace elements measured in any of the SiC AB grains that are not attributable to either distinct subgrains or to background signal are Mg and Al. The range of Mg/Si and Al/Si (Table 3.1) is highly variable, both within a single AB grain and from grain to grain. No independent Al-Mg-rich subgrains were observed, suggesting that the Al is heterogeneously distributed and is present in solid solution with SiC, possibly in the form of AlN, which is isostructural with SiC. For most of the grains, the Al concentration varies substantially from below the detection limit (≤0.2 at%) to a maximum value in the SiC grain that ranges from 1.0 at% up to 17.3 at% in grain KJG-N4-468-1 (in all cases, this assumes a SiC grain composed of only Si, Al, and Mg; as discussed previously, C is excluded due to a large background contribution from the substrate). Magnesium was significantly less abundant than Al, ranging from undetectable in most of the SiC grains (≤0.2 at%) up to a maximum of 1.1 at% in KJG-N4-531-3.

A low Mg concentration, compared to Al, is not unexpected in SiC grains. Aluminum preferentially condenses into SiC, leading to typical concentrations of several weight percent in presolar SiC (Hoppe and Ott 1997). Conversely, Mg does not readily condense into SiC, resulting in typical concentrations of only a ~100 ppm in most presolar SiC grains (Amari et al. 1995). This suggests that most of the Mg present in presolar SiC is most likely radiogenic $^{26}$Mg from the decay of $^{26}$Al (half life = 7.4 x $10^5$ yrs) that was initially present when the SiC grain condensed. This is further supported by

isotopic evidence that the Mg in mainstream SiC grains is nearly monoisotopic $^{26}$Mg (Hoppe and Ott 1997), and allows an initial $^{26}$Al/$^{27}$Al ratio to be inferred.

The highest inferred $^{26}$Al/$^{27}$Al ratios are found in SiC X grains, with ratios typically as high as 0.6 (and in one unusual grain, as high as 0.9) (Nittler et al. 1995; Zinner et al. 2010). The inferred $^{26}$Al/$^{27}$Al ratios measured in AB grains are significantly lower than those in X grains (typically as high as $10^{-2}$ in AB grains), but are higher than those measured in SiC mainstream grains (typically less than $10^{-3}$). The work discussed in Section 2.4.1 showed that within a 2σ error, the $^{26}$Al/$^{27}$Al ratios inferred from EDXS Mg/Al elemental ratios are consistent with the $^{26}$Al/$^{27}$Al ratios inferred from isotopic data. For the AB grains in this study, the maximum Mg/Al ratios in the AB grains range from 0.04 – 0.08, although it is difficult to calculate a Mg/Al ratio for many of the AB grains due to their low Mg content. However, for the AB grains in this study with a sufficiently high Mg concentration, if the Mg/Al ratios are taken as upper limits to the inferred $^{26}$Al/$^{27}$Al ratios, they are consistent with the inferred $^{26}$Al/$^{27}$Al ratios typically measured in AB grains by isotopic analysis.

## 3.4 Discussion

### 3.4.1 Implications for SiC Formation and Growth in Circumstellar Outflows

Previous studies (e.g., Daulton et al. 2003; Hynes et al. 2010; Stroud and Nittler 2004) have observed only the 3C and 2H polytypes, as well as intergrowths of the two and a small number of grains (1% by number) that are heavily disordered. With the exception of disordered grains, the same polytypes were observed in this study, despite

the different stellar origins of the grains. It is not surprising that no disordered grains were observed in this study, given their rarity and the comparatively small sample size compared to that of Daulton et al. (2003). Subsequent isotopic analysis of some of the disordered grains found by Daulton et al. (2003) indicates that they occur in all of the major types of presolar SiC (Daulton et al. 2009).

It is, however, not obvious that SiC grains that condense in a wide variety of circumstellar environments should all have the same polytypes, especially given that there are over 250 polytypes of SiC, although most higher order hexagonal and rhombohedral polytypes have only been observed to form in a lab and require temperatures in excess of ~2800 K (Fisher and Barnes 1990). Even grains that originate in sources as disparate as turbulent, rapidly evolving SNe outflows (Hynes et al. 2010) and the envelopes of comparatively quiescent AGB stars (Daulton et al. 2003) have, thus far, indexed to only two polytypes.

In an attempt to better understand the details surrounding the formation of SiC polytypes and the factors that most strongly influence it, detailed experimental and theoretical work has been done by the materials science community (SiC has a number of important materials science applications). Apparently, a large number of factors can influence polytype formation, including the: temperature; pressure; Si/C ratio; the technique used to trigger growth; and the growth substrate, and it is not currently well understood which of these factors is most dominant. An extended discussion of the details and findings of these experiments is given in Section 2.4.2 of this work. The reader is referred there, as well as to Daulton et al. (2003) and references therein for more detailed information. Despite the plethora of experiments, it is clear that no laboratory

setting can completely simulate the conditions present in the circumstellar environments in which presolar SiC condenses. All of these factors make it difficult to give a precise temperature at which any given polytype begins to form or ceases to grow in an astrophysical setting. However, experimental evidence consistently shows that 2H is the lowest temperature polytype to form, followed by 3C, making the corresponding transition from 2H to 3C and the formation of intergrowths of these two polytypes the lowest temperature transition (e.g., Kern et al. 1998; Krishna and Marshall 1971). These are also the only polytypes observed to form at temperatures roughly consistent with those predicted for SiC condensation in AGB stars (e.g., Lodders and Fegley 1995; Sharp and Wasserburg 1995).

The presence of only two polytypes in presolar SiC grains, regardless of the type of SiC or the astrophysical source from which the grains originated, suggests two possible explanations. One possibility is that physical conditions, like temperature and pressure, under which SiC can condense in stellar atmospheres do not vary significantly in different types of stellar sources. The other possibility is that polytype formation is relatively insensitive to the range of these conditions present in stars. Instead, other factors, such as the Si/C ratio or free energy constraints, may play a more dominant role in polytype formation, but may not vary significantly between stellar sources (Fissel 2000). For example, nucleation theory suggests that 3C SiC may be the most abundant polytype of SiC at relatively low temperatures like those found in stellar envelopes, even when higher order polytypes of SiC are able to form, because 3C-SiC provides the most energetically favorable stacking sequence of Si-C bilayers (Heine et al. 1991). However,

a more complete theory of polytype formation is needed to determine which of these scenarios is most applicable and influential to polytype formation in presolar SiC grains.

Although the observed polytypes in presolar SiC grains and the relative abundances of these polytypes are virtually identical for all types of SiC, the crystal domain size has been observed to vary significantly between types of SiC. The comparison of the crystal domain sizes observed in various studies is somewhat problematic, however. Some properties of presolar SiC, such as trace element abundances (Amari et al. 1995) and the relative abundances of SiC grains of different types (Hoppe et al. 1996; Zinner et al. 2007) have been observed to vary with grain size. In order to avoid the possible influence of grain size effects on the interpretation of crystal domain size in different types of SiC, grains of the same total size will be compared. SiC X grains and mainstream grains (Sections 2.3.3 and 2.4.2 of this work), as well as the AB grains in this study, are all from the KJG size fraction (3 μm average observed size) of the Murchison meteorite (Amari et al. 1994).

As discussed in Chapter 2 and in this chapter, the mainstream, X, and AB grains are composed of multiple crystal domains that are epitaxially aligned, indicating that these grains are not mechanical aggregates of independently formed crystalliltes. The size and number of the domains vary significantly between grain types, however. Each mainstream grain is composed of 2 – 3 crystal domains that range from 0.5 – 1.7 μm in diameter. At the other extreme, the X grains are composed of a large number of small crystal domains, which have an average diameter of 140 nm. The crystal domain sizes for most of the AB grains in this study fall somewhere in between the other types of SiC, with a median diameter of 331 nm and an average of 4 – 5 crystal domains in each AB

grain. Only AB grain KJG-N4-369-5 is composed of three large crystal domains that range in size from 0.516 – 1.30 μm, as well as a small 0.290 μm crystal domain. The size distribution for this AB grain closely resembles the crystal sizes observed in the mainstream grains described in Chapter 2.

The disparity in the crystal domain sizes in mainstream and X grains most likely reflects the differences in their formation environments. The large number of crystal domains in each SiC X grain implies a large number of nucleation sites, which, in turn, suggests that the gas from which the X grains condensed was supersaturated. Conditions of supersaturation foster rapid nucleation and growth, but at the expense of other crystallites. This results in a large number of small crystal domains that grow together into a single grain, which is what was observed in the X grains. In conditions of lower degrees of supersaturation, the crystals grow more slowly with lower number densities of nuclei, but are also able to grow bigger, resulting in fewer, but larger crystal domains within a single SiC grain, such as was observed in the mainstream grains.

Additional theoretical and experimental work supports these conclusions. Calculations based on a number of factors, including observations of carbon stars, thermodynamic constraints, and considerable observational evidence for the existence of presolar grains larger than 1μm in size, led Bernatowicz et al. (2005) to conclude that the likely timescale available for the growth of SiC grains in AGB stars is ~2 – 10 years. In contrast to this timescale, analysis of the Ti and V isotopic compositions of SiC X grains found evidence of extinct $^{49}$V (half life = 338 days), which suggests a timescale of less than 25 months for SiC X grains to form if live $^{49}$V must be incorporated into the growing grains (Hoppe and Besmehn 2002). When coupled with observations of SN

1987A, which indicate the onset of dust formation 300 – 500 days after the explosion (Wooden 1997), the timeframe available for X grain growth may be less than a year. Therefore, the combination of a short growth timescale, coupled with a rapid rate of nucleation, supports the observational evidence that X grains are composed of a large number of small crystal domains, relative to mainstream grains with the same total grain size.

There are substantially fewer domains in the AB grains than in the X grains, indicating less rapid growth and lower degrees of supersaturation, but almost all of the AB crystal domains are distinctly smaller than those observed in mainstream grains. This suggests that the saturation level of the parent gas in which AB grains condensed was between that of the X grains and of the mainstream grains. J stars, which are the most likely source for most of the AB grains in this study, have similar effective temperatures to AGB stars and are thought to be evolutionarily similar to AGB stars (Abia and Isern 2000; Amari et al. 2001c), so it is not surprising that the crystal domain sizes differ from those of X grains. The observed difference in the size of the crystal domains in AB grains and mainstream grains suggests, however, that there may be at least some variation in the nucleation and growth rates in these two types of astrophysical environments, although without detailed theoretical models of J stars, it is difficult to determine what may cause this dissimilarity. Possible differences could result from the diverging evolutionary histories of J stars and AGB stars, the influence of a binary star companion that is theorized to exist with J stars, or the effects of different nucleosynthetic processes in the stars (Abia et al. 2001; Chen et al. 2007).

The crystal domains in KJG-N4-369-5 are significantly larger than the domains observed in the other AB grains in this study, but similar in size to the crystal domains observed in mainstream grains. Grain KJG-N4-369-5 is the most intact AB grain in this study, so the observed domain sizes are therefore likely to be close to the true domain size and probably not significantly affected by the ultramicrotomy process. However, it is not accurate to assume that the crystal domains observed in the other AB grains in this study are all lower limits as a result of the loss of material during the ultramicrotomy process, and that the true domain sizes of all of the other AB grains are actually similar to those observed in KJG-N4-369-5. Many of the crystal domains in the other AB grains are in unbroken, intact sections of the grains, suggesting that at least some of the smaller crystal domains observed in these AB grains are also close to the true domain size. This implies that the observed difference in the crystal domain sizes in KJG-N4-369-5 and the rest of the AB grains in this study is most likely a real difference.

A potential explanation of this difference is that grain KJG-N4-369-5 originated from a different type of astrophysical source than the other AB grains in this study. The isotopic composition of grain KJG-N4-369-5 does not differ significantly from the other AB grains in any way, nor were s-process enrichments or other unusual trace elements observed in this grain that would suggest a different stellar origin. However, since the stellar sources of AB grains are not well constrained, an isotopic difference may not be obvious; instead, different stellar origins may be indicated by the crystal domain size. If some AB grains originated in a source other than J stars and born-again AGB stars, analysis of additional AB grains could reveal a connection between a particular stellar source and isotopic or elemental trends that are correlated with the domain size. These

trends, however, may not be obvious from the limited sample size of this study. Analysis of additional AB grains, as well as mainstream grains, would also provide significantly better statistics on the number of crystal domains in each SiC grain and on the relative size of these domains.

### 3.4.2 TiC Subgrain Condensation

Subgrains are commonly observed in carbonaceous presolar grains (e.g., Bernatowicz et al. 1992; Bernatowicz et al. 1996; Hynes et al. 2010). While the number of presolar SiC grains that have been analyzed for the presence of subgrains is limited, there are abundant analyses of subgrains in presolar graphite. For example, Croat et al. (2005) analyzed roughly 850 slices of presolar graphite and observed (Ti, Zr, Mo, Ru)C subgrains in ~20% of them. The s-process abundances measured in these subgrains are, on average, 200 times the solar abundance, clearly indicating an AGB origin. TiC subgrains have also been observed in presolar graphite grains that originated in Type II SNe (Croat et al. 2003). While these subgrains contain significant amounts of V (83% of the solar V/Ti ratio), no s-process elements were observed in these subgrains. Large numbers of (Ti, V)C are found in most of these graphite grains, with an abundance by volume of 110 – 2400 ppm.

The crystallographic, morphological, and chemical properties of the TiC subgrains (which here refer to all of the subgrains in this study that are predominantly composed of Ti and C) can help constrain the mechanism responsible for their formation. Previous TEM observations indicate that TiC initially condensed in solid solution with SiC and subsequently exsolved to form subgrains (Bernatowicz et al. 1992; Stroud and

Bernatowicz 2005). This scenario is consistent with the observations of this study. The observed epitaxial alignment between the TiC subgrains and the adjacent SiC crystal domains strougly suggests that the TiC subgrains exolved from solid solution. If the TiC subgrains instead formed independently and were later incorporated into the growing SiC grain at random orientations, as is the case for TiC subgrains in presolar graphite (Bernatowicz et al. 1991; Croat et al. 2003; Croat et al. 2005), then the TiC would not be expected to exhibit crystallographic alignment with the surrounding SiC. It is exceedingly unlikely that in every case, the subgrains would stick to the growing SiC grain in a random orientation that coincided with the alignment of the SiC crystal domains. The location of the TiC subgrains at the SiC crystal domain boundaries, coupled with the relative compositional homogeneity among TiC subgrains in a single AB grain, further argue for the initial condensation of the subgrains in solid solution with SiC.

### 3.4.3 S-Process Enrichments and Their Implications for Stellar Origin

Measurements of trace elements in SiC AB grains have been performed on only a limited number of grains, but of those grains, 57% have s-process enrichments (Amari et al. 1995; Pellin et al. 2000b). Although these grains display some variation in their trace-element abundance patterns, all of the patterns from the grains in the Amari et al. (1995) study could be successfully reproduced using theoretical models of equilibrium condensation in AGB stars (Lodders and Fegley 1995). These patterns correspond to s-process enrichments of 3 – 5 times the solar abundance of these elements. Amari et al. (2001c) proposed that the most likely stellar sources for these AB grains are born-again AGB stars. Sakurai's object, the only well-documented example of a born-again AGB

star, was observed to have s-process enrichments up to ~2 times the solar abundance (Asplund et al. 1999), which is roughly consistent with the enrichments observed in the AB grains. Theoretical models of born-again AGB stars predict large enrichments in $^{14}N$ (Herwig 2001; Miller Bertolami and Althaus 2007), which would limit them to the possible parent stars of AB grains with s-process enrichments and high $^{14}N/^{15}N$ ratios. Ten to twenty percent of AGB stars that pass through the planetary nebula phase are predicted to become born-again AGB stars (Iben et al. 1983). Assuming roughly half of AB grains originate in born-again AGB stars (the other half having solar abundances of the s-process elements and possibly originating in J stars), the frequency of born-again AGB stars could plausibly account for AB grains (Amari et al. 2001c).

Only one AB grain in this study was observed to have any s-process enrichments (grain KJG-N4-259-1). EDXS detection limits are at approximately solar s-process abundances, so even small enrichments should be able to be detected. However, if s-process enrichments in AB grains are found predominantly in grains with $^{14}N/^{15}N$ > solar, then it may be expected that there are very few grains in this study with s-process enrichments. As previously discussed, the low $^{12}C/^{13}C$ ratios used to identify AB grain candidates tend to be accompanied by low $^{14}N/^{15}N$ ratios, a relationship borne out by the fact that only two AB grains in this study have $^{14}N/^{15}N$ > solar, and only one AB grain has a $^{14}N/^{15}N$ ratio that is significantly higher than the solar value. However, s-process enrichments were not observed in either of these grains; KJG-N4-468-1 has $^{14}N/^{15}N$ = 351.6 and contains TiC, oldhamite, and Fe carbide subgrains, while KJG-N4-451-6 has $^{14}N/^{15}N$ = 882.0, but had no subgrains observed in it, despite having several large, intact slices available for study.

The Zr/Ti and Mo/Ti ratios measured in the two (Ti, V, Zr, Mo)C subgrains in KJG-N4-259-1 indicate enrichments of 9 – 16 times the solar abundance of these elements. This is slightly higher than the enrichments determined for the AB grains with trace element abundance measurements (Amari et al. 1995), but up to eight times higher than the enrichments measured in Sakurai's Object (Asplund et al. 1999). Given the errors associated with the spectroscopic measurements, the variation in abundance over time (which is substantial for some elements), and the fact that these abundances come from only a single example of a born-again AGB star, the difference in s-process enrichments between grain KJG-N4-259-41 and born-again AGB stars may not be significant. The enrichments are, at least, of a similar magnitude, unlike the enrichments of 200 times the solar abundance that are measured in graphite grains from AGB stars (Croat et al. 2005).

However, there is one significant problem with AB grain KJG-N4-259-1 originating in a born-again AGB star like Sakurai's Object: born-again AGB stars are predicted to have large enrichments in $^{14}N$, while grain KJG-N4-259-1 has $^{14}N/^{15}N = 71.5 \pm 0.9$. In fact, KJG-N4-259-1 has the lowest $^{14}N/^{15}N$ ratio of any AB grain in this study. Grain KJG-N4-259-1 is not, however, the only AB grain to have both s-process enrichments and less than solar $^{14}N/^{15}N$; this is also true of 17% of all the AB grains for which trace elements have previously been measured (Amari et al. 1995; Pellin et al. 2000b). There appears to be no strong correlation between s-process abundances and $^{14}N/^{15}N$ ratios in AB grains; $^{14}N/^{15}N >$ solar and s-process enrichments were observed in 37% of AB grains, $^{14}N/^{15}N <$ solar and no s-process enrichments were observed in 21% of AB grains, and $^{14}N/^{15}N >$ solar and no s-process enrichments were observed in 21% of

AB grains, while the s-process abundance of one grain was not classified (Amari et al. 1995; Pellin et al. 2000b). Furthermore, resonant ionization mass spectrometry (RIMS) measurements of the Zr and Mo isotopes of three AB grains showed unusual isotopic ratios (Pellin et al. 2000b). All three grains, which were previously identified during SIMS analysis as AB grains with $^{14}N/^{15}N$ < solar, have relatively solar Mo isotopic compositions and display a lack of any s-process signature. One of the AB grains also has a solar Zr isotopic composition, suggesting a likely circumstellar origin in a J star. However, the other two grains have large excesses in $^{96}Zr$, compared to the reference isotope $^{92}Zr$. Although Zr is an s-process element, $^{96}Zr$ is the only isotope of Zr that is not enriched in the s-process. Instead, it is usually produced in the r-process, which is thought to occur in SNe, and $^{96}Zr$ is expected to be significantly depleted by the s-process (Nicolussi et al. 1997). The production of $^{96}Zr$ is largely controlled by the strength of the $^{22}Ne$ source, which is dependent upon the temperature at the base of the He intershell, and therefore on stellar mass and metallicity (Barzyk et al. 2007; Lugaro et al. 2003). If the neutron density is sufficiently high, it is possible to bypass the s-process branch point at $^{95}Zr$ (half life = 64 days) and produce $^{96}Zr$, although such enrichments have not been observed in mainstream grains (Barzyk et al. 2007; Nicolussi et al. 1997).

Although the $^{13}C$ neutron source is responsible for the production of most of the heavy s-process elements, the $^{22}Ne$ source produces much higher neutron fluxes via the reaction $^{22}Ne(\alpha,n)^{25}Mg$, such as would be required to bypass the typical branching points in the s-process. However, it operates for a much shorter duration (typically only during the TP of the AGB star) than the $^{13}C$ source because of the high temperatures required for

the $^{14}N(\alpha,\gamma)^{18}F(\beta^{+}, \nu)^{18}O(\alpha,\gamma)^{22}Ne$ chain reaction that is responsible for the production of $^{22}Ne$ (Lugaro et al. 2003).

Another element whose production is dominated by the $^{22}Ne$ source is Si, which is veritably unaffected by the $^{13}C$ source (Lugaro et al. 1999; Zinner et al. 2006). However, for mainstream grains, the predicted effects of the $^{22}Ne$ source are small, but for stars of higher mass or lower metallicity than the stellar parents of mainstream grains, the effect on the Si isotopic composition can become significant, substantially increasing the $^{29,30}Si/^{28}Si$ ratios (Zinner et al. 2006). If the $^{22}Ne$ source is appreciably increased to produce the large $^{96}Zr$ enrichments observed in some AB grains (Pellin et al. 2000b), the Si isotopic composition could be shifted and the heavy Si isotopes would be significantly enriched, an effect which is not observed in the AB grains. However, additional theoretical calculations must be carried out to determine if it is possible for the $^{22}Ne$ source to produce the enrichments observed in $^{96}Zr$ and to calculate the results on other isotopic ratios.

The Zr and Mo patterns measured with RIMS in two AB grains (Pellin et al. 2000b) also bear a similarity to unusual patterns measured in several SiC X grains, which showed Zr and Mo isotopic compositions that do not correspond to typical s-process or r-process signatures (Davis et al. 1999; Pellin et al. 2000a; Pellin et al. 1999). These X grain patterns are potentially explained by a neutron burst, which can occur during the explosion of a Type II SN. It is unclear, however, if there is a similar scenario that could explain the isotopic compositions of the AB grains, since their C and Si isotopic compositions rule out a SN origin. Unfortunately, theoretical models do not currently exist to answer this question.

Since AB grains like KJG-N4-259-1 in this study and the two AB grains with $^{96}$Zr enrichments do not fit the description of either of the proposed types of stellar sources for AB grains, an alternate explanation must exist. Three possibilities could explain these grains: the models for born-again AGB stars are incorrect and they can produce a wide range of $^{14}$N/$^{15}$N ratios; some type of atypical process affected the grains; or they originated in a different type of stellar environment than those already proposed. If a problem exists in the models of born-again AGB stars, it is highly possible that the predicted $^{14}$N enrichments are not as large as expected. The production of $^{15}$N is notoriously poorly understood, with models for AGB stars, born-again stars, and SNe falling well short of the measured $^{15}$N enrichments (e.g., Amari et al. 2001c; Travaglio et al. 1999). This could be a result of neglecting neutron capture effects in current models of born-again AGB stars; the effect of neutron capture may decrease the $^{14}$N/$^{15}$N ratio in these stars, but full-scale models are needed to see if the $^{14}$N/$^{15}$N ratios are sufficiently low to explain the full range of AB grains (Amari et al. 2001c; Herwig 2001). Models also suggest that the production of $^{15}$N can be significantly increased if rotational mixing is taken into account, at least for massive stars (Nittler and Hoppe 2005). However, the potential effects on born-again AGB stars are unknown at this time. Further complicating matters is recent experimental evidence that the p-capture reaction rates for the production of N need revision (Palmerini et al. 2010), but such changes have not yet been factored into models.

While the model predictions of the $^{14}$N/$^{15}$N ratios in stars are not well understood, it is also possible that updated models would still fail to produce significant $^{15}$N enrichments in born-again AGB stars. Some type of atypical process, such as an

extremely high neutron flux due to the $^{22}$Ne source suggested by Pellin et al. (2000b) as a possible explanation for the unusual Zr isotopic compositions observed in two AB grains, is possible. However, as previously discussed, theoretical predictions for the effects of such processes do not exist, so the effects on the $^{14}$N/$^{15}$N ratio, as well as other isotopic ratios, are uncertain.

The final possibility is that AB grains like KJG-N4-259-1 could originate from a source other than born-again AGB stars. Novae and SNe produce significant amounts of $^{15}$N via the hot CNO cycle, with novae and X grains having the lowest $^{14}$N/$^{15}$N ratios ($^{14}$N/$^{15}$N $\geq$ 5.22) of all types of presolar SiC grains (Wiescher et al. 2010; Hynes and Gyngard 2009). However, the $^{29,30}$Si/$^{28}$Si ratios of AB grains seem to preclude them from either a nova or a SN origin. Amari et al. (2001c) discuss a number of potential sources, but significant issues like high $^{12}$C/$^{13}$C ratios or very low metallicity eliminates them as potential sources for AB grains, as discussed in Section 3.1. Of the sources discussed by Amari et al. (2001c), only an origin in AGB stars that undergo CBP may potentially explain most of the isotopic signatures of AB grains. However, He burning during CBP results in high $^{14}$N/$^{15}$N ratios, which presents the same problem previously discussed. While no firm constraints on the $^{14}$N/$^{15}$N ratios in J stars currently exist, observations clearly indicate solar s-process abundances in these stars (Abia and Isern 2000). Although AB grains with both s-process enrichments and $^{14}$N/$^{15}$N < solar, like grain KJG-N4-259-1, do not fit with predictions for the proposed sources of AB grains, at this time, there is no clearly better solution to the puzzle of their origin. Depending on the range of $^{14}$N/$^{15}$N ratios in J stars, AB grains with solar s-process abundances and either $^{14}$N/$^{15}$N > solar or $^{14}$N/$^{15}$N < solar may also require an alternate explanation of their

origin. Unfortunately, these questions are difficult to answer until additional work is done on theoretical models that can potentially help explain the isotopic and elemental signatures of many AB grains.

### 3.4.4 Grain KJG-N4-468-1

SiC AB grain KJG-N4-468-1 contains a variety of subgrains, including oldhamite, (Ti, V)C, and Fe carbide. Oldhamite is a predicted stable condensate in most models of AGB stars, but it has not previously been observed either spectroscopically or in presolar grains (e.g., Lodders and Fegley 1995; Sharp and Wasserburg 1995). The mechanism by which oldhamite was incorporated into SiC was also unknown (Lodders and Fegley 1995; Sharp and Wasserburg 1995). Condensation in solid solution is predicted for condensates that are similar to the host phase (in this case, SiC) in a variety of ways, including: stoichiometry, crystal structure, chemical bonding, and size of the atomic radii of the elements in the compound (Hoppe et al. 2001; Upadhyaya 1996). A mineral, such as AlN, that meets all of these requirements is considered an ideal solid solution. TiC is isostructural to SiC and has similar lattice parameters and is therefore expected to also form in solid solution with SiC, making it nearly ideal. Observational evidence that both AlN and TiC readily condense in solid solution with SiC, both in this study and in several previous studies (e.g., Bernatowicz et al. 1992; Stroud and Bernatowicz 2005), supports this. Although both Fe carbide and oldhamite are predicted to condense around AGB stars, formation in solid solution with SiC is less favorable. Neither $Fe_3C_7$ nor $Fe_3C$, which are the best mineral candidates for the Fe carbide subgrains observed in this study, have a cubic crystal structure, nor do they have the same stoichiometry as SiC. In order for these Fe carbides to form in solid solution with SiC, their lattices must be distorted,

which suggests a moderate probability of condensation in solid solution with SiC (Hoppe et al. 2001). While CaS and SiC have identical stoichiometries and fcc crystal structures, the crystal lattice of oldhamite is ~30% larger than that of SiC. The chemical bonding in oldhamite is also different from that in SiC (ionic versus covalent, respectively). This suggests that a solid solution of oldhamite in SiC is not particularly favorable (Hoppe et al. 2001; Upadhyaya 1996).

Despite these considerations, all three types of subgrains in KJG-N4-468-1 display a clear epitaxial alignment with the surrounding SiC crystal domains and are located at the boundaries of these domains. These are clearly exsolution features, suggesting that all three types of subgrains initially condensed in solid solution with SiC and later exsolved. As with the TiC subgrains found in other AB grains, if the subgrains formed independently, prior to incorporation in SiC, then it is unlikely that there would be precise alignment between the crystallographic planes of the subgrains and the SiC domains.

The observational evidence of exsolution from solid solution for the subgrains in KJG-N4-468-1 is also consistent with thermodynamic considerations. The condensation sequence for compounds in the atmospheres of C-rich AGB stars depends upon a number of factors, including temperature, pressure, C/O ratio, and elemental abundances, although the relative importance of these factors varies significantly with each mineral species (Lodders and Fegley 1995; Sharp and Wasserburg 1995). Graphite condensation, for example, is strongly dependent upon the C/O ratio, but relatively insensitive to pressure and temperature. In contrast, the condensation of carbides like TiC and SiC are relatively insensitive to the C/O ratio, but strongly dependent upon pressure. This makes

the condensation sequence and the temperatures at which various compounds condense somewhat variable. For most reasonable temperatures, pressures, and C/O ratios in the envelopes of AGB stars where grains are able to condense, refractory carbides like ZrC and TiC condense first, followed by graphite; however, at higher C/O ratios or lower pressures, graphite is predicted to condense before TiC. The condensation of TiC before graphite over a large range of parameters is consistent with the condensation sequence implied by TEM observations of presolar graphite grains with centrally located TiC subgrains (Bernatowicz et al. 1996; Croat et al. 2003; Croat et al. 2005). These subgrains likely served as nucleation centers for the growing graphite grains. TiC grains form first and then, at slightly lower temperatures, are incorporated into the growing graphite grains. For the full range of pressures, temperatures, and C/O ratios, SiC is predicted to condense next, at ~160 – 200 K below TiC (Lodders and Fegley 1995; Sharp and Wasserburg 1995). Finally AlN, Fe carbide, and CaS condense at similar temperatures, ~250 – 350 K below SiC.

These temperatures reflect the independent condensation of each compound directly from the gas; however, there is no evidence that any of the subgrains found in presolar SiC condensed and were incorporated into SiC in this way (e.g., Bernatowicz et al. 1992; Hynes et al. 2010). Instead, TEM analyses indicate that the subgrains condensed in solid solution with SiC. Because the actual activity coefficients of the relevant compounds were not (and are still not) generally available for solid solutions with SiC, Lodders and Fegley (1995) calculated the temperature at which 50% of a compound will have condensed in solid solution with SiC, assuming an ideal solid solution, which may not be accurate for minerals such as oldhamite and Fe carbide, as

already discussed. It is important to note that all of the aforementioned calculations for the condensation temperatures of both pure compounds and compounds in solid solution with SiC are done under the assumption of thermodynamic equilibrium (Lodders and Fegley 1995; Sharp and Wasserburg 1995).

Based on these calculations, compounds with a higher independent condensation temperature than SiC, such as TiC, will have a solid solution condensation temperature equal to that of SiC. For compounds like CaS and AlN, the temperature at which they condense in solid solution is actually somewhat higher than the temperature at which the pure compound condenses (Lodders and Fegley 1995). For example, at C/O $\geq$ 1.05 and a pressure of 5 Pa, pure TiC is predicted to condense at 1702 K, followed by SiC at 1544 K, Fe carbide at 1278 K, AlN at 1242 K, and finally CaS at 1220 K. In contrast, for condensation in solid solution under the same conditions, TiC and SiC are both predicted to condense at 1544 K, followed by AlN at 1274 K, Fe carbide at 1254 K, and CaS at 1252 K. This effect may also explain why both ZrC, which condenses at higher temperatures than TiC, and VC, which condenses at lower temperatures than TiC, are observed in solid solution within the same TiC subgrain in AB grain KJG-N4-259-1; all three carbides are predicted to condense at the same temperature in solid solution (Lodders and Fegley 1995).

The presence of refractory TiC subgrains in the same SiC grain as comparatively low temperature phases like oldhamite and Fe carbide, which are predicted to condense more than 300 K below SiC, has important implications for the stellar environment in which grain KJG-N4-468-1 condensed. Additionally, the Al content, which is most likely in the form of AlN, is much higher in KJG-N4-468-1 than in any other AB grain in

this study (at least ten times the Al/Si ratio measured in any other AB grain). Oldhamite, Fe carbide, and AlN are some of the lowest temperature condensates predicted to condense in solid solution with SiC, with oldhamite being the lowest temperature condensate observed to be present in presolar SiC (Lodders and Fegley 1995; Sharp and Wasserburg 1995). Therefore, in order for all of these compounds to have condensed in solid solution with SiC, equilibrium must have been maintained over a large temperature range of at least 300 K, from the temperature at which the TiC condensed to the temperature at which the oldhamite condensed.

Predictions indicate that at temperatures less than 1500 K (at 5 Pa), ~50% of the available Si has been removed from the gas via the condensation of SiC (Lodders and Fegley 1995). At this temperature, however, SiC is no longer the dominant Si-rich compound; instead, most of the Si is tied up in the gaseous forms of pure Si and SiS (Lodders and Fegley 1995; Sharp and Wasserburg 1995). When oldhamite begins to condense at 1220 K, it removes some of the S from the gas, thereby freeing up some Si to form additional SiC. Approximately 11% of the total amount of SiC is predicted to condense through this mechanism (Lodders and Fegley 1995). All of the Ca is predicted to be removed from the gas within 100 K of the onset of oldhamite formation, which subsequently causes SiC condensation to cease completely. The onset of forsterite ($Mg_2SiO_4$) condensation and the continued presence of gaseous SiS preclude the formation of additional SiC (Lodders and Fegley 1995).

The onset of low temperature SiC condensation triggered by oldhamite condensation may help to explain the presence of oldhamite and the other low temperature phases present in SiC. If SiC formation effectively ceases below 1500 K and

does not resume until oldhamite begins to condense, AB grain KJG-N4-468-1 may contain both high and low temperature SiC. The majority of TiC is predicted to condense before the beginning of SiC condensation at 1544 K, with the remainder of the TiC subsequently condensing into solid solution with SiC near this temperature. This scenario explains the TiC subgrains observed in both graphite grains and in SiC grains like KJG-N4-468-1 (e.g., Bernatowicz et al. 1992; Croat et al. 2005). If some SiC crystal domains of AB grain KJG-N4-468-1 condensed around 1544 K, the grain could then have acted as a nucleation center for the low temperature SiC that subsequently condensed, along with the low temperature condensates in solid solution with this SiC, as a result of the onset of oldhamite condensation.

The polytypes of the SiC crystal domains in KJG-N4-468-1, as well as the location of the subgrains in the SiC grain, may support this scenario. All of the AB grains in this study were predominantly 3C-SiC, with the exception of KJG-N4-468-1. In this grain, roughly half of the crystal domains were either 2H-SiC or an intergrowth of 2H- and 3C-SiC. The disproportionately high number of crystal domains that index, at least partially, to the lowest temperature polytype is consistent with SiC condensation at a lower temperature than most of the other SiC crystals. In fact, low temperature SiC condensation, triggered by oldhamite condensation, could potentially explain some, if not most, of the occurrences of 2H-SiC. Furthermore, while the location of the TiC subgrains have no apparent relation to the other subgrains, the Fe carbide and oldhamite subgrains, as well as the highest Al contents, are all located at the crystal domain boundaries of SiC crystals that have been indexed to either the 2H polytype or to an intergrowth of the 2H and 3C polytypes (Figure 3.8). This suggests that the low

temperature phases may have all been in solid solution with the 2H and intergrowth polytypes of SiC and later exsolved (in the case of oldhamite and Fe carbide) or remained in solid solution with these SiC crystal domains (in the case of AlN).

However, it is extremely important to study additional grains with low temperature condensates like oldhamite to determine if the subgrain locations and the polytypes observed in grain KJG-N4-468-1 are simply coincidental or if they are a hallmark of low temperature condensation. It is also possible that the presence of low temperature condensates and the relatively high number of occurrences of the 2H polytype could reflect some difference between J stars and AGB stars. Although observations indicate both have similar surface temperatures (Abia and Isern 2000), without grain condensation models particular to J stars, it is difficult to tell what effects, if any, the difference in stellar environments may have on grain condensation. However, previous studies have indicated that SiC polytypes do not vary significantly between stellar sources, even in stellar environments as disparate as AGB stars and SNe (Daulton et al. 2003; Hynes et al. 2010). In general, it is also surprising that there are not more examples of low temperature condensation in presolar SiC if the prediction that the formation of ~11% of SiC is triggered by oldhamite condensation is correct (Lodders and Fegley 1995).

Although both the Fe carbide subgrains and the oldhamite subgrains are low temperature condensates (compared to TiC, graphite, and most SiC), there is no apparent reason why every Fe carbide subgrain should be found in close proximity to an oldhamite subgrain in KJG-N4-468-1. That this assemblage is observed in six separate cases strongly suggests that some type of relationship exists, but, to the best of our knowledge,

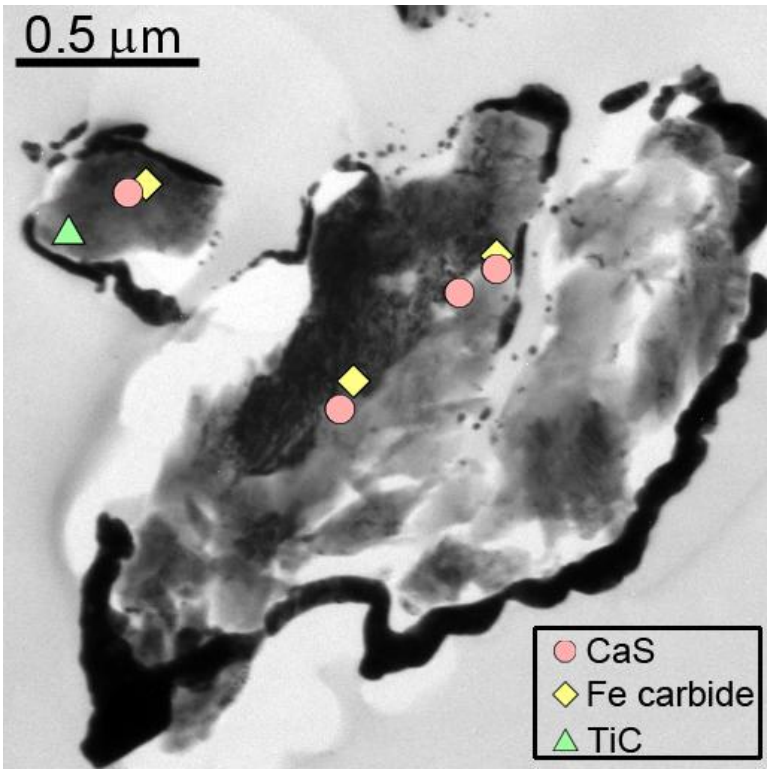


Figure 3.8: TEM BF image of one slice of AB grain KJG-N4-468-1 (also pictured in Figure 3.4a), with the locations and types of subgrains in this slice indicated by the overlaid figures. All of the subgrains in this slice are located along the boundaries of a single SiC crystal domain (indicated in green in Figure 3.4a). This domain is broken into two pieces – a large, strongly diffracting crystal domain and a smaller, unattached fragment. In this figure, the domain is oriented along the [001] direction, but as indicated in Figure 3.4a, this domain also indexes to an intergrowth between the 3C and 2H polytypes. In other slices of KJG-N4-468-1 in which subgrains were observed, both the Fe carbide and oldhamite subgrains are similarly located along the boundaries of crystal domains that index to either the 2H polytype or to an intergrowth. The other TiC subgrain observed in KJG-N4-468-1 is located between two 3C-SiC domains.

there are no theoretical or experimental data that suggest a casual connection. It is possible that if the oldhamite exsolved before the Fe carbide, it could act as a nucleation center for the subsequent exsolution of the Fe carbide. Also unexplained (and potentially related) are the morphologies of the Fe carbide and oldhamite subgrains. The oldhamite is clearly in the process of some type of back-reaction that resulted in the complete loss of the primary crystal growth faces, while the Fe carbide was left with well-defined crystal faces. As previously discussed, the morphology of the oldhamite subgrains cannot be the result of dissolution due to contact with water or of weathering resulting from the grains forming independently of the SiC (e.g., Croat et al. 2003). One possibility is that a significant amount of Fe initially existed in solid solution with the oldhamite subgrain and later exsolved to form independent Fe carbide subgrains. This reaction could have also eroded the crystal faces of the oldhamite subgrain, causing the anhedral morphology. There is, however, no clear evidence at this time that this process is definitively responsible for the apparent back-reaction or phase instability of the oldhamite, and some other process may be responsible.

Some recent studies of SiC grains with extreme $^{29,30}$Si enrichments (termed "Type C" grains), which are thought to have originated in the outflows of Type II SNe, have large S anomalies (Gyngard et al. 2010a; Hoppe et al. 2010). Oldhamite has been proposed as the possible carrier of these anomalies, but Ca isotopic and elemental measurements do not exist for these grains, nor do crystallographic analyses. The presence of oldhamite in AB grains confirms theoretical predictions that while oldhamite does not form an ideal solid solution with SiC, it nevertheless does condense in solid solution with SiC in circumstellar environments. However, whether or not oldhamite can

condense in the SN outflows in which Type C grains are believed to have formed is currently unknown.

## 3.4 Summary and Conclusions

SiC AB grains are rather enigmatic, both in their stellar origin and in the details of the nucleosynthetic processes that produce the isotopic signatures of AB grains. TEM analysis of seven AB grains has provided some new insights into the morphology, chemical composition, and internal subgrains present in these SiC grains, as well as their possible stellar origin. Each AB grain is composed of an aggregate of SiC crystal domains, which vary significantly in size. However, there were no obvious correlations between the isotopic composition of the AB grains and the crystal domain size, suggesting that if AB grains form in multiple types of astrophysical environments, the growth conditions are not substantially different. As with previous studies, only two polytypes (2H and 3C), in addition to intergrowths of the two, were observed in the AB grains (e.g., Daulton et al. 2003; Hynes et al. 2010). Polytype formation appears to either be insensitive to the limited range of temperatures and pressures at which SiC can condense in stellar outflows or else other factors, such as the Si/C ratio, may play a more dominant role in SiC formation.

The first direct evidence of subgrains in SiC AB grains was observed, the size of which were all on the order of tens of nanometers in diameter. Most of the subgrains were (Ti, V)C that likely condensed in solid solution with SiC and later exsolved, a formation scenario that is consistent with previous observations of TiC in presolar SiC

(Bernatowicz et al. 1992; Stroud and Bernatowicz 2005). Only one AB grain contained any indication of s-process abundances greater than the solar abundance, with enrichments of 9 – 16 times. Grains with significant s-process enrichments are theorized to originate in born-again AGB stars, a type of stellar source for which large $^{14}N$ enrichments are also predicted (Herwig 2001). However, the AB grain in this study with s-process enrichments is extremely enriched in $^{15}N$. This suggests that either the models for born-again AGB stars are incorrect, at least in their predictions of the $^{14}N$ abundance; that some grains, such as the one in this study, experienced an atypical process that affected their isotopic and elemental composition; or that this AB grain originated in a different type of circumstellar environment. Additional theoretical models are needed to determine which of these scenarios is correct. The rest of the grains in this study are consistent with an origin in J stars. However, these stars remain highly enigmatic and additional spectroscopic observations, as well as theoretical models, would significantly help in understanding the most likely type of parent star for AB grains with solar s-process abundances.

Only one AB grain in this study contained additional types of subgrains: oldhamite and Fe carbide, both of which likely condensed in solid solution with SiC and later exsolved. The observation of seven oldhamite subgrains represents the discovery of a new presolar phase, which has long been a predicted condensate in AGB stars (e.g., Lodders and Fegley 1995; Sharp and Wasserburg 1995). Due to their low condensation temperature relative to that of SiC, the oldhamite (which is the lowest temperature condensate observed in presolar SiC to date) and Fe carbide subgrains, as well as the high Al content in the grain, indicate that thermodynamic equilibrium must have been

maintained in the grain over a large temperature range. This AB grains also supports the prediction of low temperature SiC, the condensation of which is triggered by the condensation of oldhamite (Lodders and Fegley 1995; Sharp and Wasserburg 1995). In all six cases in which Fe carbide subgrains were observed, they were always in close proximity to an oldhamite subgrain, strongly suggesting a relationship between the two types of subgrains. However, the nature of this relationship is, at this time, unclear. Models of grain condensation in J stars may provide insight into the low temperature condensates observed in this AB grain. The analysis of additional AB grains, particularly those containing low temperature condensates and those with s-process enrichments, may help answer some of these outstanding questions or reveal isotopic trends between AB grains with different trace element and subgrain compositions.

# Chapter 4

---

## The Presolar Grain Database

> "We are bits of stellar matter that got cold by accident, bits of a star gone wrong."
>
> ~Sir Arthur Eddington, from *The New York Times Magazine*, 1932

The discovery of presolar grains meant that individual pieces of stardust could be microanalyzed in the lab, rather than simply studied in bulk with a telescope. Examples of the advantages of such microanalysis have been discussed in Chapters 2 and 3. As demonstrated in these chapters, combined isotopic, structural, mineralogical, and chemical analysis can provide the most complete constraints on grain formation. However, for a variety of reasons, including the difficulty of TEM sample preparation and the time consuming nature of TEM analysis, the bulk of presolar grain research (~95% of the total number of grains analyzed) has concentrated on the isotopic properties of the grains. While the full range of these data and their implications can obviously not be presented in a single thesis, the general properties of the various types of presolar grains will be discussed in this chapter, along with a description of a system developed not only to organize the isotopic data that has been reported on more than twelve-thousand presolar grains, but also to provide better accessibility to these data for the astrophysical community.

## 4.1 Carbonaceous Presolar Grains

### 4.1.1 Silicon Carbide

Although SiC is not the most abundant type of presolar grain (see Table 1.1), it is, by far, the most studied type for several reasons: all SiC that has been found in meteorites is presolar, eliminating the problem of contamination from solar grains that is a major difficulty with other grain types: nearly every isotopic system that has been measured is anomalous; a wide variety of trace-elements and internal subgrains have been found in SiC; the size of SiC is relatively large compared to other types of presolar grains, with SiC typically a few microns or smaller; and SiC grains originate from a wide variety of stellar sources, with analyses of different types of SiC allowing for ready comparisons between different types of stellar sources. Mainstream SiC was one of the three types of presolar grains discovered almost simultaneously between 1987 and 1990. Its discovery was due to the presence of the "exotic" noble gas components Ne-E and Xe-S in SiC (Bernatowicz et al. 1987; Tang and Anders 1988; Zinner et al. 1987), the latter of which matched predictions for the production of Xe isotopes in the s-process (Clayton and Ward 1978). A second clear indication that mainstream grains originated in carbon stars is that the $^{12}C/^{13}C$ ratios measured in mainstream grains closely match spectroscopic measurements of carbon stars (Lambert et al. 1986) (Figure 4.1), which produce and inject up to 50% of the total dust in the ISM (Thronson et al. 1987). SiC X grains were discovered several years later in 1992 and so named as a word play on what was described as their "extremely exotic" isotopic composition (compared to mainstream

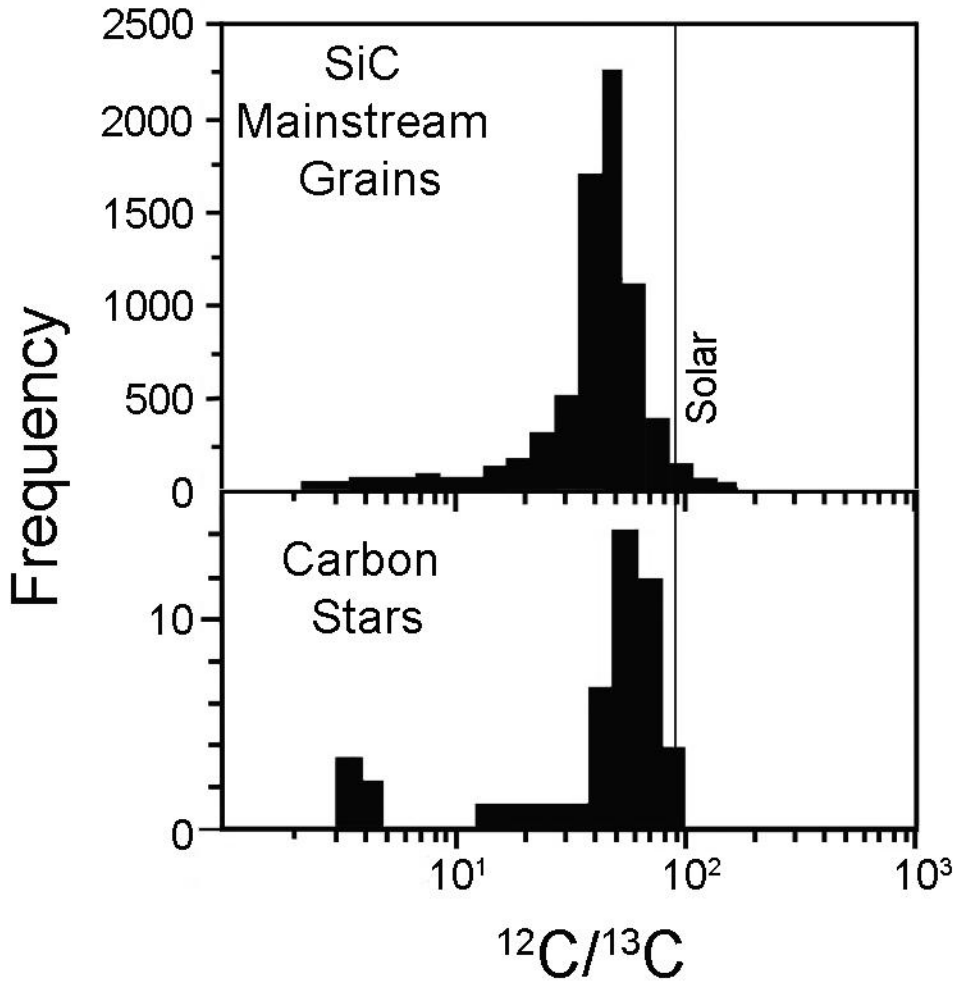


Figure 4.1: Histogram of the $^{12}C/^{13}C$ ratios of SiC mainstream grains and of the atmospheres of carbon stars (Lambert et al. 1986). Although the methods for acquiring isotopic data are very different for carbon stars (spectroscopic measurements) than for presolar grains (typically SIMS measurements), both carbon stars and mainstream SiC grains have nearly identical distributions of their $^{12}C/^{13}C$ ratios, indicating that the atmospheres of carbon stars are the likely source of SiC mainstream grains. The vertical line indicates the solar $^{12}C/^{13}C$ ratio of 89. Figure courtesy of E. Zinner.

grains) (Amari et al. 1992). The discovery of the other types of presolar SiC followed, with each simply named for the next successive letter, resulting in SiC Y, Z, and AB grains, along with a few other minor types.

The different types of SiC are largely defined by their $^{29,30}Si/^{28}Si$, $^{12}C/^{13}C$, and $^{14}N/^{15}N$ ratios. The Si, C, and N ratios of the different types of presolar SiC grains, along with the relative abundance of each type, are plotted in Figure 4.2 and 4.3. As mainstream grains, X grains, and AB grains have already been extensively covered in previous chapters, a description of these grain types will not be repeated here. SiC Y and Z grains each comprise ~1% of the total SiC population and, like mainstream grains, are believed to originate in low-mass stars of 1 – 3 $M_{\odot}$. However, unlike mainstream and AB grains, which plot along a line of slope 1.37 on a $\delta^{29}Si/^{28}Si$ versus $\delta^{30}Si/^{28}Si$, indicating that they originated in stars of approximately solar metallicity (Zinner et al. 2007), both Y and Z grains have $\delta^{29}Si/^{28}Si < \delta^{30}Si/^{28}Si$ (with Z grains having $\delta^{29}Si/^{28}Si << \delta^{30}Si/^{28}Si$), indicating that both of these types of SiC originated in low-metallicity stars. Depletions in both $^{29}Si$ and $^{30}Si$, relative to $^{28}Si$, are strongly indicative of Galactic Chemical Evolution (GCE), which assumes an age-metallicity relationship based on the evolution over time of the ratio of primary nuclei to secondary nuclei (Zinner et al. 2006). The earliest stars were extremely metal-poor (deficient in elements heavier than H and He) and were composed mainly of primary nuclei, such as $^{12}C$, $^{16}O$, and $^{28}Si$, which can be made from a star composed solely of H and He. Secondary nuclei, like $^{29}Si$ and $^{30}Si$, require the presence of elements heavier than He to act as a seed nuclei to which protons or neutrons can be added, thereby increasing the metallicity of the star. As metal-poor massive stars in the early Galaxy rapidly evolved and ejected their nucleosynthetic

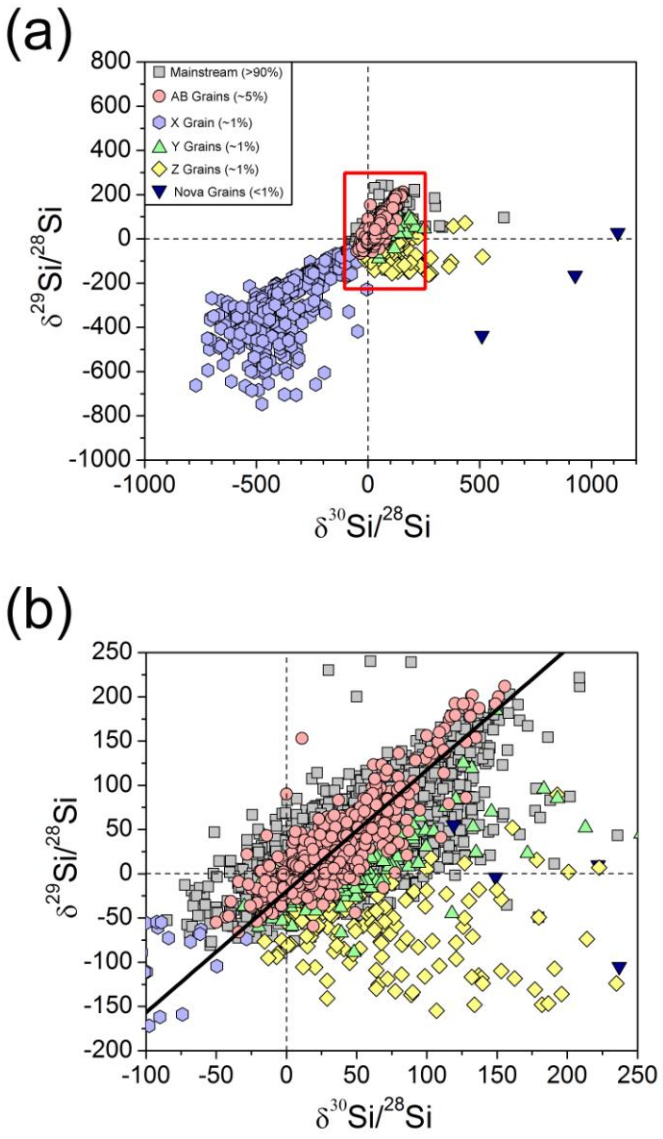


Figure 4.2: Plot of the Si isotopic compositions of all the presolar SiC grains in the Presolar Database, expressed as delta values, showing all of the major SiC types. The area indicated by the red box in (a) is magnified in (b) to show a detailed view of the Si isotopic ratios of mainstream, AB, Y, and Z grains. The solid black line in (b) is the mainstream correlation line [$\delta^{29}Si/^{28}Si = 1.37 \times \delta^{30}Si/^{28}Si - 19.9$ (Zinner et al. 2007)], along which most mainstream and AB grains fall. The equation of this line was determined utilizing data from the Presolar Database, which is also where all the plotted data points, along with references to their original discovery, can be found (Hynes and Gyngard 2009).

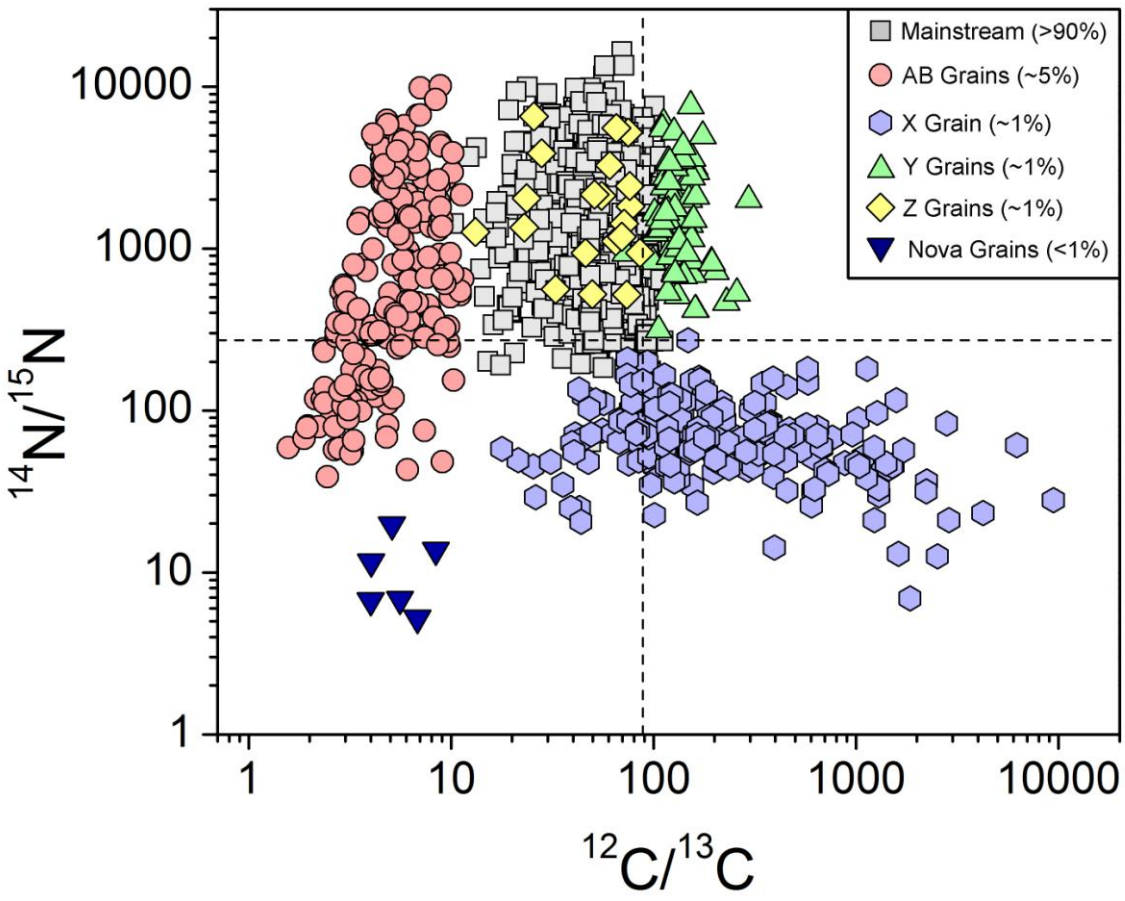


Figure 4.3: Plot of the C and N isotopic ratios of presolar SiC grains, showing all of the major SiC sub-types. As in Figure 4.3, all of the data can be found in the Presolar Database (Hynes and Gyngard 2009).

products into the ISM, each subsequent generation of stars inherited some of this material and became progressively more metal-rich. In this way, GCE traces the evolution of the $^{29,30}Si/^{28}Si$ isotopic ratios over time. The Si isotopic ratios of Y grains match predictions for stars of approximately one-half solar metallicity (Amari et al. 2001b), while Z grains match predictions for stars of approximately one-third solar metallicity (Hoppe et al. 1997).

SiC Y grains are defined as having $^{12}C/^{13}C$ ratios > 100, which agrees with models of low-metallicity stars with enrichments in the products of He burning (e.g., $^{12}C$) (Amari et al. 2001b). Z grains, however, have $^{12}C/^{13}C$ ratios similar to those of mainstream grains due to the effects of extra-mixing processes, such as CBP (Zinner et al. 2006). Both Y and Z grains have $^{14}N/^{15}N$ ratios similar to those of mainstream grains, indicative of H burning in low-mass stars (Meyer and Zinner 2006). The $^{26}Al/^{27}Al$ ratios inferred for Y and Z grains are also similar to those in mainstream grains and are typical of an AGB star origin.

Besides the major types of presolar SiC described above, a few minor subpopulations exist. Some grains, (less than 1% of presolar SiC grains) are believed to be from ONe novae. These grains have extremely low $^{12}C/^{13}C$ ratios similar to those in AB grains ($1 < ^{12}C/^{13}C < 9$) coupled with extremely low $^{14}N/^{15}N$ ratios ($5 < ^{14}N/^{15}N < 20$), large excesses in $^{30}Si$ relative to $^{28}Si$, and high inferred $^{26}Al/^{27}Al$ ratios (Amari et al. 2001a). However, Ti and Ca isotopic measurements indicate that at least two grains previously ascribed to a nova origin may, indeed, have a SN origin, leading to questions about the remaining nova grains (Nittler and Hoppe 2005). Despite this uncertainty, the

$^{12}C/^{13}C$ ratio ($^{12}C/^{13}C$ = 1.04 ± 0.01) of at least one grain strongly argues that at least some SiC grains have a nova origin (Nittler et al. 2006).

Several grains (<<1 %) have extreme enrichments in $^{29,30}Si$, with $\delta^{29,30}Si/^{28}Si$ > 1000 (e.g., Amari et al. 1999; Croat et al. 2010b). Most of these unusual SiC grains are very small (< 500 nm) (Hoppe et al. 2010; Gyngard et al. 2010a) and several have been discovered as inclusions within presolar graphite grains (Croat et al. 2010b). The extreme Si isotopic ratios of these grains indicate that they most likely originated in massive stars (Type II SNe). With only a handful of these grains currently known, isotopic data are extremely limited, but they suggest that these grains have isotopically light C. The isotopic compositions of trace elements in these grains may also be extremely unusual, as indicated by S measurements on two grains, which have large depletions in $^{33,34}S$, relative to $^{32}S$ (Gyngard et al. 2010a; Hoppe et al. 2010). It has been suggested that this type of unusual SiC may constitute a new group of presolar SiC, termed "Type C" grains, but the discovery of more grains with extremely large enrichments in $^{29,30}Si$ is needed to better understand their origin.

### 4.1.2 Graphite

Presolar graphite was discovered in 1990 as the carrier of Ne-E(L) (Amari et al. 1990). Unlike presolar SiC, presolar graphite is categorized as either high-density graphite or low-density graphite, with the different densities displaying very different isotopic, chemical, and structural properties. Most isotopic and TEM measurements of

presolar graphite have been done on grains from the Murchison meteorite. TEM studies of hundreds of high-density graphite slices [2.15 – 2.20 g $cm^{-3}$ for the best-studied fraction, KFC1 (Amari et al. 1994)] reveal two basic morphologies named for their general appearance: "onion" and "cauliflower" (Figure 4.4a-c). The onion-type graphite grains are composed of well-ordered, concentric shells of graphene sheets with long-range order, like the layers of an onion vegetable (Croat et al. 2005). About two-thirds of these onion-type grains also contain nanocrystalline cores, which are made of randomly oriented sheets of graphene ~3 – 4 nm in diameter (Figure 4.4a) (Bernatowicz et al. 1996). Cauliflower graphite grains, on the other hand, have turbostratic layering of the graphene sheets, which results in wavy layers and visible gaps, much like the wrinkled surfaces of their namesake vegetable (Figure 4.4c). While there is some short-range order (<50 nm), they do not have the long-range order and concentric shells that the onion-type graphite grains display. Both types of grains are spherical and are generally ≥1 μm in size. Onion and cauliflower graphite grains both frequently contain refractory carbides like (Ti, Zr, Mo)C, which have average s-process enrichments of times the solar abundance, clearly indicating an origin in AGB stars. High-density graphite grains have a wide range of $^{12}C/^{13}C$ ratios ($2 < {}^{12}C/{}^{13}C < 4000$) and typically have solar $^{16}O/^{18}O$ and $^{14}N/^{15}N$ ratios (Hynes and Gyngard 2009).

Low-density graphite grains (1.6 – 2.05 g $cm^{-3}$) also display a wide range of $^{12}C/^{13}C$ ratios ($3 < {}^{12}C/{}^{13}C < 7000$) (Hynes and Gyngard 2009). They are believed to originate in SNe, which is indicated by the excesses in $^{18}O$, $^{15}N$, and $^{28}Si$ that are measured in many of the grains. These grains are typically larger than their high-density

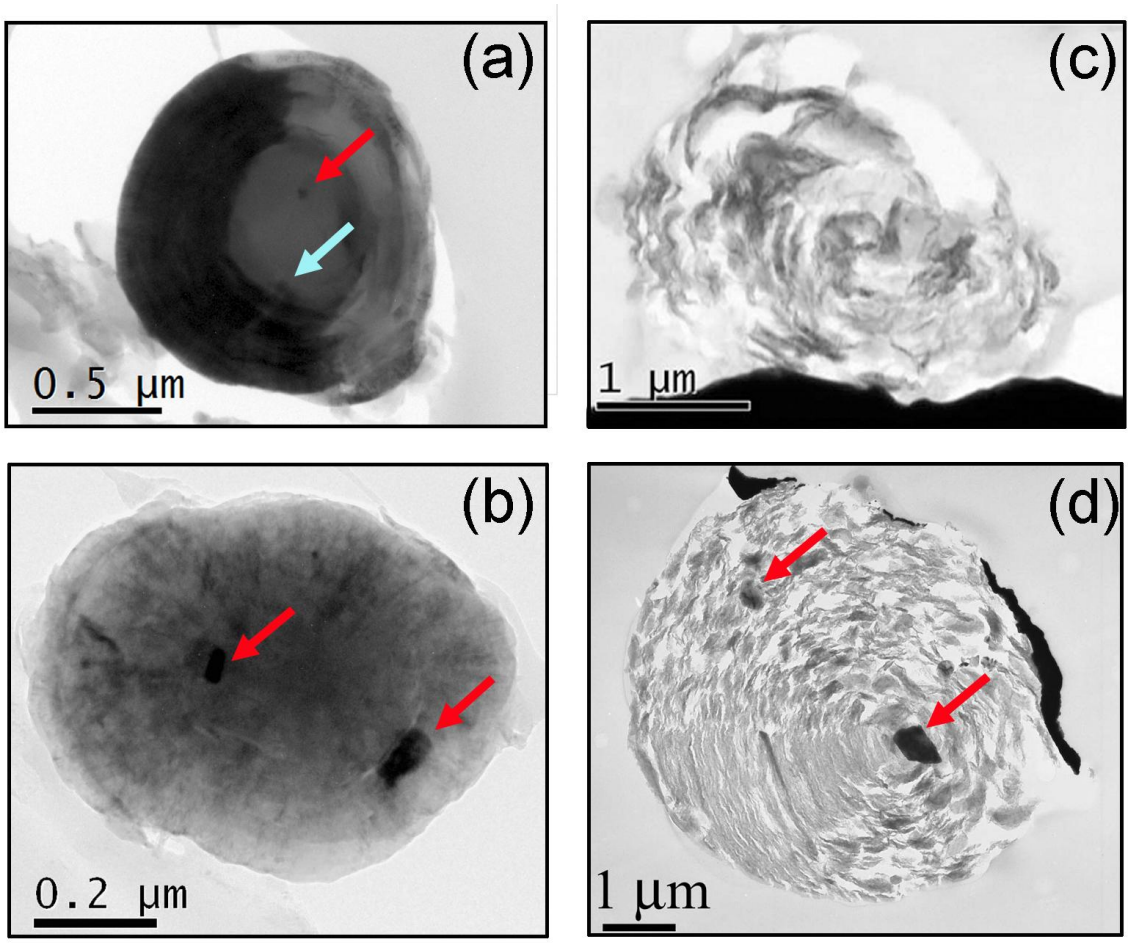


Figure 4.4: TEM BF images of typical examples of each of the major morphologies of presolar graphite from the Murchison meteorite. The different morphologies are differentiated by the local ordering of the graphene sheets (Croat et al. 2005). (a) High-density graphite grain with an onion-type morphology and a nanocrystalline core, which is observed in ~66% of onion-type graphite grains. The red arrow indicates a TiC subgrain and the blue arrow indicates a SiC subgrain (Hynes et al. 2006). (b) High-density graphite grain with an onion-type morphology, but lacking a nanocrystalline core. The arrows indicate two examples of internal (Ti,Zr)C subgrains (Croat et al. 2005). (c) High-density graphite grain with a cauliflower-type morphology. Subgrains are less common in cauliflower-type graphite grains, although due to slicing effects, abundances are difficult to compare between density fractions (Croat et al. 2005). (d) Low-density graphite grain with a SN origin. The arrows indicate two examples of TiC subgrains (Croat et al. 2003).

counterparts and range in size from 4 – 12 μm in diameter. TEM analysis indicates low-density graphite is composed of concentric turbostratic layers, somewhere between the onion and cauliflower morphologies in terms of degree of graphitization (Figure 4.4d) (Croat et al. 2003). TiC and Fe-Ni subgrains like those described in detail in sections 2.1 and 2.4.3 also indicate a SN origin.

Until recently, it was believed that presolar graphite grains fell neatly into two categories, with high-density grains having an AGB origin and low-density grains having a SN origin. However, several recent examples have challenged this overly simplified view. The extreme $^{29,30}Si/^{28}Si$ isotopic ratios measured in SiC subgrains (the possible Type C grains described above) found within high-density graphite grains suggest an origin in the outflows of Type II SNe (Croat et al. 2010b and see Appendix). Numerous isotopic measurements on high-density graphite grains with low $^{12}C/^{13}C$ ratios from the Orgueil meteorite have also provided some surprises (Jadhav et al. 2008). Three grains contain significant excesses in $^{44}Ti$, a clear indicator of a SN origin, although the $^{13}C$ excesses are atypical of grains with a SN origin. Several other grains contain extremely large Ca and Ti isotopic anomalies that are not consistent with model predictions for AGB stars. When coupled with the extremely low $^{12}C/^{13}C$ ratios (similar to those measured in AB grains), these data suggest a possible origin in born-again AGB stars for these unusual graphite grains. Preliminary TEM analyses of low-density graphite grains from Orgueil revealed some unique subgrains, such as possible silicate and troilite subgrains, but additional work is needed to determine if the subgrains in Orgueil graphite grains differ considerably from those in graphite grains from Murchison (Croat et al. 2010a).

### 4.1.3 Nanodiamonds

Nanodiamonds are the most abundant type of presolar grain. They were also the first type of presolar grain to be discovered; their isolation was the result of the fact that nanodiamonds are the carriers of Xe-HL (Lewis et al. 1987). Despite their relatively high abundance, nanodiamonds are the least-studied type of presolar grain. Isotopically anomalous Xe and Te are indicative of a SN origin (Lewis et al. 1987; Richter et al. 1998), but bulk C isotopic measurements reveal solar $^{12}C/^{13}C$ ratios (Russell et al. 1996). As their name indicates, nanodiamonds are very small (2.6 nm mean diameter) and it is impossible, even with extremely high spatial resolution mass spectrometers like the NanoSIMS, to analyze individual nanodiamonds. Therefore, the $^{12}C/^{13}C$ measurements confirm only that bulk nanodiamonds are solar; there could, in theory, be a significant population with $^{12}C$ excesses and another significant population with $^{13}C$ excesses and the opposite effects essentially "cancel" each other out, resulting in a bulk solar composition. Alternatively, there could be only a small number of presolar nanodiamonds within a much larger number of solar nanodiamonds, which would greatly dilute any isotopic anomalies and make them difficult to observe in a sea of solar composition nanodiamonds. This problem could eventually be resolved by the application of a new technique, the atom probe, to measure the isotopic ratios of individual nanodiamonds (Stadermann et al. 2010). Recent work shows signs of promise, but is still in the testing stages.

Despite the limitations on making isotopic measurements of individual nanodiamonds, an extremely successful study on the structure and formation mechanism of nanodiamonds has been carried out by Daulton et al. (1996). However, as this chapter

deals primarily with the isotopic properties of presolar grains, which are not available for individual nanodiamonds, the reader is referred to the sources mentioned in this discussion for additional information on nanodiamonds.

## 4.2 Oxygen-rich Phases and Other Types of Presolar Grains

### 4.2.1 Oxides

One of the reasons that SiC is the best studied type of presolar grain is that it is extremely easy to distinguish presolar SiC from solar SiC in the meteorite because there is essentially no solar SiC in carbonaceous meteorites. Unlike their carbonaceous counterparts, O-rich presolar phases are far more challenging to find, due to the fact that since the SS formed under oxidizing conditions, most rocks, including the meteorite matrix in which the presolar grains are located, are made up of O-rich minerals. This makes it exceedingly difficult to locate the presolar O-rich grains amongst their isotopically normal neighbors, and, in fact, only about 0.3% of the oxide grains found in meteorites are actually presolar.

Until recently, techniques designed to locate presolar O-rich grains had been largely inefficient. One method was to automatically image extremely densely packed areas of a grain mount (Figure 4.5b-c), which allowed for a large number of grains to be measured, thus also increasing the total number of presolar grains located (Nguyen and Zinner 2004). A less efficient method was to manually measure single grains that were sparsely distributed on a grain mount (Zinner et al. 2003) (Figure 4.5a). Due to the

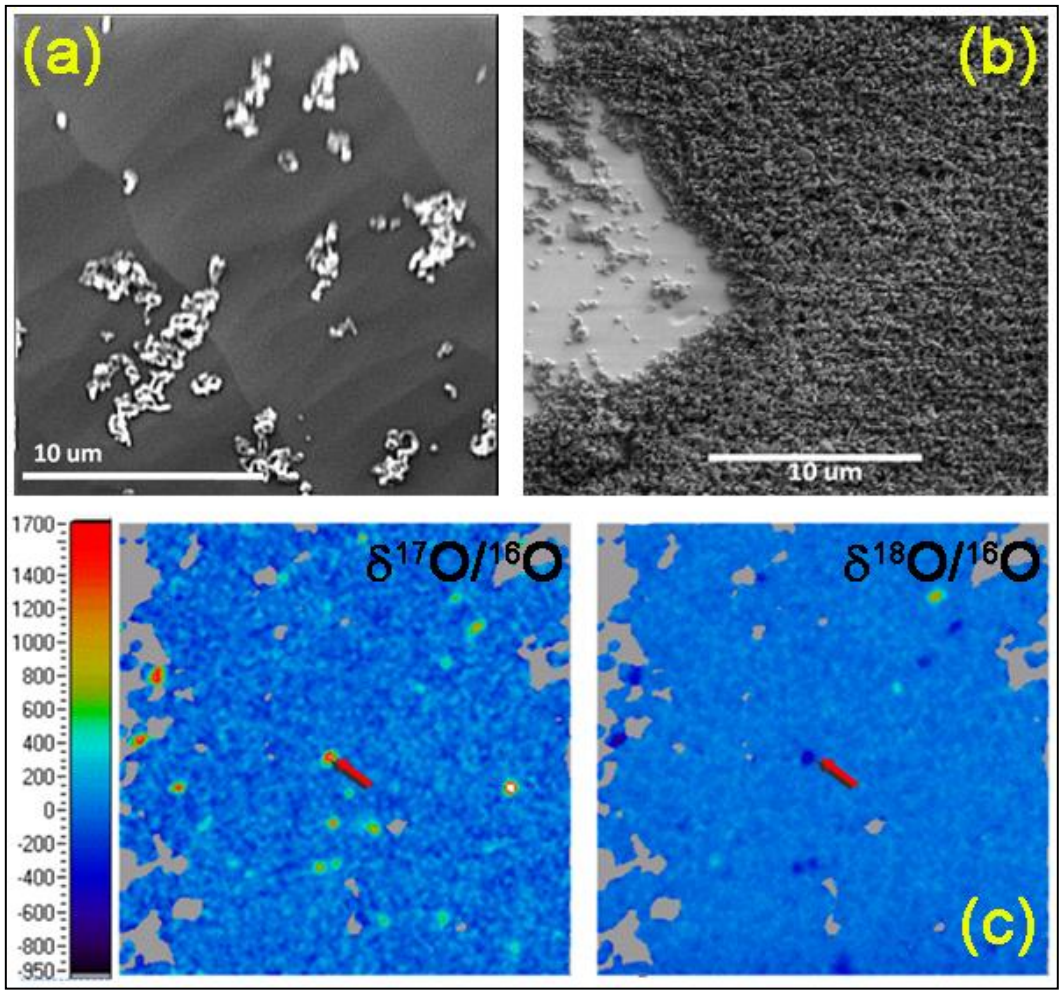


Figure 4.5: (a) NanoSIMS secondary electron image of well-separated oxide grains from the Murray meteorite. The isotopic compositions of these grains can be individually measured in the NanoSIMS (Figure courtesy of Frank Gyngard). (b) SEM image of a densely packed area of a grain mount from the Murray meteorite. Ion imaging (c) is the most efficient way to measure the isotopic compositions of this type of densely packed area. (c) The $^{17}O/^{16}O$ (left) and the $^{18}O/^{16}O$ (right) NanoSIMS ratio images of a densely packed area like the one pictured in (b). Grains with solar composition appear in shades of blue (deviations of ~0‰). Presolar grains deviate significantly from the solar value and therefore stand out as noticeable color variations, known as hotspots, like the presolar grain indicated with an arrow (Figures (b) and (c) from Nguyen 2005).

significant amount of man-hours required of the NanoSIMS user to perform these measurements, only a relatively small number of grains could be analyzed. However, this technique has recently been automated and successfully applied to oxides [as well as SiC (Hynes et al. 2009) – see Appendix], drastically reducing the amount of time a NanoSIMS user is required to manually operate the instrument, and thus increasing the total time the machine can measure grains (Gyngard et al. 2010b). The other advantage to this method is that the grains are well separated, allowing for many additional isotopic measurements without isotopic dilution from nearby isotopically normal grains.

Presolar oxide grains were discovered in 1994 based on their anomalous O compositions, well after their carbonaceous counterparts (Hutcheon et al. 1994; Nittler et al. 1994). The later discovery date came, in part, from the fact that oxides do not carry any of the exotic noble gases that led to the initial discovery of carbonaceous presolar grains. The $^{17}O/^{16}O$ and $^{18}O/^{16}O$ ratios for both presolar oxides and presolar silicates are plotted in Figure 4.6, along with the processes responsible for producing the O isotopic signatures of these grains. Both the $^{17}O/^{16}O$ and $^{18}O/^{16}O$ ratios are expected to increase with time and thus chart GCE (Timmes et al. 1995), with the $^{17}O/^{16}O$ ratio also being affected by stellar mass. Based on this idea, presolar oxides and silicates have been divided into four groups, based on their O isotopic ratios (Nittler et al. 1997). Group 1 grains are defined as $^{17}O/^{16}O \gtrsim$ solar ($3.82 \times 10^{-4}$) and solar ($2.01 \times 10^{-3}$) $\gtrsim {}^{18}O/^{16}O \gtrsim 8 \times 10^{-4}$. These isotopic ratios closely match observations of RG and AGB stars of roughly solar metallicty (e.g., Harris et al. 1987). This range of O isotopic ratios results from H burning in low- to intermediate-mass stars, followed by dredge-up events (Boothroyd and

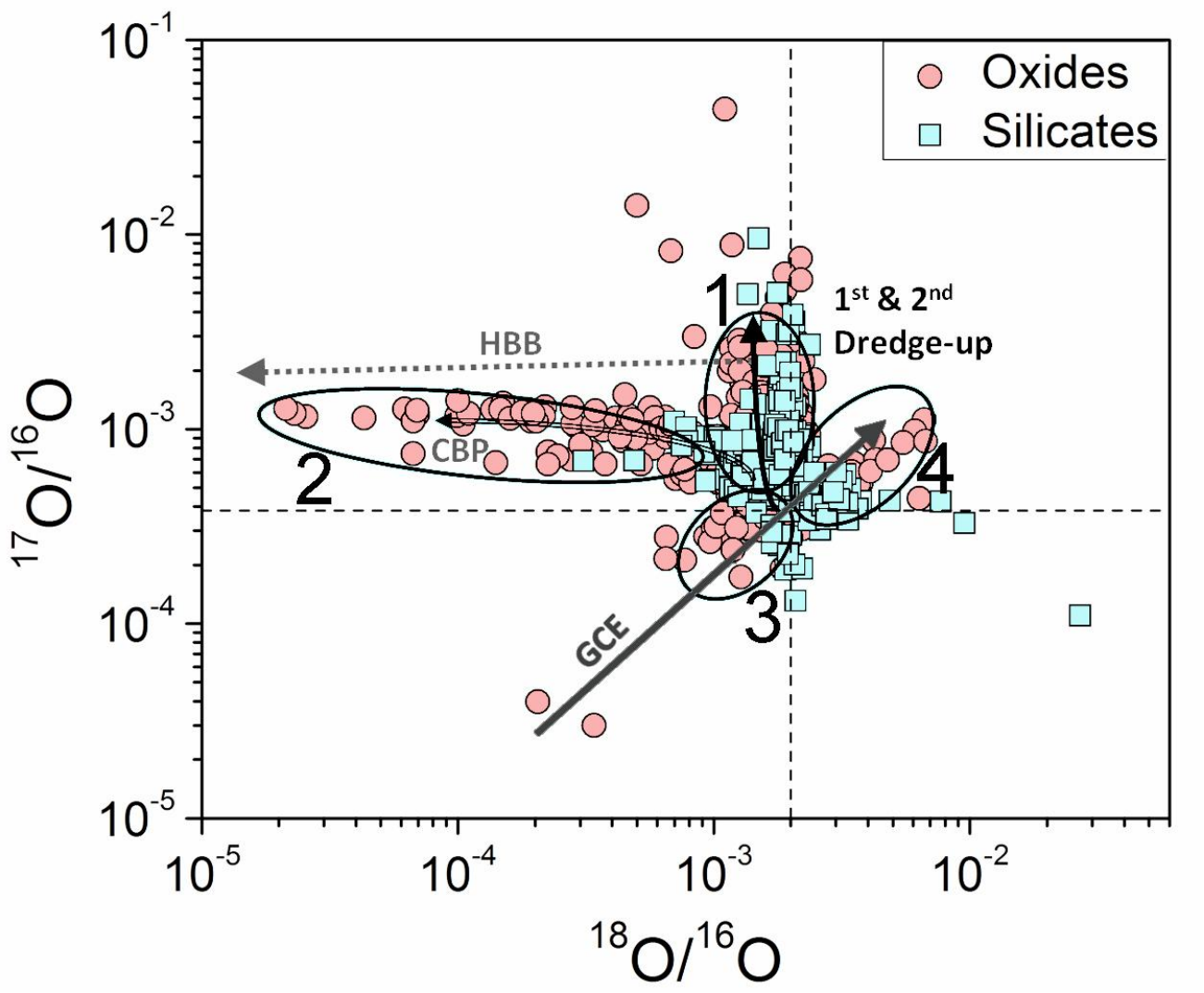


Figure 4.6: Plot of O isotopic ratios of presolar silicate and oxide grains. The groups of presolar O-rich grains, as defined by Nittler et al. (1997), are indicated by the ellipses. The processes responsible for producing these ratios are also schematically indicated in the plot. The maximum $^{17}O/^{16}O$ ratio encompassed by the Group 1 ellipse indicates the highest $^{17}O/^{16}O$ ratio that can be produced by AGB stars (Boothroyd and Sackmann 1999), indicating that the grains with $^{17}O/^{16}O$ ratios higher than this value (~4 x $10^{-3}$) are produced in novae (Gyngard et al. 2010b). The solar values of $^{17}O/^{16}O$ and $^{18}O/^{16}O$ are indicated with dashed lines. Data for all the presolar grains can be found in Hynes and Gyngard (2009). (Figure partially adapted from Gyngard et al. 2010b)

Sackmann 1999). Also believed to originate in RGB and AGB stars, group 2 grains have $^{17}O$ excesses, but these are coupled with large depletions in $^{18}O$ ($^{18}O/^{16}O < 10^{-3}$). These low $^{18}O/^{16}O$ ratios cannot be explained by first and second dredge-up events, and, like Z grains, extra mixing in the form of CBP is required to explain the measured ratios (Zinner 2007). While group 3 grains are also thought to have a RGB and AGB origin, they have significant depletions in both $^{17}O$ and $^{18}O$, indicating that their parent stars were both low-metallicity and low-mass. The isotopic compositions of group 3 grains were compared to models of stellar evolution and GCE to obtain an age of the Galaxy of 14.4 ± 1.3 Gyr (Nittler and Cowsik 1997), which is consistent with the extremely high-precision age of 13.7 ± 0.2 Gyr obtained from measurements of the cosmic microwave background (Spergel et al. 2003). The $^{18}O$ excesses found in group 4 grains are suggestive of a SN origin, likely from the mixing of $^{18}O$-rich material from the He/C zone into the O-rich zones (Choi et al. 1998). In addition, there are several grains that have indicators of a nova origin, namely $^{17}O/^{16}O >> 4 \times 10^{-3}$, which is the maximum $^{17}O/^{16}O$ ratio that can be produced by standard AGB nucleosynthesis models (Gyngard et al. 2010b; Nittler et al. 1997). New reaction rates and models may, however, revise these numbers (Nittler et al. 2010).

A variety of presolar oxide phases have been identified based on their compositions, including $Al_2O_3$ (compositionally like corundum), $MgAl_2O_4$ (compositionally like spinel), and $CaAl_{12}O_{19}$ (compositionally like hibonite). These are not only the most abundant types of presolar oxides, but they are also the most refractory. As the circumstellar environment in which presolar grains condense begins to cool, the first phase to condense (for C/O < 1) is $Al_2O_3$, at temperatures between ~1400 – 1600 K

for reasonable pressures, followed by $CaAl_{12}O_{19}$ and $MgAl_2O_4$ (Lodders and Fegley 1995). The best studied phase [true abundances are difficult to give due to sampling biases of spinel-rich and spinel-poor grain fractions (Zinner 2007)] is $Al_2O_3$. However, the mineral identification of these grains is somewhat problematic. While in older literature, these grains are referred to as corundum (e.g., Choi et al. 1998; Nittler et al. 1997), recent TEM analysis has revealed that while some of these grains are, in fact, truly corundum (meaning they have both the composition and the crystal structure of corundum), others are amorphous (Stroud et al. 2004a). Because a true mineral phase is defined by both its composition and its crystal structure, some of the grains are truly corundum, while others just have a corundum-like composition, but can only be correctly referred to as alumina (of which corundum is one type).

The second and third most studied types of presolar oxides are $MgAl_2O_4$ and $CaAl_{12}O_{19}$. Unlike $Al_2O_3$, TEM measurements (although quite limited in number), indicate that all presolar $MgAl_2O_4$ and $CaAl_{12}O_{19}$ are actually spinel and hibonite, respectively (Stroud et al. 2008; Zega et al. 2010). A few cases of presolar chromite ($FeCr_2O_4$), which can also contain some Mg and Al, have also been observed (Nittler et al. 2005; Zega et al. 2008). This phase is not predicted by thermodynamic equilibrium calculations to condense from a gas of solar composition (Ebel 2006); spinel and Fe metal grains are expected to condense instead. However, both isotopic and microstructural data indicate that presolar chromite does, in fact, exist, possibly suggesting non-equilibrium condensation. Finally, five cases of presolar $TiO_2$ have been observed, although no additional TEM data are available to determine exactly which phases of $TiO_2$ are present (Bose et al. 2010; Nittler et al. 2008).

### 4.2.2 Silicates

Almost two decades before their discovery, presolar silicates were believed to exist based on spectroscopic observations of young main sequence stars and O-rich AGB stars, which indicated a high abundance of both crystalline and amorphous silicate grains (Little-Marenin 1986; Waelkens et al. 1996; Waters et al. 1996). Although the spectroscopic evidence proved that silicates condense around O-rich stars, it was feared that these particles were not as resistant to processing in the ISM, the solar nebula, or the meteoritic parent body as other grain types, and were therefore destroyed. It was not until 2003 that presolar silicates were first discovered in IDPs (Messenger et al. 2003) and until 2004 that they were discovered in meteorites (Nguyen and Zinner 2004), well after the other major types of presolar grains. The delay in their discovery was due to several factors, including: their small size (usually < 500 nm); their destruction by the harsh acid treatments used to isolate the carbonaceous phases; and the difficulty in locating presolar silicates amongst large amounts of surrounding isotopically solar meteorite matrix material. Their discovery was only made possible by the high spatial resolution of the NanoSIMS.

Since their comparatively late discovery, presolar silicates have been in the limelight of presolar grain research and are currently one of the most often studied types of presolar grains. Even more so than presolar oxides, presolar silicates are difficult to locate amongst the surrounding matrix material. Automatic isotopic imaging with the NanoSIMS of large, densely packed areas of thousands of silicate grains has proven the most effective way to locate presolar silicates grains (Nguyen et al. 2007), as well-separated grain residues of silicate are not able to be produced. Such analysis has

revealed that presolar silicates are the second most abundant type of presolar grains, with an average abundance of ~375 ppm in IDPs and ~180 ppm in meteorites, although this abundance is highly dependent upon the type of meteorite analyzed, with the most primitive (and therefore least altered) meteorites like Acfer 094 having significantly higher abundances than more altered meteorites. It is unclear at this time if the difference in abundances between meteorites is the effect of thermal and/or aqueous alteration of the parent body, the heterogeneous distribution of silicates within the chondrite forming regions of the early solar nebula, or the result of instrumental biases, such as different estimates of grain detection efficiency, which is dependent upon both grain size and instrumental conditions (Floss and Stadermann 2009).

Like presolar oxides, presolar silicates are categorized into four groups, which have similar isotopic characteristics and are thought to have the same stellar origins as their oxide counterparts in each group. When comparing the $^{17}O/^{16}O$ and $^{18}O/^{16}O$ ratios of presolar silicates and oxides in Figure 4.6, it is evident that, for the most part, the silicates have smaller isotopic anomalies than do the oxides. However, this is most likely not a real difference, but instead is due to the fact that silicate measurements are made in densely packed areas and silicate grains are generally smaller than oxide grains. This results in the primary beam of the NanoSIMS overlapping small areas of the densely packed grains adjacent to the target grain being measured. If a presolar silicate is the target grain, the surrounding grains are all most likely isotopically normal and will contribute some of their normal O isotopic composition to the measurement. The measured O ratios are therefore somewhat diluted by this normal component. This effect has been clearly demonstrated on measurements of spinel that were individually

measured in well-distributed areas and also imaged in densely packed areas (Nguyen et al. 2003). While isotopic dilution is only a minor problem with the NanoSIMS, which can routinely get a beam size of ~100 nm or smaller, previous mass spectrometers had beam sizes of ~1 μm, which measured so many surrounding normal grains that any isotopic anomaly present in the presolar grain was completely diluted, making it appear isotopically normal. This is one of the major reasons why presolar silicates were not discovered until the advent of the NanoSIMS.

The mineralogy of presolar silicate grains has proven to be quite complex. While TEM is still the best way to absolutely determine both the composition and the crystal structure of a grain, the sample preparation is quite difficult on such small grains and bulk isolation of the type used for carbonaceous grains and oxides is inherently destructive to the silicate grains. To an even greater extent than for carbonaceous grains, this severely limits the number of presolar silicate grains that can be analyzed in the TEM (e.g., Messenger et al. 2003; Vollmer et al. 2007). However, the use of the Auger Nanoprobe has significantly improved the compositional analysis of presolar silicates (Floss and Stadermann 2009). This instrument, in addition to being non-destructive and not requiring extensive sample preparation, can measure just the grain in question, without getting signal from surrounding grains. Unlike EDXS, which samples a large volume of material (with a depth of ~1 μm below the surface that the beam hits the sample), Auger spectrometry uses Auger electrons to sample just the top few atomic layers. The volume sampled with EDXS does not present a problem in TEM analysis due to the small sample thickness that is required for electron transparency, but the volume sampled by EDXS in traditional non-destructive techniques, like SEM, measures not only the grain of interest,

but the underlying material as well. By sampling multiple grains, the true composition can become ambiguous or even be entirely disguised.

With the use of the Auger Nanoprobe, the NanoSIMS, and TEM, a number of compositional types of presolar silicate grains have been identified. These include: $(Mg,Fe)_2SiO_4$ (olivine); $(Mg,Fe,Ca)SiO_3$ (pyroxene); $CaTiO_3$ (perovskite); $Mg_2SiO_4$ (forsterite); glass with embedded metals and sulfides (GEMS); $SiO_2$ (silica); as well as grains with nonstoichiometric compositions (see Hynes and Gyngard 2009 and references therein). A relatively small number of these grains have been analyzed in the TEM to confirm their mineralogy. These include the crystalline phases of olivine (e.g., Messenger et al. 2003) and perovskite (Vollmer et al. 2007), as well as nonstoichiometric silicates that are nanocrystalline or amorphous (e.g., Nguyen et al. 2007).

### 4.2.3 Other Types of Presolar Grains

One significant type of presolar grain that has not yet been discussed is presolar $Si_3N_4$. These grains are isotopically very similar to SiC X grains, with excesses in $^{28}Si$, $^{12}C$, and $^{15}N$, along with relatively high inferred $^{26}Al/^{27}Al$ ratios (Hynes and Gyngard 2009). Because of their isotopic similarity to X grains, $Si_3N_4$ grains are also believed to originate in SNe under reducing conditions (C/O > 1) combined with high N concentrations (Nittler et al. 1995). Equilibrium condensation models predict that $Si_3N_4$ is not a stable condensate in AGB stars; instead, other nitrides like AlN and TiN should form (Lodders and Fegley 1995), which may explain why no $Si_3N_4$ with isotopic signatures indicative of formation around an AGB star have been observed. Although

quite rare, with an abundance of only ~0.002 ppm, the use of automatic imaging has led to the discovery of nearly forty $Si_3N_4$ grains (Hynes and Gyngard 2009).

While the vast majority of presolar grains fall into one of the six types described above, there are numerous additional phases that have been observed, mainly as subgrains during TEM analysis, particularly in graphite (Bernatowicz et al. 1991; Croat et al. 2003; Croat et al. 2005; Croat 2007; Croat et al. 2009) and SiC (Bernatowicz et al. 1992; Hynes et al. 2010). Many examples of these rare grain types have already been described in detail in Chapters 2 – 3 and will therefore not be repeated here. However, it is important to further note the importance of TEM studies in addition to NanoSIMS analysis on all grain types: many of these presolar phases are too small and too rare to be identified by astronomical observations, while NanoSIMS analysis can only provide a suggestion of what the detected subgrain could be. Because NanoSIMS isotopic analysis can only measure a limited number of elements at one time, it may miss a major compositional constituent. Furthermore, it provides no crystallographic data for conclusive mineral identification.

## 4.3 The Presolar Grain Database

### 4.3.1 Motivation

The presolar grain types, sub-types, groups, and trends described above only became apparent after a large number of grains were measured. After twenty-three years of work, there are over twelve-thousand individual grains reported in the literature.

However, the amount of data is actually significantly larger because almost every grain measured has at least two reported isotopic ratios, with most having at least three or four and some having as many as fourteen ratios for a single grain. Furthermore, there is additional important information for each grain that must be considered, such as grain size, meteorite of origin, and the type of instrument with which the measurements were made. These data are themselves collected within hundreds of different papers, some of which are difficult to find or which may not be accessible except by paper copy. All together, this is a staggering amount of data. It becomes quite a struggle for an individual to simply create a plot of their data and compare it to previous isotopic measurements, such as the plots in Figures 2.1 and 2.2.

Although a few personal data compilations existed (S. Amari, pers. comm.; L. Nittler, pers. comm.; E. Zinner, pers. comm.), there was no comprehensive, easily accessible database of presolar grain isotopic data available to the entire presolar grain community. To fill this void, the idea for a database was conceived that would: include all of the available presolar isotopic data, as well as related additional information; be regularly updated as new data are published; and be created as a website so it could be available to the astrophysical community as a whole, not just to the presolar grain community. The collection of presolar grain data that was subsequently created and named the Presolar Database is intended for any interested party's professional or personal use, the only request being that the database be cited as Hynes and Gyngard (2009) in any papers for which the tool was utilized. The development, structure, limitations, and uses of this website (http://presolar.wustl.edu/~pgd) are presented in this chapter.

### 4.3.2 Organization

In order to best catalog the immense quantity of presolar grain isotopic data, a spreadsheet system was developed utilizing Microsoft Excel. Information on each grain was listed in a spreadsheet, with all the grains in a paper listed together in a single spreadsheet. Each paper was then compiled into a larger spreadsheet, which gives all the data for a particular grain type (e.g., SiC, graphite, oxides). Additionally, for convenience of use, each grain type (e.g., SiC) has the data for each sub-type (e.g., X, Y, Z, mainstream) put into a separate spreadsheet so that the database user can easily access a very specific type of grain.

A separate spreadsheet was created for every presolar grain paper, with data on each grain in the paper listed in separate rows. The columns contain all of the isotopic ratios and the corresponding 1σ errors measured for each grain, with each isotopic ratio and each error listed in separate columns (Figure 4.7). The isotopic ratios are listed as those most commonly used in the literature (e.g., $^{12}C/^{13}C$, $^{14}N/^{15}N$, $\delta^{29}Si/^{28}Si$). In some cases, papers list their isotopic compositions in alternate, less common forms (e.g., $\delta^{13}C/^{12}C$ values). In these instances, both the ratios and their corresponding errors were recalculated into the standard isotopic form (e.g., into $^{12}C/^{13}C$) and listed in this form in the database. Errors were also adjusted, when necessary, to be 1σ. These recalculations and adjustments were done to maximize the usability of the database; the user can always be assured he or she is comparing the proverbial apples to apples.

Even though the same isotopic ratios are not reported in each paper, all column headings for a given type of presolar grain (e.g., SiC, graphite, oxides) are the same. The

most illustrative example of this is SiC. A total of forty-six different isotopic ratios have been measured in SiC during various studies, primarily due to the large number of trace elements present in SiC and the relative ease with which they can be measured. While the $^{12}C/^{13}C$ and $^{14}N/^{15}N$ ratios, as well as $\delta^{29}Si/^{28}Si$ and $\delta^{30}Si/^{28}Si$ values, are reported for most SiC grains, only a handful have $^{7}Li/^{6}Li$ isotopic ratios or $\delta^{137}Ba/^{136}Ba$ values reported. However, for every paper with SiC data, all forty-six columns of isotopic ratios (and the corresponding forty-six columns of errors associated with each isotopic ratio or delta value) are listed. If a given isotopic ratio was not measured, the corresponding column is left blank. This allows every paper with SiC data to be easily transferred, combined, and sorted with every other paper and thereby avoids any problem with column mismatch; if each paper only contained columns for the isotopic data that are reported in it, sets of data from different papers could not be easily combined into a single spreadsheet.

In addition to isotopic data, other important information is included for each grain (Figure 4.8). The publication reference for each grain is given. This reference includes the first author's name (followed by et al. when appropriate), the journal in which the paper was published, and the publication year. In addition, for SiC and graphite, the sub-type (AB, X, Y, Z, nova, unusual, or mainstream grains for SiC and high- or low-density grains for graphite) is listed. For oxides and silicates (which both have the same column headings for easy comparison), the group number (e.g., 1, 2, 3, 4, or ungrouped), the grain phase (e.g., oxide or silicate), and the compositional mineralogy (e.g., pyroxene, olivine, spinel, corundum) are listed. The mineralogy is intended only to give a compositional description of the grain and does not include any structural information. If

TEM analysis determined the complete structural and compositional mineralogy of a grain, this is indicated under the "Techniques" section, in which the technique(s) and instrument(s) used to measure the grain (e.g., Washington University NanoSIMS; Naval Research Lab TEM) are included. Also included are additional data on each grain, such as the name by which the author refers to the grain in the original paper, the meteorite of origin, and the grain size, if available. Additionally, there is a spot for notes on the grain to explain any supplementary information. With this information about each grain provided, the database user has sufficient information to locate the specific paper and grain should they require additional information beyond what the database provides.

The data are available for download from the website in the choice of several formats. First, all of the data are compiled into a large spreadsheet containing all of the data for a specific grain type. The user can therefore download a file of all the available: SiC data; graphite data; oxide and silicate data, either combined into one file or as two distinct files; and $Si_3N_4$ data. Furthermore, for each grain sub-type (e.g., SiC AB grains or low-density graphite grains) a spreadsheet containing data for just that subset is also available for download. For example, if a user is interested just in SiC, he or she has the choice of downloading spreadsheets that contain all of the available grain data on: all SiC grains; SiC of sub-type mainstream, AB, X, Y, Z, or nova; unusual SiC grains that do not fit into any of the major sub-types, such as the Type C grains; and grains for which only heavy metal data are available (Nicolussi et al. 1997; Nicolussi et al. 1998a; Nicolussi et al. 1998b; Savina et al. 2003; Savina et al. 2004) that cannot be classified into a standard sub-type due to unmeasured $^{12}C/^{13}C$ and $^{14}N/^{15}N$ ratios, as well as $\delta^{29}Si/^{28}Si$ or $\delta^{30}Si/^{28}Si$ values. These grains were all measured with RIMS at Argonne

National Laboratory, in which lasers are utilized to selectively ionize only a single element at a time. This technique is extremely useful for precisely measuring heavy elements, which can provide valuable information about the s- and r-processes. These measurements are difficult, if not impossible, with conventional mass spectrometers like SIMS, due to the large number of isobaric and molecular interferences encountered during analysis of heavy elements. However, only certain elements are currently able to be ionized, and the lighter elements, such as C, N, and Si are currently unable to be measured with RIMS. If these elements are of interest, it is necessary to use another type of mass spectrometer, such as the NanoSIMS, to make these measurements. The two techniques were successfully combined to provide complimentary information on SiC mainstream grains in a study by Barzyk et al. (2007). It should also be noted here that until the advent of this database, the large suite of heavy element isotopic data generated by RIMS for presolar graphite and SiC grains was virtually unavailable to the community, as much of it is unpublished. Unfortunately, spreadsheets of data grouped by individual paper, which were used primarily as an organizational tool during the database construction, are currently unavailable for download on the website, although these spreadsheets are available upon request. Eventually, these spreadsheets will hopefully also be included for download on the website.

The website is intuitive to navigate. Upon entering the website address, http://presolar.wustl.edu/~pgd/, a welcome screen appears with a password request. As a security measure, the website is password protected, with the password available upon request via email to the address listed on the introductory webpage. After entering the password, a menu on the left side of the webpage displays each of the presolar grain

types and is the primary navigation tool. Once the user selects the grain type (e.g., SiC) for which they wish to download isotopic information, they are directed to a page where each of the grain sub-types (e.g., AB, X, mainstream, etc.) are listed as files available for download (Figure 4.9). Each of the spreadsheets described above is available as both an Excel 2003 file (compatible with both PC and Apple computers) and as a tab-delimited text file, for easy importation into custom plotting utilities. Clicking on the appropriate grain sub-type opens a dialog box that allows the user to download and save the file on their computer. As an additional precaution to ensure the integrity of the database, data can only be downloaded from the website; nothing can be uploaded, thus avoiding the possibility of a malicious user tampering with the data. However, user feedback, including the submission of additional data, corrections to the existing data, and suggestions for improvement, are strongly encouraged through email correspondence.

| $^{7}Li/^{6}Li$ | Error[$^{7}Li/^{6}Li$] | $^{12}C/^{13}C$ | Error[$^{12}C/^{13}C$] | $^{14}N/^{15}N$ | Error[$^{14}N/^{15}N$] | d($^{29}Si/^{28}Si$) | Error[d($^{29}Si/^{28}Si$)] | d($^{30}Si/^{28}Si$) | Error[d($^{30}Si/^{28}Si$)] |
|---|---|---|---|---|---|---|---|---|---|
| 9.3 | 0.4 | 47.5 | 0.4 | | | 45 | 4 | 73 | 7 |
| 10.7 | 0.2 | 55.7 | 0.4 | | | 70 | 4 | 75 | 7 |
| 9.8 | 0.4 | 48 | 0.4 | | | 51 | 4 | 74 | 7 |
| 10.9 | 0.4 | 47.4 | 0.4 | | | 36 | 4 | 57 | 7 |
| 10.5 | 0.2 | 47.5 | 0.4 | | | 57 | 4 | 71 | 7 |
| 10.8 | 0.3 | 48 | 0.4 | | | 55 | 4 | 65 | 7 |
| 9.7 | 0.2 | 47.9 | 0.4 | | | 57 | 4 | 66 | 7 |
| 11.3 | 0.3 | 90.8 | 0.7 | | | 15 | 3 | 21 | 7 |
| 11.4 | 0.4 | 47.4 | 0.4 | | | 54 | 4 | 76 | 7 |

Figure 4.7: Example of a spreadsheet of isotopic ratios and the corresponding errors of SiC mainstream grains from the Presolar Database. The most commonly used form of each isotopic ratio and its corresponding error are listed as column headings and are the same for every SiC grain in the database, even though every isotopic ratio was not measured for every grain (e.g., $^{14}N/^{15}N$ in this example). In the case that a particular isotopic ratio was not measured, the column for this ratio is left blank. This allows the data from any given study to be easily combined with data from any other study into a single spreadsheet, thus allowing for maximum flexibility. Data originally from Gyngard et al. (2009).

| Group | Phase | Mineralog | Grain Label | Reference | Meteorite | Technique | Size (nm) | Notes | $^{17}O/^{16}O$ |
|---|---|---|---|---|---|---|---|---|---|
| 3 | Oxide | Spinel | 10-11-4 | Gyngard ApJ 2010 | Murray | Wash U NanoSIMS | | | 3.544E-04 |
| 1 | Oxide | Spinel | 10-7-16 | Gyngard ApJ 2010 | Murray | Wash U NanoSIMS | | | 9.151E-04 |
| 1 | Oxide | Spinel | 11-1-1 | Gyngard ApJ 2010 | Murray | Wash U NanoSIMS | | | 9.500E-04 |
| 1 | Oxide | Spinel | 12-12-4 | Gyngard ApJ 2010 | Murray | Wash U NanoSIMS | | | 6.390E-04 |
| 4 | Oxide | Spinel | 12-13-3 | Gyngard ApJ 2010 | Murray | Wash U NanoSIMS | | | 1.116E-03 |
| U | Oxide | Spinel | 12-20-10 | Gyngard ApJ 2010 | Murray | Wash U NanoSIMS | | | 8.801E-03 |
| 1 | Oxide | Corundum | 1-2-8 | Gyngard ApJ 2010 | Murray | Wash U NanoSIMS | | | 1.045E-03 |
| 1 | Oxide | Spinel | 13-28-12 | Gyngard ApJ 2010 | Murray | Wash U NanoSIMS | | | 4.820E-04 |
| 2 | Oxide | Spinel | 13-30-9 | Gyngard ApJ 2010 | Murray | Wash U NanoSIMS | | | 1.189E-03 |
| 1 | Oxide | Spinel | 13-3-12 | Gyngard ApJ 2010 | Murray | Wash U NanoSIMS | | | 5.830E-04 |
| 2 | Oxide | Spinel | 13-34-3 | Gyngard ApJ 2010 | Murray | Wash U NanoSIMS | | | 1.009E-03 |
| 1 | Oxide | Spinel | 13-6-3 | Gyngard ApJ 2010 | Murray | Wash U NanoSIMS | | | 4.639E-04 |
| 2 | Oxide | Corundum | 14-1-14 | Gyngard ApJ 2010 | Murray | Wash U NanoSIMS | | | 9.876E-04 |
| 2 | Oxide | Spinel | 14-12-7 | Gyngard ApJ 2010 | Murray | Wash U NanoSIMS | | | 7.649E-04 |
| 1 | Oxide | Spinel | 14-13-6 | Gyngard ApJ 2010 | Murray | Wash U NanoSIMS | | | 4.445E-04 |
| 1 | Oxide | Spinel | 14-14-5 | Gyngard ApJ 2010 | Murray | Wash U NanoSIMS | | | 6.508E-04 |
| 1 | Oxide | Spinel | 14-19-2 | Gyngard ApJ 2010 | Murray | Wash U NanoSIMS | | | 1.367E-03 |
| 1 | Oxide | Spinel | 14-6-3 | Gyngard ApJ 2010 | Murray | Wash U NanoSIMS | | | 5.249E-04 |

Figure 4.8: Example of a spreadsheet from the Presolar Database containing additional information about oxide grains in Gyngard et al. (2010b). The data can be sorted by any of the columns, which are the same for every oxide and silicate grain.

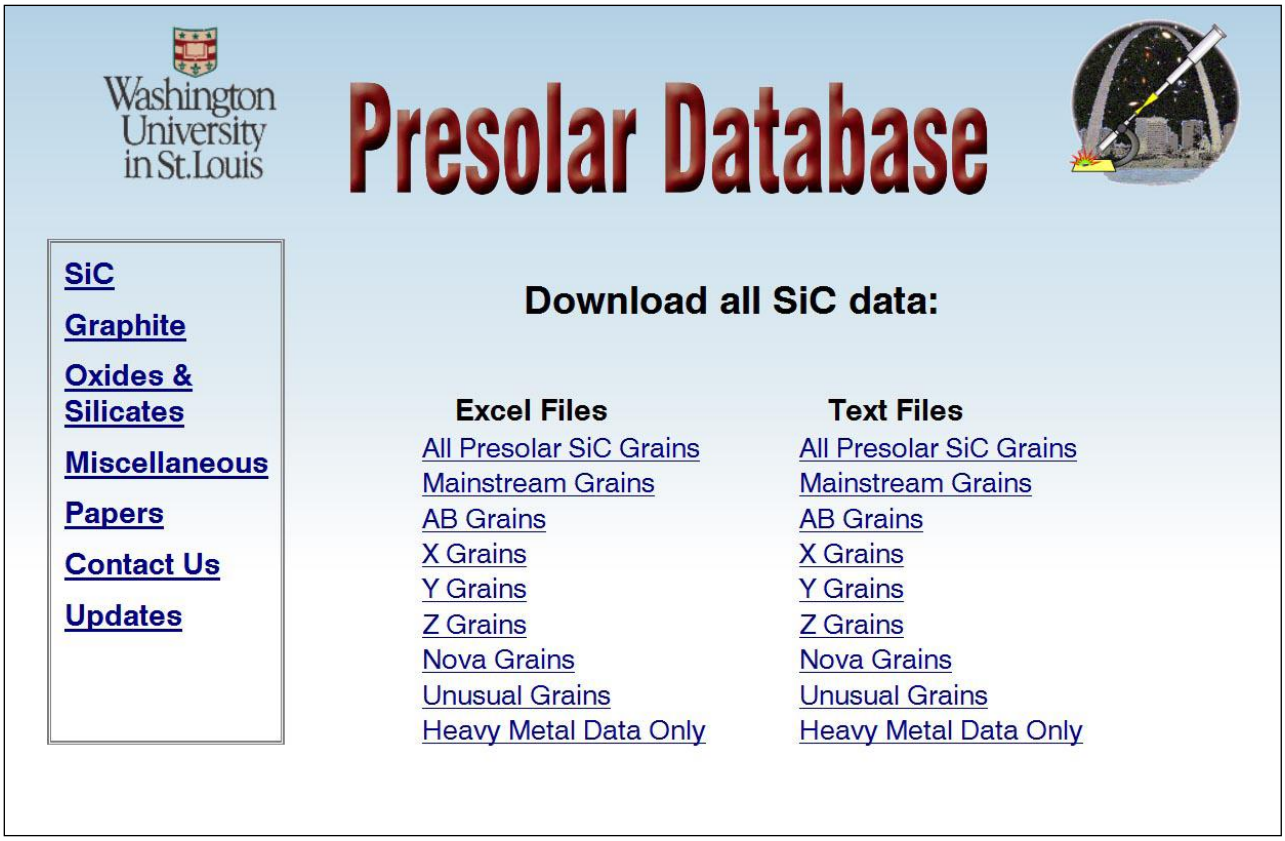


Figure 4.9: Sample image of the Presolar Database webpage (http://presolar.wustl.edu/~pgd) from which the user can download either all of the presolar SiC isotopic data in the database or a sub-set of the SiC data. The data are available for download by clicking the link on the webpage under the user's choice of two formats: a Microsoft Excel 2003 file or a tab-delimited text file. Similar pages exist for downloading graphite, silicate, and oxide data, to which the user can navigate using the links on the left side of the webpage

### 4.3.3 Uses and Successes

The Presolar Database is intended as a tool for the entire presolar grain and cosmochemistry community, as well as for scientists in other fields. The most useful feature of the database is the ease of locating and plotting data for any grain type or isotope of interest. Plots of large quantities of isotopic data, such as those shown in Figure 4.2 and 4.3, are readily created utilizing the presolar database. This type of graph was previously quite difficult to create, particularly for those who did not have access to a private compilation of presolar grain data. With the Presolar Database, access to updated data files is available to anyone who requests it.

For experimentalists, this is quite useful for comparing new data to all of the data previously acquired on any presolar grain type or sub-type of interest. This is essential in identifying trends in data and to determine if the experimentalist's data are consistent with previous measurements or if it represents some new result not previously observed. For example, Croat et al. (2010b) cite the database in their paper on the discovery of extremely anomalous SiC subgrains in graphite, which may constitute the new sub-type of group C grains. By plotting all of the SiC data in the database, it was readily apparent that only one previously measured SiC grain has similarly large $^{29,30}$Si excesses (Amari et al., 1999) and a quick perusal of the database provided the relevant reference information needed to locate this paper. In addition to comparing one set of data to another, the database is also useful to look at overarching trends in presolar grain data. For example, it has long been clear that mainstream SiC grains all fall roughly along a single line, known as the mainstream correlation line (shown as a solid line in Figure 4.2b), which is largely the result of GCE. The equation of this line was initially reported as $\delta^{29}Si/^{28}Si =$

1.34 x $\delta^{30}Si/^{28}Si$ – 15.7 (Hoppe and Ott 1997), which was based on the isotopic ratios of around six hundred grains from the KJG and KJH size fractions of the Murchison meteorite (at the time, this was one of the only large datasets of SiC mainstream grains). Although the mainstream correlation line has been amended several times utilizing various available datasets (Lugaro et al. 1999; Nittler and Alexander 2003), Zinner et al. (2007) used the more than six-thousand mainstream grains in the Presolar Database to determine a new equation for the mainstream correlation line: $\delta^{29}Si/^{28}Si = (1.37 \pm 0.01)$ x $\delta^{30}Si/^{28}Si - (19.9 \pm 0.6)$. Access to a substantially larger data set (by an order of magnitude) than that used by Hoppe and Ott allowed Zinner et al. to determine a value for the mainstream correlation line that better describes all SiC mainstream grains. This includes grains from a variety of parent meteorites as well as grains with a wide assortment of sizes. Furthermore, the updated equation has very small errors, particularly on the slope.

In addition to creating isotope plots, information about a particular ratio can be quickly obtained by sorting the data contained in a given spreadsheet by an isotope of interest. It is then extremely easy for an experimentalist to survey the entire range of data collected on that particular isotopic ratio, quickly focus in on the most anomalous ratios, and then locate the references for these ratios for further study. For example, in sections 2.2.3 and 2.4.1 of this thesis on the inferred $^{26}Al/^{27}Al$ ratios in SiC X grains, the database provided exceptionally quick access to the range of $^{26}Al/^{27}Al$ ratios previously measured in X grains, along with the most extreme value and the errors on this measurement (analyzed by Nittler et al., 1995). This allowed a simple determination on whether the EDXS Mg/Al ratios were, within errors, consistent with the isotopic measurements of the

inferred $^{26}Al/^{27}Al$ ratios in X grains. Instead of manually looking through the ~20 papers on SiC X grains and searching for the range of the inferred $^{26}Al/^{27}Al$ ratios in these grains, the database provided the same information in seconds.

Furthermore, the database is also useful in allowing an experimentalist to quickly identify which grain types or isotopic ratios are particularly well studied or for which there is a dearth of data, possibly suggesting a new line of study. For example, the database indicated there was only one SiC Z grain for which the Fe and Ni isotopic ratios were measured and that this grain has quite anomalous $^{54}Fe/^{56}Fe$ and $^{62}Ni/^{58}Ni$ ratios, which prompted additional measurements on SiC Z grains (Hynes et al., 2009), as discussed in the Appendix.

As useful as the database can be to experimentalists, access to a large, comprehensive dataset is just as, if not more, useful to theorists. The database is a valuable tool to help theoreticians ultimately determine if their models reflect physically reasonable results, which is typified by experimentally determined data. Because a wide variety of isotopic ratios can be very precisely measured in presolar grains, they provide important constraints on theoretical models of nucleosynthesis, stellar mixing, and GCE, as a few examples. While a few theoreticians work closely with the presolar grain community and may therefore have easy access to a private collection of data, many more know only that presolar grains provide useful constraints for their models. These theoreticians, who may be astronomers, astrophysicists, or nuclear physicists, probably do not have close connections to presolar grain experimentalists, or even to the cosmochemistry community, nor are these theoreticians likely to even know where to start finding data with which to compare their models.

The Presolar Database has received high praise for its usefulness in constraining models from a variety of theoreticians. For example, one important problem for traditional models of the photospheres of low-mass RGB and AGB stars is that the isotopic abundances of C, N, O, and Al that have been measured in presolar grains do not match theoretical predictions. As discussed earlier, extra mixing, called cool bottom processing (CBP) has been invoked to explain these discrepancies. Various models have attempted to explain experimental data by different methods and degrees of extra-mixing and convection, to various degrees of success. Two good tests of such models are the $^{18}O/^{16}O$ and inferred $^{26}Al/^{27}Al$ ratios of the Group 2 oxide grains. Two different groups of modelers have asked for access to the database for just this purpose (Busso et al. 2010, M. Lugaro, pers. comm.)

In addition to its use by seasoned scientists, the database is also an excellent place for students new to the field of presolar grain research to begin getting acquainted with it. The references provide a veritable card catalog of presolar grain papers, which are easily sorted by whatever grain type, sub-type, or isotopic system is of interest. A significant number of students have requested use of the database for just this purpose. One user even requested access to the database in order to locate papers on presolar grains when he became interested in presolar grain research after reading a theoretical paper that referenced them.

### 4.3.4 Limitations

Although the database is a powerful tool for locating and utilizing isotopic data on presolar grains, there are limitations to the website. For example, although the website

and files are simple to navigate, there is no independent search or sort feature associated with the website. If a user wishes to look at only Ti data for SiC grains, he or she cannot simply download a file of "Ti data"; instead, the user must first download the entire file of SiC data and subsequently sort the data by the column of Ti isotopic data (e.g., $\delta^{46}Ti/^{48}Ti$ values) in which the user is interested. However, this sorting process is quite simple with Microsoft Excel or a similar program of the user's choosing when all the relevant data are provided in one location.

A second limitation in the database is in the presentation of errors, which, for the most part, are quite straightforward, but which can occasionally be problematic. Although different people use different methods to calculate errors, this is not reflected in the database; to somehow present this information would make the database excessively complicated. The errors that are presented in the database are directly copied from the paper in which they were originally published, with the exception of being recalculated to $1\sigma$ and put in the most common isotopic ratio format, as discussed above. If the user wishes to know additional details on the methods by which the errors were calculated, they are referred back to the original paper.

Measurements that have no error associated with them are excluded from the database, as are measurements with errors that are a significant fraction of the reported value. In both cases, the data are omitted because they lack statistical significance and could affect overall trends in the data. While this effect would not be noticeable for a commonly measured value like $\delta^{29}Si/^{28}Si$ for SiC, it could be particularly pronounced for isotopic ratios for which only a limited number of grains have been measured. Rather than risk skewing trends with the inclusion of poorly constrained data, these were

excluded from the database. However, for each grain with this type of isotopic ratio, only the problematic isotopic ratios are omitted; all other isotopic data are still included.

In some cases, the errors given in a paper are asymmetrical. In such instances, only the larger of the two errors are reported in the database for convenience and ease of plotting, since many graphing programs cannot easily handle asymmetrical errors. If the more precise details of the asymmetrical errors are required by the user, they are, once again, referred back to the original paper for these details. Similarly, correlated errors (i.e., non-axisymmetric) are not addressed in the database and are beyond its scope, both because of the difficulty associated with the calculation of correlated errors, which are not given in most papers, and the difficulty this would present in making the database an easy to use spreadsheet with data that can be readily graphed, even in simple programs. As a general rule, the database is intended as a simple online library of all presolar grain data, presented in the most commonly used formats. For any user who requires more complicated or uncommon calculations, the database can serve as a starting point to assemble the relevant data. The reference list (which provides the author, publication journal, and publication year) should provide sufficient information to allow the user to easily locate the works from which these data originated.

The compilation of all the available isotopic presolar grain data in the database is its primary strength, but this also presents a limitation in one aspect: the abundances of each type and sub-type of presolar grain. For example, X grains make up only ~1% by number of the total SiC population, but they comprise ~5% of the total number of SiC grains in the database. This is largely because researchers often choose to study the more unusual sub-types of SiC as opposed to mainstream grains. As such, grain searches either

target a certain rare type (e.g., X grains) or in large automatic searches, data on mainstream grains are simply not reported and are therefore not available for inclusion in the database. There are ~7300 mainstream grains in the database, but based on the number of X grains in the database and assuming that X grains are 1% of the SiC population, while mainstream grains make up 93% of the population, there should be ~49,000 mainstream grains in the database. An even more extreme case is the abundances of the grain types, themselves. As discussed above, SiC is the best studied type of presolar grain, despite not having the highest abundance. There are ~8860 SiC grains listed, compared to just ~470 silicates, despite these grain types having abundances of 15 ppm and ~180 – 375 ppm, respectively (Zinner 2007). From these two examples, it is obvious that the true abundances of presolar grains cannot be directly obtained via the database. Instead, isotopic analysis of a large, randomly selected collection of grains is necessary to obtain unbiased abundances for grain sub-types (e.g., Hoppe et al. 1996; Nittler and Alexander 2003) and matrix normalization is required to compare the abundances between grain types. However, this limitation of the database accurately reflects the same limitations that can be present in the presolar grain literature as a whole, and the database can actually help remedy such problems. For example, it was generally believed that most presolar grains with a nova origin were SiC, despite astronomical observations indicating enhancements of O-rich minerals in nova dust-shells (Gyngard et al. 2010b). However, using the database Gyngard et al. (2010b - see Appendix) noted that this was likely a statistical effect, resulting from the fact that comparatively few oxides and silicates, compared to SiC, have been analyzed, almost necessarily leading to fewer O-rich nova grains. The problem was compounded by several likely O-rich nova

grains not being reported in the literature as such. A closer inspection of the O-rich grains in the database for the diagnostically high $^{17}O/^{16}O$ ratio ($> 4 \times 10^{-3}$, which is the maximum that can be produced by a single RGB star), revealed several additional nova candidates. When the number of O-rich and SiC nova grains were adjusted for the measurement bias, O-rich nova grains were found to be several times, up to an order of magnitude, more common than SiC nova grains, which is qualitatively consistent with the astronomical observations.

## 4.4 Conclusions

Since the Presolar Database was first brought on line, user response has been overwhelmingly positive. Various users have wondered why such a tool was not previously developed and have expressed thanks that it is now available. The overall reception is that the database has made effectively utilizing the vast amount of presolar data a bit easier. The database has also been growing in popularity, both in the academic and public arenas; it appears as the first entry in Google under "presolar database", can be found in the Wikipedia article on "presolar grains", and has received password requests from over fifty people from all over the world, including Japan, Switzerland, China, Finland, Australia, and of course, around the United States. While a number of these requests have come from well-known people in the presolar grain or cosmochemistry communities, a sizable number of requests have been from people who have no obvious affiliation with presolar grains, but who are interested in them for various reasons, the most common being to compare theoretical models to experimental data.

The database has proven useful to a variety of scientists, including experimentalists, theoreticians, and students. By keeping both experimentalists and theoreticians informed about the latest presolar grain data, the database helps facilitate the back-and-forth that is required between the two types of researchers. Experimentalists need theoretical models to help explain from what type of stars their grains originated, how this type of star produced the measured isotopes and in what quantities, and how this type of star mixed different layers to produce the ratios observed in the grains. Conversely, theoreticians need experimental data to help them constrain their models and let them know if their calculations are based in reality. Although the database certainly has some limitations, it has certainly fulfilled its intended role as a simple, easy to use, easy to access collection of isotopic data for presolar grains, as well as to serve as a quick reference library of presolar grain publications.

# Chapter 5

## Concluding Remarks

**"**We do not ask for what useful purpose the birds do sing, for song is their pleasure since they were created for singing. Similarly, we ought not to ask why the human mind troubles to fathom the secrets of the heavens…The diversity of the phenomena of Nature is so great, and the treasures hidden in the heavens so rich, precisely in order that the human mind shall never be lacking in fresh nourishment."

~Johannes Kepler, from *Mysterium Cosmographicum*, 1596

Presolar grains provide a unique opportunity to analyze stardust in a laboratory setting. The isotopic, elemental, and morphological information obtained from these grains, in conjunction with astronomical observations and theoretical models, can, in turn, provide a variety of insights into astrophysical sources and processes. Some of these insights include, but are not limited to, a better understanding of: the most likely stellar sources of presolar grains; nucleosynthetic processes and yields in a variety of astrophysical objects; mixing and dredge-up events in stars, particularly AGB stars and SNe; temperature and pressure constraints on condensation sequences; the chemical evolution of the Galaxy; and the identification of a host of types of presolar grains that are not able to currently be detected by astronomical observations.

This thesis has sought to emphasize the importance of combined NanoSIMS and TEM analyses of presolar grains. NanoSIMS analysis is necessary to determine the isotopic composition and the probable stellar origin, while TEM analysis is essential to determine the mineralogy of each presolar grain, quantify trace elements in the grain, identify whether these trace elements are present in solid solution or as individual subgrains, and constrain the growth conditions under which the grain condensed. In some cases, additional NanoSIMS analysis is then possible on subgrains that have been identified, further constraining the nucleosynthetic processes and mixing in the parent star of the presolar grain.

As important as the combination of NanoSIMS and TEM analyses are, the number of grains that have been analyzed in the TEM is miniscule compared to the number of grains that have been analyzed for their isotopic compositions. For example, while the isotopic compositions of over ten-thousand presolar SiC grains have been reported in the literature (Hynes and Gyngard, 2009), prior to the work of this thesis, only eight SiC grains have been analyzed in the TEM for the presence of internal subgrains. The work performed in this thesis on presolar SiC grains represents a 200% increase in the number of grains that have been so analyzed. This enormous disparity represents one of the most critical areas of need in the field of presolar grain research, but also corresponds to one of the areas ripest for future work.

There is great need for an extensive coordinated NanoSIMS and TEM study of SiC mainstream grains. Although Daulton et al. (2003) have extensively characterized the polytypes of SiC grains, the lack of coordinating isotopic data for most of the grains in the study makes it impossible to know the specific polytype distribution of individual

SiC types. To supplement this information, a large-scale study of the crystal domain size and structure, chemical composition, and possible subgrains present in mainstream SiC grains is essential. Mainstream grains represent over 90% of presolar grains by number, but only four have been analyzed in the TEM for any properties other than their polytype. An extensive TEM study of mainstream grains, coupled with the comparatively advanced theoretical framework for AGB stars, would provide a useful point of comparison for all of the minor types of SiC.

In general, very few of the minor types of SiC grains have been analyzed in the TEM. There are data for only nine X grains, seven AB grains, one Z grain, and no Y grains. In the work presented in this thesis, two new types of presolar grains were discovered, present as subgrains in SiC X and AB grains. With few to no SiC grains analyzed to date of several of these minor types, there may be a wealth of additional types of subgrains yet to be discovered. Furthermore, since some types of subgrains are quite rare in SiC grains (e.g., silicides are observed in 22% of the X grains analyzed and oldhamite is observed in just 14% of the AB grains analyzed), it is likely that there are even rarer types of subgrains yet to be discovered in SiC grains. These subgrains could potentially be observed in additional studies of each type of presolar SiC. The observation of new types of presolar grains, whether as independent grains or as subgrains, also provides important constraints on theoretical models, either confirming predictions or presenting new puzzles that must be understood and in so doing, leads to the development of a better understanding of each type of stellar grain formation environment.

A final area in which additional TEM analysis could significantly benefit the field of presolar grain research is in the analysis of the rarest types of grains, such as independent SiC Type C grains, nova grains of any mineralogy, and the extremely large grains from the Murchison LS+LU series (e.g., see Gyngard et al. 2009). While these grains are exceedingly rare and every atom of the grain is precious, none of these grains have yet been made available for TEM analysis. With such rare grains, it is difficult to determine what type of analysis to perform, since every isotope could potentially reveal new, exotic anomalies in the grain. However, TEM analysis is the only way to conclusively determine how trace elements are distributed throughout the grain (i.e., in solid solution or as subgrains) and in what mineral form. These grains may also have drastically different crystal structures, grain sizes, or subgrains than other presolar grains of the same general mineralogy, which could then lead to significant new insights into the growth conditions present in the parent stars while these grains formed. The conditions that produced these rare types of grains may be significantly different from the conditions inferred from the more abundant types of presolar grains.

While this list of unanswered questions is by no means exhaustive, it represents several of the areas currently in need of additional work. There are many other interesting problems, from the absolute ages of presolar grains to the number of independent stellar sources from which presolar grains originate (a problem for which the Presolar Database may be a significant help), that require further study. While presolar grains have now been analyzed for almost a quarter of a century, there are still many questions about astrophysical environments and processes that are unanswered and that presolar grains can help to illuminate.

# References


Abbas M. M., LeClair A., Owen T., Conrath B. J., Flasar F. M., Kunde V. G., Nixon C. A., Achterberg R. K., Bjoraker G., Jennings D. J., Orton G., and Romani P. N. 2004. The nitrogen isotopic ratio in Jupiter's atmosphere from observations by the composite infrared spectrometer on the Cassini spacecraft. *The Astrophysical Journal* 602: 1063-1074.

Abia C. and Isern J. 2000. The chemical composition of carbon stars. II. The J-type stars. *The Astrophysical Journal* 536: 438-449.

Abia C., Busso M., Gallino R., Domínguez I., Straniero O., and Isern J. 2001. The $^{85}$Kr s-process branching and the mass of carbon stars. *The Astrophysical Journal* 559: 1117-1134.

Amari S., Anders E., Virag A., and Zinner E. 1990. Interstellar graphite in meteorites. *Nature* 345: 238-240.

Amari S., Hoppe P., Zinner E., and Lewis R. S. 1992. Interstellar SiC with unusual isotopic compositions: Grains from a supernova? *The Astrophysical Journal* 394: L43-L46.

Amari S., Lewis R. S., and Anders E. 1994. Interstellar grains in meteorites: I. Isolation of SiC, graphite, and diamond; size distributions of SiC and graphite. *Geochimica et Cosmochimica Acta* 58: 459-470.

Amari S., Hoppe P., Zinner E., and Lewis R. S. 1995. Trace-element concentrations in single circumstellar silicon carbide grains from the Murchison meteorite. *Meteoritics* 30: 679-693.

Amari S., Zinner E., and Lewis R. S. 1999. A singular presolar SiC grain with extreme $^{29}$Si and $^{30}$Si excesses. *The Astrophysical Journal* 517: L59-L62.

Amari S., Zinner E., and Lewis R. S. 2000. Isotopic compositions of different presolar silicon carbide size fractions from the Murchison meteorite. *Meteoritics and Planetary Science* 35: 997-1014.

Amari S., Gao X., Nittler L. R., Zinner E., José J., Hernanz M., and Lewis R. S. 2001a. Presolar grains from novae. *The Astrophysical Journal* 551: 1065-1072.

Amari S., Nittler L. R., Zinner E., Gallino R., Lugaro M., and Lewis R. S. 2001b. Presolar SiC grains of type Y: Origin from low-metallicity asymptotic giant branch stars. *The Astrophysical Journal* 546: 248-266.

Amari S., Nittler L. R., Zinner E., Lodders K., and Lewis R. S. 2001c. Presolar SiC grains of type A and B: Their isotopic compositions and stellar origins. *The Astrophysical Journal* 559: 463-483.

Anikin M. and Madar R. 1997. Temperature gradient controlled SiC crystal growth. *Materials Science and Engineering B (Solid-State Materials for Advanced Technology)* B46: 278-286.

Asplund M., Gustafsson B., Lambert D. L., and Kameswara Rao N. 1997. A stellar endgame - the born-again Sakurai's object. *Astronomy and Astrophysics* 321: L17-L20.

Asplund M. 1999. Sakurai's object - stellar evolution in real time. Proceedings, International Astronomical Union Symposium #191. pp. 481-486.

Asplund M., Lambert D. L., Kipper T., Pollacco D., and Shetrone M. D. 1999. The rapid evolution of the born-again giant Sakurai's object. *Astronomy and Astrophysics* 343: 507-518.

Aston F. W. 1920. The mass-spectra of chemical elements. *Philosophical Magazine and Journal of Science* 39: 611-625.

Bahcall J. 2000. How the sun shines. *Journal of the Royal Astronomical Society of Canada* 946: 219-227.

Barbuy B., Cayrel R., Spite M., Beers T. C., Spite F., Nordström B., and Nissen P. E. 1997. Analysis of two CH/CN-strong, very metal-poor stars. *Astronomy and Astrophysics* 317: L63-L66.

Barzyk J. G., Savina M. R., Davis A. M., Gallino R., Gyngard F., Amari S., Zinner E., Pellin M. J., Lewis R. S., and Clayton R. N. 2007. Constraining $^{13}C$ neutron source in AGB stars through isotopic analysis of trace elements in presolar SiC. *Meteoritics and Planetary Science* 42: 1103-1119.

Becket J. R., Connolly H. C., Ebel D. S. 2006. Chemical processes in igneous calcium-aluminum-rich inclusions: A mostly CMAS view of melting and crystallization. In *Meteorites and the Early Solar System II*, edited by Lauretta D. S. and Mcsween H. Y., Jr. Tucson: University of Arizona Press. pp. 399-429.

Bender H., De Veirman A., Van Landuyt J., and Amelinckx S. 1986. HREM investigation of twinning in very high dose phosphorus ion-implanted silicon. *Applied Physics A (Solids and Surfaces)* A39: 83-90.

Bernatowicz T., Fraundorf G., Tang M., Anders E., Wopenka B., Zinner E., and Fraundorf P. 1987. Evidence for interstellar SiC in the Murray carbonaceous meteorite. *Nature* 330: 728-730.

Bernatowicz T. J., Amari S., Zinner E. K., and Lewis R. S. 1991. Interstellar grains within interstellar grains. *The Astrophysical Journal* 373: L73-L76.

Bernatowicz T. J., Amari S., and Lewis R. S. 1992. TEM studies of a circumstellar rock. Proceedings, 23rd Lunar and Planetary Science Conference. pp. 91-92.

Bernatowicz T. J., Cowsik R., Gibbons P. C., Lodders K., Fegley B., Jr., Amari S., and Lewis R. S. 1996. Constraints on stellar grain formation from presolar graphite in the Murchison meteorite. *The Astrophysical Journal* 472: 760-782.

Bernatowicz T. J. and Zinner E. 1997. *Astrophysical implications of the laboratory study of presolar materials.* New York: American Institute of Physics. 750 p.

Bernatowicz T., Bradley J., Amari S., Messenger S., and Lewis R. 1999. New kinds of massive star condensates in a presolar graphite from Murchison (abstract #1392). 30th Lunar and Planetary Science Conference. CD-ROM.

Bernatowicz T. J., Akande O. W., Croat T. K., and Cowsik R. 2005. Constraints on grain formation around carbon stars from laboratory studies of presolar graphite. *The Astrophysical Journal* 631: 988-1000.

Bernatowicz T. J., Croat T. K., and Daulton T. L. 2006. Origin and evolution of carbonaceous presolar grains in stellar environments. In *Meteorites and the Early Solar System II*, edited by Lauretta D. S. and Mcsween H. Y., Jr. Tucson: University of Arizona Press. pp. 109-126.

Bethe H. A. 1939. Energy production in stars. *Physical Review* 55: 434-456.

Black D. C. and Pepin R. O. 1969. Trapped neon in meteorites II. *Earth Planetary Science Letters* 6: 395-406.

Black D. C. 1972. On the origins of trapped helium, neon and argon isotopic variations in meteorites II. Carbonaceous meteorites. *Geochimica et Cosmochimica Acta* 36: 377-394.

Boothroyd A. I., Sackmann I.-J., and Wasserburg G. J. 1995. Hot bottom burning in asymptotic giant branch stars and its effect on oxygen isotopic abundances. *The Astrophysical Journal* 442: L21-L24.

Boothroyd A. I. and Sackmann I.-J. 1999. The CNO isotopes: Deep circulation in red giants and first and second dredge-up. *The Astrophysical Journal* 510: 232-250.

Bose M., Floss C., and Stadermann F. J. 2010. An Investigation into the origin of Fe-rich presolar silicates in Acfer 094. *The Astrophysical Journal* 714: 1624-1636.

Bradley J. 2007. Interplanetary dust particles. In *Treatise on Geochemistry Volume 1*, 2nd ed., edited by Holland D. and Turekian K. Oxford: Pergamon. pp. 1-24.

Brahe, Tycho. 1573. *De nova stella*, translated by Shapley H. and Howarth A. E.

Burbidge E. M., Burbidge G. R., Fowler W. A., and Hoyle F. 1957. Synthesis of the elements in stars. *Reviews of Modern Phyiscs* 29: 547-650.

Busso M., Gallino R., and Wasserburg G. J. 1999. Nucleosynthesis in asymptotic giant branch stars: relevance for Galactic enrichment and solar system formation. *Annual Review of Astronomy and Astrophysics* 37: 239-309.

Busso M., Palmerini S., Maiorca E., Cristallo S., Straniero O., Abia C., Gallino R., and La Cognata M. 2010. On the need for deep-mixing in asymptotic giant branch stars of low mass. *The Astrophysical Journal Letters* 771: L47-L51.

Cameron A. G. W. 1957. Nuclear reactions in stars and nucleogenesis. *Publications of the Astronomical Society of the Pacific.* 69: 201-222.

Cameron A. G. W. and Fowler W. A. 1971. Lithium and the s-process in red-giant stars. *The Astrophysical Journal* 164: 111-114.

Carroll B. W. and Ostlie D. A. 2007. *An introduction to modern astrophysics,* 2nd ed. San Francisco: Addison Wesley. 1278 p.

Chen P.-S., Yan X.-H., and Zhang P. 2007. Infrared study of J-type carbon stars based on Infrared Astronomical Satellite, two micron all sky survey, and Infrared space observatory data. *The Astronomical Journal* 134: 214-222.

Choi B.-G., Huss G. R., Wasserburg G. J., and Gallino R. 1998. Presolar corundum and spinel in ordinary chondrites: Origins from AGB stars and a supernova. *Science* 282: 1284-1289.

Clayton D. D. and Ward R. A. 1978. S-process studies: Xenon and krypton isotopic abundances. *The Astrophysical Journal* 224: 1000-1006.

Clayton R. N., Grossman L., and Mayeda T. K. 1973. A component of primitive nuclear composition in carbonaceous meteorites. *Science* 182: 485-488.

Comte, Auguste. 1830-1842. *Cours de philosophie positive,* translated by Harriet Martineau. New York: Calvin Blanchard. 838 p.

Croat T. K., Bernatowicz T. J., Amari S., Messenger S., and Stadermann F. J. 2003. Structural, chemical, and isotopic microanalytical investigations of graphite from supernovae. *Geochimica et Cosmochimica Acta* 67: 4705-4725.

Croat T. K., Stadermann F. J., and Bernatowicz T. J. 2005. Presolar graphite from AGB stars: Microstructure and s-process enrichment. *The Astrophysical Journal* 631: 976-987.

Croat T. K. 2007. Rutile found within presolar graphites from Murchison (abstract). *Meteoritics and Planetary Science* 42: A34.

Croat T. K., Jadhav M., Lebsack E., and Bernatowicz T. J. 2009. Low-density presolar graphite spherules from the Orgueil meteorite (abstract #2175). 40th Lunar and Planetary Science Conference. CD-ROM.

Croat T. K., Jadhav M., Lebsack E., and Bernatowicz T. J. 2010a. Microstructural differences among the isotopic groups of low-density Orgueil graphites (abstract #1867). 41st Lunar and Planetary Science Conference. CD-ROM.

Croat T. K., Stadermann F. J., and Bernatowicz T. J. 2010b. Unusual $^{29,30}$Si-rich SiCs of massive star origin found within graphites from the Murchison meteorite. *The Astronomical Journal* 139: 2159-2169.

Crozaz G. and Lundberg L. 1995. The origin of oldhamite in unequilibrated enstatite chondrites. *Geochimica et Cosmochimica Acta*: 59: 3817-3831.

Darwin C. 1859. *On the origin of the species by natural selection or the preservation of favored races in the struggle for life*. London: Hurst. 501 p.

Daulton T. L., Eisenhour D. D., Bernatowicz T. J., Lewis R. S., and Buseck P. R. 1996. Genesis of presolar diamonds: Comparative high-resolution transmission electron microscopy study of meteoritic and terrestrial nano-diamonds. *Geochimica et Cosmochimica Acta* 60: 4853-4872.

Daulton T. L., Bernatowicz T. J., Lewis R. S., Messenger S., Stadermann F. J., and Amari S. 2003. Polytype distribution of circumstellar silicon carbide: Microstructural characterization by transmission electron microscopy. *Geochimica et Cosmochimica Acta* 67: 4743-4767.

Daulton T. L., Stadermann F. J., Bernatowicz T. J., Amari S., and Lewis R. S. 2006. First systematic TEM-NanoSIMS coordinated study of crystal structure and isotopic composition of presolar silicon carbide (abstract). *Meteoritics and Planetary Science* 41: A42.

Daulton T. L., Stadermann F. J., Bernatowicz T. J., Amari S., and Lewis R. S. 2009. Coordinated TEM/NanoSIMS microanalysis of structurally or isotopically rare presolar silicon carbide (abstract). *Meteoritics and Planetary Science* 44: A56.

Davis A. M., Pellin M. J., Lewis R. S., Amari S., and Clayton R. N. 1999. Molybdenum- and zirconium-isotopic compositions of supernova grains (abstract). *Meteoritics and Planetary Science* 34: A30-A31.

Dominy J. F. 1984. The chemical composition and evolutionary state of the early R stars. *The Astrophysical Journal Supplement Series* 55: 27-43.

Duerbeck H. W. and Benetti S. 1996. Sakurai's object - a possible final helium flash in a planetary nebula nucleus. *The Astrophysical Journal* 468: L111-L114.

Ebel D. S. and Grossman L. 2000. Condensation in dust-enriched systems. *Geochimica et Cosmochimica Acta* 64: 339-366.

Ebel D. S. 2006. Condensation of Rocky Material in Astrophysical Environments. In *Meteorites and the Early Solar System II*, edited by Lauretta D. S. and Mcsween H. Y., Jr. Tucson: University of Arizona Press. pp. 253-277.

Eddington A. S. 1920. The Internal constituion of the stars. *Observatory* 557: 341-358.

Einstein A. 1905. Electrodynamics of moving bodies. *Annalen der Physik* 17: 891-921.

Fedkin A. V., Meyer B. S., Grossman L., and Desch S. J. 2009. Condensation in Supernova Ejecta at High Spatial Resolution (abstract #1699). 40th Lunar and Planetary Science Conference. CD-ROM.

Fisher G. R. and Barnes P. 1990. Towards a unified view of polytypism in silicon carbide. *Philosophical Magazine B (Physics of Condensed Matter, Electronic, Optical and Magnetic Properties)* 61: 217-236.

Fissel A. 2000. Thermodynamical consideration of the epitaxial growth of SiC polytypes. Proceedings, International Conference on Silicon Carbide and Related Materials. pp. 209-212.

Floss C. and Crozaz G. 1993. Heterogeneous REE patterns in oldhamite from the aubrites: Ttheir nature and origin. *Geochimica et Cosmochimica Acta* 57: 4039-4057.

Floss C. and Stadermann F. J. 2009. Auger Nanoprobe analysis of presolar ferromagnesian silicate grains from primitive CR chondrites QUE 99177 and MET 00426. *Geochimica et Cosmochimica Acta* 73: 2415-2440.

Fujimoto M. Y. 1977. On the origin of R-type carbon stars: Possibility of hydrogen mixing during helium flicker. *Publications of the Astronomical Society of Japan* 29: 331-350.

Gallino R., Busso M., Picchio G., and Raiteri C. M. 1990. On the astrophysical interpretation of isotope anomalies in meteoritic SiC grains. *Nature* 348: 298-302.

Gamow G. 1946. Expanding universe and the origin of elements. *Physical Review* 70: 572-573.

Gyngard F. 2009. Isotopic studies of presolar silicon carbide and oxide grains as probes of nucleosynthesis and the chemical evolution of the galaxy. Ph.D. thesis. Washington University, St. Louiss, MO, USA.

Gyngard F., Amari S., Zinner E., and Ott U. 2009. Interstellar exposure ages of large presolar SiC grains from the Murchison meteorite. *The Astrophysical Journal* 694: 359-366.

Gyngard F., Nittler L. R., and Zinner E. 2010a. Presolar SiC grains of Type C (abstract). *Meteoritics and Planetary Science* 45: A72.

Gyngard F., Zinner E. K., Nittler L. R., Margand A., Stadermann F. J., and Hynes K. M. 2010b. Automated NanoSIMS measurements of spinel stardust from the Murray meteorite. *The Astrophysical Journal* 717: 107-120.

Hajduk M., Zijlstra A. A., Herwig F., van Hoof P. A. M., Kerber F., Kimeswenger S., Pollacco D. L., Evans A., Lopez J. A., Bryce M., Eyres S. P. S., and Matsuura M. 2005. The real-time stellar evolution of Sakurai's object. *Science* 308: 231-233.

Harris M. J., Lambert D. L., Hinkle K. H., Gustafsson B., and Eriksson K. 1987. Oxygen isotopic abundances in evolved stars. III - 26 carbon stars. *The Astrophysical Journal* 316: 294-304.

Heck P. R., Gyngard F., Ott U., Meier M. M. M., Avila J. N., Amari S., Zinner E. K., Lewis R. S., Baur H., and Wieler R. 2009. Interstellar residence times of presolar SiC dust grains from the Murchison carbonaceous meteorite. *The Astrophysical Journal* 698: 1155-1164.

Heine V., Cheng C., and Needs R. J. 1991. The preference of silicon carbide for growth in the metastable cubic form. *Journal of the American Ceramic Society* 74: 2630-2633.

Helmholtz V. H. 1856. Lecture "On the interaction of natural forces". *In Philisophical Magazine* 11: 489-518.

Herwig F., Blöcker T., Langer N., and Driebe T. 1999. On the formation of hydrogen-deficient post-AGB stars. *Astronomy and Astrophysics* 349: L5-L8.

Herwig F. 2001. Internal mixing and surface abundance of [WC]-CSPN. *Astrophysics and Space Science* 275: 15-26.

Hoppe P., Amari S., Zinner E., Ireland T., and Lewis R. S. 1994. Carbon, nitrogen, magnesium, silicon, and titanium isotopic compositions of single interstellar silicon carbide grains from the Murchison carbonaceous chondrite. *The Astrophysical Journal* 430: 870-890.

Hoppe P., Strebel R., Eberhardt P., Amari S., and Lewis R. S. 1996. Small SiC grains and a nitride grain of circumstellar origin from the Murchison meteorite: Implications for stellar evolution and nucleosynthesis. *Geochimica et Cosmochimica Acta* 60: 883-907.

Hoppe P., Annen P., Strebel R., Eberhardt P., Gallino R., Lugaro M., Amari S., and Lewis R. S. 1997. Meteoritic silicon carbide grains with unusual Si-isotopic compositions: Evidence for an origin in low-mass, metallicity asymptotic giant branch stars. *The Astrophysical Journal* 487: L101-L104.

Hoppe P. and Ott U. 1997. Mainstream silicon carbide grains from meteorites. In *Astrophysical Implications of the Laboratory Study of Presolar Materials,* edited

by Bernatowicz T. J. and Zinner E. New York: American Institute of Physics. pp. 27-58.

Hoppe P., Lodders K., Strebel R., Amari S., and Lewis R. S. 2001. Boron in presolar silicon carbide grains from supernovae. *The Astrophysical Journal* 551: 478-485.

Hoppe P. and Besmehn A. 2002. Evidence for extinct vanadium-49 in presolar silicon carbide grains from supernovae. *The Astrophysical Journal* 576: L69-L72.

Hoppe P., Leitner J., Gröner E., Marhas K., Meyer B., and Amari S. 2010. NanoSIMS studies of small presolar SiC grains: New insights into supernova nucleosynthesis, chemistry, and dust formation. *The Astrophysical Journal* 719: 1370-1384.

Hoyle F. 1946. The synthesis of the elements from hydrogen. *Monthly Notices of the Royal Astronomical Society.* 106: 343-383.

Hsu W. 1998. Geochemical and petrographic studies of oldhamite, diopside, and roedderite in enstatite meteorites. *Meteoritics and Planetary Science* 33: 291-301.

Huss G. R., Hutcheon I. D., Fahey A. J., and Wasserburg G. J. 1993. Oxygen isotope anomalies in Orgueil corundum: Confirmation of presolar origin. *Meteoritics* 28: 369-370.

Hutcheon I. D., Huss G. R., Fahey A. J., and Wasserburg G. J. 1994. Extreme $^{26}$Mg and $^{17}$O enrichments in an Orgueil corundum: identification of a presolar oxide grain. *The Astrophysical Journal* 425: L97-L100.

Hynes K. M., Croat T. K., Amari S., Mertz A. F., and Bernatowicz T. J. 2006. A transmission electron microscope study of internal subgrains in SiC-X grains (abstract). *Meteoritics and Planetary Science* 41: A83.

Hynes K. M. and Croat T. K. 2007. Silicon carbide subgrains in presolar graphite from Murchison. *Meteoritics and Planetary Science* 42: A72.

Hynes K. M., Croat T. K., and Bernatowicz T. J. (2007) Microstructure of silicon carbides found within presolar graphite (abstract #1693). 38th Lunar and Planetary Science Conference. CD-ROM.

Hynes K. M. and Gyngard F. 2009. The Presolar Grain Database: http://presolar.wustl.edu/~pgd (abstract #1198). 40th Lunar and Planetary Science Conference. CD-ROM.

Hynes K. M., Gyngard F., Zinner E., and Nittler L. R. 2009. Iron and nickel isotopic compositions of silicon carbide Z grains (abstract). *Meteoritics and Planetary Science* 72: A96.

Hynes K. M., Croat T. K., Amari S., Mertz A. F., and Bernatowicz T. J. 2010. Structural and isotopic microanalysis of presolar SiC from supernovae. *Meteoritics and Planetary Science* 45: 596-614.

Iben I., Jr., Kaler J. B., Truran J. W., and Renzini A. 1983. On the evolution of those nuclei of planetary nebulae that experience a final helium shell flash. *The Astrophysical Journal* 264: 605-612.

Jadhav M., Amari S., Marhas K. K., Zinner E., Maruoka T., and Gallino R. 2008. New stellar sources for high-density, presolar graphite grains. *The Astrophysical Journal* 682: 1479-1485.

Kaempffert, W. 1932. Eddington expounds a mystical cosmos: Beyond the seen world and underlying laws of physics, a famous scientist finds a new religious meaning. *The New York Times Magazine* October 1932 Part 5: SM9.

Kelvin W. T. 1862. On the age of the sun's heat. *Macmillan's Magazine*: 283-293.

Kepler, Johannes. 1596. *Mysterium Cosmographicum*. Quoted in *Cosmos*, written by Carl Sagan. 1985. New York: Ballantine Books. 324 p.

Kern R. S., Tanaka S., Rowland L. B., and Davis R. F. 1998. Reaction kinetics of silicon carbide deposition by gas-source molecular-beam epitaxy. *Journal of Crystal Growth* 183: 581-593.

Krishna P. and Marshall R. C. 1971. Direct transformation from the 2H to the 6H structure in single-crystal silicon carbide. *Journal of Crystal Growth* 11: 147-150.

Krishna P., Marshall R. C., and Ryan C. E. 1971. The discovery of 2H-3C solid state transformation in silicon carbide single crystals. *Journal of Crystal Growth* 8: 129-131.

Lambert D. L., Gustafsson B., Eriksson K., and Hinkle K. H. 1986. The chemical composition of carbon stars. I - Carbon, nitrogen, and oxygen in 30 cool carbon stars in the Galactic disk. *The Astrophysical Journal Supplement Series* 62: 373-425.

Lattanzio J. C. and Boothroyd A. I. 1997. Nucleosynthesis of elements in low to intermediate mass stars through the AGB phase. In *Astrophysical Implications of the Laboratory Study of Presolar Materials,* edited by Bernatowicz T. J. and Zinner E. New York: American Institute of Physics. pp. 85-114.

Lattimer J. M., Schramm D. N., and Grossman L. 1978. Condensation in supernova ejecta and isotopic anomalies in meteorites. *The Astrophysical Journal* 219: 230-249.

Lawlor T. M. and MacDonald J. 2003. Sakurai's Object, V605 Aquilae, and FG Sagittae: An Evolutionary Sequence Revealed. *The Astrophysical Journal* 583: 913-922.

Lewis R. S., Tang M., Wacker J. F., Anders E., and Steel E. 1987. Interstellar diamonds in meteorites. *Nature* 326: 160-162.

Lin Y., Amari S., and Pravdivtseva O. 2002. Presolar grains from the Qingzhen (EH3) meteorite. *The Astrophysical Journal* 575: 257-263.

Little-Marenin I. R. 1986. Carbon stars with silicate dust in their circumstellar shells. *The Astrophysical Journal* 307: L15-L19.

Lodders K. and Fegley B., Jr. 1995. The origin of circumstellar silicon carbide grains found in meteorites. *Meteoritics* 30: 661-678.

Lodders K. 2003. Solar system abundances and condensation temperatures of the elements. *The Astrophysical Journal* 591: 1220-1247.

Lodders K. 2006. They came from the deep in the supernova: The origin of TiC and metal subgrains in presolar graphite grains. *The Astrophysical Journal* 647: L37-L40.

Lugaro M., Zinner E., Gallino R., and Amari S. 1999. Si isotopic ratios in mainstream presolar SiC grains revisited. *The Astrophysical Journal* 527: 369-394.

Lugaro M., Davis A. M., Gallino R., Pellin M. J., Straniero O., and Käppeler F. 2003. Isotopic compositions of strontium, zirconium, molybdenum, and barium in single presolar SiC grains and asymptotic giant branch stars. *The Astrophysical Journal* 593: 486-508.

Marhas K. K., Amari S., Gyngard F., Zinner E., and Gallino R. 2008. Iron and nickel isotopic ratios in presolar SiC grains. *The Astrophysical Journal* 689: 622-645.

Marty B., Zimmermann L., Burnard P. G., Wieler R., Heber V. S., Burnett D. L., Wiens R. C., and Bochsler P. 2010. Nitrogen isotopes in the recent solar wind from the analysis of Genesis targets: Evidence for large scale isotope heterogeneity in the early solar system. *Geochimica et Cosmochimica Acta* 74: 340-355.

Merrill P. W. 1952. Spectroscopic observations of stars of class S. *The Astrophysical Journal.* 116: 21-26.

Messenger S., Keller L. P., Stadermann F. J., Walker R. M., and Zinner E. 2003. Samples of stars beyond the solar system: Silicate grains in interplanetary dust. *Science* 300: 105-108.

Meyer B. S., Weaver T. A., and Woosley S. E. 1995. Isotope source table for a 25 $M_{\odot}$ supernova. *Meteoritics* 30: 325-334.

Meyer B. S. and Zinner E. 2006. Nucleosynthesis. In *Meteorites and the Early Solar System II*, edited by Lauretta D. S. and Mcsween H. Y., Jr. Tucson: University of Arizona Press. pp. 69-108.

Miller Bertolami M. M. and Althaus L. G. 2007. The born-again (very late thermal pulse) scenario revisited: The mass of the remnants and implications for V4334 Sgr. *Monthly Notices of the Royal Astronomical Society* 380: 763-770.

Miura H., Kato M., and Mori T. 1990. Determination of boundary energies of Cu from the shape of boundary $SiO_2$ particles. *Colloque de Physique* C1: 263-268.

National Nuclear Data Center at Brookhaven National Laboratory. Interactive chart of the nuclides. http://www.nndc.bnl.gov/chart/.

Nguyen A., Zinner E., and Lewis R. S. 2003. Identification of small presolar spinel and corundum grains by isotopic raster imaging. *Publications of the Astronomical Society of Australia* 20: 382-388.

Nguyen A. N. and Zinner E. 2004. Discovery of ancient silicate stardust in a meteorite. *Science* 303: 1496-1499.

Nguyen A. 2005. Characterization of presolar silicate grains in primitive meteorites by multi-detection raster ion imaging in the NanoSIMS. Ph.D. thesis. Washington University, St. Louis, MO, USA.

Nguyen A. N., Stadermann F. J., Zinner E., Stroud R. M., Alexander C. M. O'D., and Nittler L. R. 2007. Characterization of presolar silicate and oxide grains in primitive carbonaceous chondrites. *The Astrophysical Journal* 656: 1223-1240.

Nicolussi G. K., Davis A. M., Pellin M. J., Lewis R. S., Clayton R. N., and Amari S. 1997. S-process zirconium in presolar silicon carbide grains. *Science* 277: 1281-1283.

Nicolussi G. K., Pellin M. J., Lewis R. S., Davis A. M., Amari S., and Clayton R. N. 1998a. Molybdenum isotopic composition of individual presolar silicon carbide grains from the Murchison meteorite. *Geochimica et Cosmochimica Acta* 62: 1093-1104.

Nicolussi G. K., Pellin M. J., Lewis R. S., Davis A. M., Clayton R. N., and Amari S. 1998b. Strontium isotopic composition in individual circumstellar silicon carbide grains: A record of s-process nucleosynthesis. *Physical Review Letters* 81: 3583-3586.

Nittler L. R., Alexander C. M. O'D., Gao X., Walker R. M., and Zinner E. K. 1994. Interstellar oxide grains from the Tieschitz ordinary chondrite. *Nature* 370: 443-446.

Nittler L. R., Hoppe P., Alexander C. M. O'D., Amari S., Eberhardt P., Gao X., Lewis R. S., Strebel R., Walker R. M., and Zinner E. 1995. Silicon nitride from supernovae. *The Astrophysical Journal* 453: L25-L28.

Nittler L. R. 1996. Quantitative isotopic ratio ion imaging and its application to studies of preserved stardust in meteorites. Ph.D. thesis, Washington University, St. Louis, MO, USA.

Nittler L. R., Amari S., Zinner E., Woosley S. E., and Lewis R. S. 1996. Extinct $^{44}$Ti in presolar graphite and SiC: Proof of a supernova origin. *The Astrophysical Journal* 462: L31-L34.

Nittler L. R., Alexander C. M. O'D., Gao X., Walker R. M., and Zinner E. 1997. Stellar sapphires: The properties and origins of presolar $Al_2O_3$ in meteorites. *The Astrophysical Journal* 483: 475-495.

Nittler L. R. and Cowsik R. 1997. Galactic age estimates from O-rich stardust in meteorites. *Physical Review Letters* 78: 175-178.

Nittler L. R. and Alexander C. M. O'D. 2003. Automated isotopic measurements of micron-sized dust: Application to meteoritic presolar silicon carbide. *Geochimica et Cosmochica Acta* 67: 4961-4980.

Nittler L. R., Alexander C. M. O'D., Stadermann F. J., and Zinner E. K. 2005. Presolar chromite in Orgueil (abstract). *Meteoritics and Planetary Science* 40: A114.

Nittler L. R. and Hoppe P. 2005. Are presolar silicon carbide grains from novae actually from supernovae? *The Astrophysical Journal* 631: L89-L92.

Nittler L. R., Alexander C. M. O'D., and Nguyen A. N. 2006. Extreme $^{13}C$ and $^{15}N$ enrichments in a Murchison presolar SiC grain (abstract). *Meteoritics and Planetary Science* 41: A134.

Nittler L. R. 2008. Presolar stardust in the Solar System: recent advances for nuclear astrophysics. Proceedings, 10th Symposium on Nuclei in the Cosmos. 10 p.

Nittler L. R., Alexander C. M. O'D., Gallino R., Hoppe P., Nguyen A. N., Stadermann F. J., and Zinner E. K. 2008. Aluminum-, calcium- and titanium-rich oxide stardust in ordinary chondrite meteorites. *The Astrophysical Journal* 682: 1450-1478.

Nittler L. R., Gyngard F., and Zinner E. 2010. Extreme O isotopic anomalies in presolar oxides from the Murray CM2 chondrite (abstract). *Meteoritics and Planetary Science* 45: A153.

Palmerini S., Busso M., La Cognata M., Maiorca E., and Cristallo S. 2010. Effects of new reaction rates on p-capture nucleosynthesis in low mass stars. Proceedings, 11th Symposium on Nuclei in the Cosmos. p. 130.

Patrick L., Hamilton D. R., and Choyke W. J. 1966. Growth, luminescence, selection rules and lattice sums of SiC with wurtzite structure. *Physical Review* 143: 528-536.

Pellin M. J., Davis A. M., Lewis R. S., Amari S., and Clayton R. N. 1999. Molybdenum isotopic composition of single silicon carbide grains from supernovae (abstract #1969). 30th Lunar and Planetary Science Conference. CD-ROM.

Pellin M. J., Calaway W. F., Davis A. M., Lewis R. S., Amari S., and Clayton R. N. 2000a. Toward complete isotopic analysis of individual presolar silicon carbide grains: C, N, Si, Sr, Zr, Mo, and Ba in single grains of type X (abstract #1917). 31st Lunar and Planetary Science Conference. CD-ROM.

Pellin M. J., Davis A. M., Calaway W. F., Lewis R. S., Clayton R. N., and Amari S. 2000b. Zr and Mo isotopic constraints on the origin of unusual types of presolar SiC grains (abstract #1934). 31st Lunar and Planetary Science Conference. CD-ROM.

Rauscher T., Heger A., Hoffman R. D., and Woosley S. E. 2002. Nucleosynthesis in massive stars with improved nuclear and stellar physics. *The Astrophysical Journal* 576: 323-348.

Reynolds J. H. and Turner G. 1964. Rare gases in the chondrite Renazzo. *Journal of Geophysical Research.* 69: 3263-3282.

Richter S., Ott U., and Begemann F. 1998. Tellurium in pre-solar diamonds as an indicator for rapid separation of supernova ejecta. *Nature* 391: 261-263.

Russell S. S., Arden J. W., and Pillinger C. T. 1996. A carbon and nitrogen isotope study of diamond from primitive chondrites. *Meteoritics and Planetary Science* 31: 233-252.

Savina M. R., Davis A. M., Tripa C. E., Pellin M. J., Clayton R. N., Lewis R. S., Amari S., Gallino R., and Lugaro M. 2003. Barium isotopes in individual presolar silicon carbide grains from the Murchison meteorite. *Geochimica et Cosmochimica Acta* 67: 3201-3214.

Savina M. R., Davis A. M., Tripa C. E., Pellin M. J., Gallino R., Lewis R. S., and Amari S. 2004. Extinct technetium in presolar silicon carbide grains: Implications for stellar nucleosynthesis. *Science* 303: 649-652.

Sharp C. M. and Wasserburg G. J. 1995. Molecular equilibria and condensation temperatures in carbon-rich gases. *Geochimica et Cosmochimica Acta* 59: 1633-1652.

Smith V. V. and Lambert D. L. 1990. On the occurrence of enhanced lithium in Magellanic Cloud red giants. *The Astrophysical Journal* 361: L69-L72.

Speck A. K., Hofmeister A. M., and Barlow M. J. 1999. The SiC problem: Astronomical and meteoritic evidence. *The Astrophysical Journal* 513:L87-L90.

Spergel D. N., Verde L., Peiris H. V., Komatsu E., Nolta M. R., Bennett C. L., Halpern M., Hinshaw G., Jarosik N., Kogut A., Limon M., Meyer S. S., Page L., Tucker G. S., Weiland J. L., Wollack E., and Wright E. L. 2003. First-year Wilkinson Microwave Anisotropy Probe (WMAP) observations: Determination of cosmological parameters. *The Astrophysical Journal Supplement Series* 148: 175-194.

Stadermann F. J., Zhao X., Daulton T. L., Isheim D., Seidman D. N., Heck P. R., Pellin M. J., Savina M. R., Davis A. M., Stephan T., Lewis R. S., and Amari S. 2010. Atom-probe tomographic study of the three-dimensional structure of presolar silicon carbide and nanodiamonds at atomic resolution (abstract #2134). 41st Lunar and Planetary Science Conference. CD-ROM.

Stan M. A., Patton M. O., Warner J. D., Yang J. W., and Pirouz P. 1994. Growth of 2H-SiC on 6H-SiC by pulsed laser ablation. *Applied Physics Letters* 64: 2667-2669.

Stroud R. M., O'Grady M., Nittler L. R., and Alexander C. M. O'D. 2002. Transmission electron microscopy of an *in situ* presolar silicon carbide grain (abstract #1785). 33rd Lunar and Planetary Science Conference. CD-ROM.

Stroud R. M., Nittler L. R., Alexander C. M. O'D., Bernatowicz T. J., and Messenger S. R. 2003. Transmission electron microscopy of non-etched presolar silicon carbide (abstract #1755). 34th Lunar and Planetary Science Conference. CD-ROM.

Stroud R. M. and Nittler L. R. 2004. A search for solar-system processing signatures in presolar grains (abstract #9091). Proceedings, *Workshop on Chondrites and the Protoplanetary Disk*.

Stroud R. M., Nittler L. R., and Alexander C. M. O'D. 2004a. Polymorphism in presolar $Al_2O_3$ grains from asymptotic giant branch stars. *Science* 305: 1455-1457.

Stroud R. M., Nittler L. R., and Hoppe P. 2004b. Microstructures and isotopic compositions of two SiC X grains (abstract). *Meteoritics and Planetary Science* 39: A101.

Stroud R. M. and Bernatowicz T. J. 2005. Surface and internal structure of pristine presolar silicon carbide (abstract #2010). 36th Lunar and Planetary Science Conference. CD-ROM.

Stroud R. M., Nittler L. R., and Alexander C. M. O'D. 2008. Transmission electron microscopy of a presolar supernova hibonite grain (abstract #1778). 39th Lunar and Planetary Science Conference. CD-ROM.

Tang M. and Anders E. 1988. Isotopic anomalies of Ne, Xe, and C in meteorites. II. Interstellar diamond and SiC: Carriers of exotic noble gases. *Geochimica et Cosmochimica Acta* 52: 1235-1244.

Thronson H. A., Jr., Latter W. B., Black J. H., Bally J., and Hacking P. 1987. Properties of evolved mass-losing stars in the Milky Way and variations in the interstellar dust composition. *The Astrophysical Journal* 322: 770-786.

Timmes F. X., Woosley S. E., and Weaver T. A. 1995. Galactic chemical evolution: Hydrogen through zinc. *The Astrophysical Journal Supplement Series* 98: 617-658.

Travaglio C., Gallino R., Amari S., Zinner E., Woosley S., and Lewis R. S. 1999. Low-density graphite grains and mixing in type II supernovae. *The Astrophysical Journal* 510: 325-354.

Twain, Mark. 1885 *The adventures of Huckleberry Finn*. New York: Barnes and Noble. 319 p.

Upadhyaya G. S. 1996. *Nature and properties of refractory carbides*. Commack, NY: Nova Science Publishers. 545 p.

Vollmer C., Hoppe P., Brenker F. E., and Holzapfel C. 2007. Stellar $MgSiO_3$ perovskite: A shock-transformed stardust silicate found in a meteorite. *The Astrophysical Journal* 666: L49-L52.

Waelkens C., Waters L. B. F. M., de Graauw M. S., Huyen E., Malfait K., Plets H., Vandenbussche B., Beintema D. A., Boxhoorn D. R., Habing H. J., Heras A. M., Kester D. J. M., Lahuis F., Morris P. W., Roelfsema P. R., Salama A., Siebenmorgen R., Trams N. R., van der Bliek N. R., Valentijn E. A., and Wesselius P. R. 1996. SWS observations of young main-sequence stars with dusty circumstellar disks. *Astronomy and Astrophysics* 315: L245-L248.

Wallerstein G., Iben I., Jr., Parker P., Boesgaard A. M., Hale G. M., Champagne A. E., Barnes C. A., Käppeler F., Smith V. V., Hoffman R. D., Timmes F. X., Sneden

C., Boyd R. N., Meyer B. S., and Lambert D. L. 1997. Synthesis of the elements in stars: forty years of progress. *Reviews of Modern Physics.* 69: 995-1084.

Wannier P. G., Andersson B.-G., Olofsson H., Ukita N., and Young K. 1991. Abundances in red giant stars: Nitrogen isotopes in carbon-rich molecular envelopes. *The Astrophysical Journal* 380: 593-605.

Wasserburg G. J., Boothroyd A. I., and Sackmann I.-J. 1995. Deep circulation in red giant stars: A solution to the carbon and oxygen isotope puzzles? *The Astrophysical Journal Letters* 447: L37-L40.

Waters L. B. F. M., Molster F. J., de Jong T., Beintema D. A., Waelkens C., Boogert A. C. A., Boxhoorn D. R., de Graauw T., Drapatz S., Feuchtgruber H., Genzel R., Helmich F. P., Heras A. M., Huygen R., Izumiura H., Justtanont K., Kester D. J. M., Kunze D., Lahuis F., Lamers H. J. G. L. M., Leech K. J., Loup C., Lutz D., Morris P. W., Price S. D., Roelfsema P. R., Salama A., Schaeidt S. G., Tielens A. G. G. M., Trams N. R., Valentijn E. A., Vandenbussche B., van den Ancker M. E., van Dishoeck E. F., van Winckel H., Wesselius P. R., and Young E. T. 1996. Mineralogy of oxygen-rich dust shells. *Astronomy and Astrophysics* 315: L361-L364.

Wiescher M., Görres J., Uberseder E., Imbriani G., and Pignatari M. 2010. The cold and hot CNO cycles. *Annual Review of Nuclear and Particle Science*. 60: 381-404.

Wooden D. H. 1997. Observational evidence for mixing and dust condensation in core-collapse supernovae. In *Astrophysical Implications of the Laboratory Study of Presolar Materials*, edited by Bernatowicz T. J. and Zinner E. New York: American Institute of Physics. pp. 317-374.

Woosley S. E. and Weaver T. A. 1995. The evolution and explosion of massive stars. II. Explosive hydrodynamics and nucleosynthesis. *The Astrophysical Journal Supplement*. 101: 181-235.

Yoo W. S. and Matsunami H. 1991. Polytype-controlled single-crystal growth of silicon carbide using 3C→6H solid-state phase-transformation. *Journal of Applied Physics* 70: 7124-7131.

Zangvil A. and Ruh R. 1988. Phase relationships in the silicon carbide-aluminum nitride system. *Journal of the American Ceramic Society* 71: 884-890.

Zega T. J., Nittler L. R., Alexander C. M. O'D., and Stroud R. M. 2008. Transmission electron microscopy analysis of a presolar Cr-rich spinel grain (abstract #2424). 39th Lunar and Planetary Science Conference. CD-ROM.

Zega T. J., Alexander C. M. O'D., Nittler L. R., and Stroud R. M. 2010. The Microstructure of a presolar spinel grain (abstract #2055). 41st Lunar and Planetary Science Conference. CD-ROM.

Zhaoqing L. and Jun N. 2005. Layered growth modelling of epitaxial growth processes for SiC polytypes. *Journal of Physics: Condensed Matter* 17: 5355-5366.

Zinner E., Tang M., and Anders E. 1987. Large isotopic anomalies of Si, C, N and noble gases in interstellar silicon carbide from the Murray meteorite. *Nature* 330: 730-732.

Zinner E., Amari S., Guinness R., Nguyen A., Stadermann F., Walker R. M., and Lewis R. S. 2003. Presolar spinel grains from the Murray and Murchison carbonaceous chondrites. *Geochimica et Cosmochimica Acta* 67: 5083-5095.

Zinner E., Nittler L. R., Gallino R., Karakas A. I., Lugaro M., Straniero O., and Lattanzio J. C. 2006. Silicon and carbon isotopic ratios in AGB stars: SiC grain data,

models, and the Galactic evolution of the Si isotopes. *The Astrophysical Journal* 650: 350-373.

Zinner E. 2007. Presolar grains. In *Treatise on Geochemistry Volume 1*, 2nd ed., edited by Holland D. and Turekian K. Oxford: Pergamon. pp. 1-33.

Zinner E., Amari S., Guinness R., Jennings C., Mertz A. F., Nguyen A. N., Gallino R., Hoppe P., Lugaro M., Nittler L. R., and Lewis R. S. 2007. NanoSIMS isotopic analysis of small presolar grains: Search for $Si_3N_4$ grains from AGB stars, and Al and Ti isotopic compositions of rare presolar SiC grains. *Geochimica et Cosmochimica Acta* 71: 4786-4813.

Zinner E., Jadhav M., Gyngard F., and Nittler L. R. 2010. Bonanza: Isotopic anatomy of a large presolar SiC grain of type X (abstract). *Meteoritics and Planetary Science* 45: A225.

# Appendix

---

# Related Presolar Grain Projects

During my tenure as a graduate student at Washington University, I have been involved in projects that are either not directly related to this thesis or in which I served in an ancillary role. This appendix briefly describes some of these projects, as well as provides references to which the reader is referred for additional information.

## A.1 SiC Subgrains in Presolar Graphite

Presolar SiC has not only been observed as independent grains, like those described in detail in Chapters 2 and 3, but also as subgrains in high density presolar graphite. As discussed in Section 3.4.4, theoretical predictions for condensation in AGB stars suggest that the condensation of SiC before graphite is unlikely under most conditions (e.g., Lodders and Fegley 1995). This was quite problematic, since all high density graphite grains were thought to originate in AGB stars, while all low density graphite grains were believed to have a SN origin (e.g., Croat et al. 2003). In an effort to identify the source of presolar graphite grains with SiC subgrains, I helped to perform preliminary TEM analysis on four of these graphite grains, the results of which are described in two published conference abstracts (Hynes and Croat 2007; Hynes et al. 2007). Subsequent NanoSIMS measurements of the $^{16}O/^{18}O$ and $^{12}C/^{13}C$ ratios of two of these graphite grains were consistent with both an AGB and a SN origin, and were

therefore non-diagnostic. However, analysis by Croat et al. (2010b) of additional graphite grains with SiC subgrains and NanoSIMS measurements of the $^{29,30}Si/^{28}Si$ ratios of these grains revealed that the SiC subgrains are extremely enriched in both $^{29}Si$ and $^{30}Si$ and may constitute a new subtype of presolar grain, unofficially termed "Type C" grains. These grains most likely originated in Type II SNe. Three examples of Type C SiC grains have also been observed independently of graphite, and extreme S isotopic anomalies, possibly carried by CaS, have been measured in two of these SiC Type C grains (Amari et al. 1999; Gyngard et al. 2010a; Hoppe et al. 2010).

## A.2 Iron and Nickel Isotopes of SiC Z Grains

Marhas et al. (2008) measured the Fe and Ni isotopic compositions of a total of 90 presolar SiC grains, the majority of which were SiC X grains. Among these grains was a single SiC Z grain, which has anomalous $^{54}Fe/^{56}Fe$ and $^{62}Ni/^{58}Ni$ isotopic ratios. The anomalous isotopic composition of this grain prompted us to measure the $^{54,56,57}Fe$, $^{58,60,61,62}Ni$, $^{59}Co$, and $^{52}Cr$ (in order to make corrections for $^{54}Cr$ interferences) isotopes of 24 additional SiC Z grains with the NanoSIMS, utilizing a combination of magnetic peak-jumping and multidetection. The results of this work have been published in a conference abstract (Hynes et al. 2009). SiC Z grains represent ~1% of the total presolar SiC population, but this percentage increases with decreasing grain size (Zinner et al. 2007). In order to obtain enough Z grains for analysis, we used the IH6 fraction (0.25 – 0.65 μm diameter) of the Indarch EH4 meteorite, which has previously been observed to have a Z grain abundance of ~8% (Zinner et al. 2007). Unfortunately, the relatively

small size of the grains, coupled with the low Fe and Ni abundances in these grains, resulted in significant measurement uncertainties; however, several of the grains had resolvable Fe and Ni isotopic anomalies. While most of the anomalies in the Z grains qualitatively match predictions for low metallicity AGB stars, several grains have unexpected anomalies that are difficult to explain, most notably excesses in $^{54}$Fe (deficits are predicted). Both Fe and Fe-Ni subgrains were also observed in several of the Z grains. Although the large errors make it difficult to give quantitative results, this study served as a test to see if Fe and Ni isotopes in SiC Z grains are anomalous and of interest for further study. The results clearly indicate Fe and Ni anomalies, some of which are contrary to predictions for AGB stars (see Marhas et al. 2008 and references therein), exist in at least some SiC Z grains. This has prompted some of my colleagues and me to pursue a suite of larger Z grains (which should yield more counts of each isotope and therefore smaller error bars) for additional analysis.

### A.3 Oxide Grains from Novae

Automated measurements of the O, Mg, and Al isotopic compositions of 41 oxide grains from the Murray meteorite revealed grains from all four of the major oxide groups, in addition to several oxide grains with unusual compositions (Gyngard et al. 2010b). One of these grains has an extremely high $^{17}O/^{16}O$ ratio of $4.4 \times 10^{-2}$ (solar = $3.8 \times 10^{-4}$), which is indicative of a nova origin. I used the Presolar Database to analyze the frequency of silicate, oxide, and SiC grains thought to originate from novae. Because the number of C-rich and O-rich grains that have been analyzed is not a true reflection of

their abundance, the data were normalized to take this effect into account. The likelihood that nova grains of each mineralogy would be observed in the lab was also determined. This led to the conclusion that O-rich presolar grains from novae are considerably more abundant than C-rich grains, which is consistent with theoretical predictions (e.g., Gyngard et al. 2010b and references therein), although prior to this analysis, experimental evidence seemed to contradict theoretical predictions for novae.